Hopf Bifurcation Control and Indices for Power System with Interacting Generator and FACTS Controllers

by

Nadarajah Mithulananthan

A thesis
presented to the University of Waterloo
in fulfillment of the
thesis requirement for the degree of
Doctor of Philosophy
in
Electrical and Computer Engineering

Waterloo, Ontario, Canada, 2002

I hereby declare that I am the sole author of this thesis.

I authorize the University of Waterloo to lend this thesis to other institutions or individuals for the purpose of scholarly research.

I further authorize the University of Waterloo to reproduce this thesis by photocopying or by other means, in total or in part, at the request of other institutions or individuals for the purpose of scholarly research.

The University of Waterloo requires the signatures of all persons using or photocopying this thesis. Please sign below, and give address and date.

ABSTRACT

Power system oscillations, especially electromechanical oscillations, have been a major concern in power system planning and operation. Given the characteristics and nature of these oscillations, these problems can be studied well using Hopf bifurcation theory, which describes the onset of an oscillatory problem in nonlinear systems.

This thesis presents two indices to predict and detect oscillatory problem in power systems using Hopf bifurcations; one of them is preferred as an on-line operational tool due to its higher computational speed. Application of these indices on several test power systems, including the IEEE 50-machines test system and two nonlinear systems, is also included in this thesis to demonstrate the usefulness of the indices. Simulation results indicate that the indices are smooth and fairly linear with respect to the loading factor of the system.

The thesis also clearly demonstrates the direct association between electromechanical oscillations and Hopf bifurcations in power systems. The mitigation of the oscillation problem or Hopf bifurcation from the generator side using PSS controllers, and from the transmission side using FACTS controllers is studied in detail. A new placement technique for a shunt-FACTS controller for the purpose of oscillation damping is also proposed.

The increasing trend in the number of FACTS controllers used in power systems could lead to some undesirable interactions between FACTS and power system controllers or among FACTS controllers. The importance of and tools needed to study this problem are demonstrated in a test system through the analysis of a negative interaction leading to an oscillatory unstable condition.

ACKNOWLEDGEMENTS

The author would like to express his profound gratitude, most sincere appreciation and special thanks to his supervisors Prof. Claudio A. Cañizares and Prof. John Reeve for their constant moral support, invaluable advice and continuous encouragement throughout his Ph.D. program in Waterloo.

It is author's pleasure to thank Prof. S. T. Ariaratnam, Dept. of Civil Engineering, Mr. Graham J. Rogers, Cherry Tree Scientific Software and Mr. Frederic Howell, Powertech for their help, suggestions and enlighten discussion.

The author acknowledges the support of Bill, Lilly and Edvina during the initial period of the stay in the University. The author will always remember Hong, author's colleague, for her help with computer problems and other things. Author also extends thanks to his office-mates big brother Sameh, Fed (Milano), Hassan and room-mate Dev.

Author also wishes to express sincere appreciation to the OGS for their financial support for the later part of the Ph.D. program.

Last but not least, the author wishes to thank with extreme gratitude to his beloved parents for all the hardships they have under gone in educating and bringing their son. This work is dedicated to his parents and their love.

" Live a good, honorable life.
When you get older and think back,
you'll enjoy it a second time. "

Contents

List of Figures

List of Tables

List of Terms

Acronyms:

AVR	:	Automatic Voltage Regulator
BPA	:	Bonneville Power Administration
CPF	:	Continuation Power Flow
DAE	:	Differential-Algebraic Equations
DLM	:	Dynamic Loading Margin
EPRI	:	Electric Power Research Institute
ETMSP	:	Extended Transient Midterm Stability Program
FACTS	:	Flexible AC Transmission Systems
FC	:	Fixed Capacitors
HB	:	Hopf Bifurcation
IEEE	:	Institute of Electrical and Electronics Engineers
MASS	:	Multi Area Small Signal Stability
ODE	:	Ordinary Differential Equation
PSS	:	Power System Stabilizer
PST	:	Power System Toolbox
PTI	:	Power Technology Inc.
PWM	:	Pulse Width Modulation
SLM	:	Static Loading Margin
SSSC	:	Static Synchronous Series Compensator
STATCOM	:	Static Synchronous Compensator
SVC	:	Static Var Compensator
TCR	:	Thyristor Controlled Reactor
TCSC	:	Thyristor Controlled Series Compensator

TSC	:	Thyristor Switched Capacitor
UPFC	:	Unified Power Flow Controller
UWPFLOW	:	University of Waterloo Power Flow
VSC	:	Voltage Source Converter
VSI	:	Voltage Source Inverter
WSCC	:	Western System Coordination Council

Symbols:

δ	:	Generator internal bus voltage angle
ω	:	Angular Speed
M_g	:	Moment of Inertia of generator
D	:	Damping constant
μ	:	Eigenvalue
P_L, Q_L	:	Total Real, Reactive Power Load
λ	:	Loading factor
B	:	Susceptance
K	:	Gain
T	:	Time constant
α	:	Real part of the eigenvalue
β	:	Imaginary part of the eigenvalue
R, r	:	Bifurcation parameters

Chapter 1

INTRODUCTION

1.1 Research Motivation

Nonlinear phenomena, including bifurcations and chaos, occurring in power system models have been the subject of several studies during the last two decades [1, 2, 3, 4, 5, 6, 7, 8]. Among the different types of bifurcations, the saddle-node, limit-induced, and Hopf bifurcations have been identified as pertinent to instability problems in power systems [9].

In the case of saddle-node bifurcations, a singularity of a system Jacobian and/or state matrix results in disappearance of steady state solutions, whereas in the case of limit-induced bifurcations, the lack of steady state solutions arises from system controls reaching limits (e.g. generator reactive power limits). Both of these bifurcation modes typically lead to voltage collapse [10]. Hopf bifurcations on the other hand, produce limit cycles (periodic orbits) that may lead the system to oscillatory instabilities as have been detected in a variety of power system models [9, 11, 12, 13, 14] and observed in practice [15, 16, 17].

In general, power system instability problems can be classified into three main categories, namely, angle, voltage, and mid and long term instability problems. Angle instability problem occurs due to torque imbalance of synchronous machines while voltage and mid-term and long-term instabilities occur due to reactive power imbalance and fault contingencies in the system, respectively. Angle instability can be subdivided into transient and small-signal instability. Transient instability or first swing instability occurs due to large disturbance in the system whereas small-signal instability results from insufficient torque. Small-signal instability is further sub divided into non-oscillatory and oscillatory instability [18].

Hopf bifurcations, which describe the onset of an oscillatory problem, could arise due to variable net damping, frequency dependence of electrical torque and voltage control issues (e.g. fast acting automatic voltage regulators in generators [13, 19]) and are triggered by system contingencies. In most cases, bifurcations occur on very stressed systems, i.e. heavily loaded systems operating close to the "tip of the nose curve" (maximum loading point on a P-V curve). This is a topical concern as many current networks operate near their stability limits due to economical and environmental constraints. Incidents of system collapses induced by Hopf bifurcation include the Sri Lankan power system disturbance of May 2, 1995 [15], and the Western System Coordination Council (WSCC) system disturbance of August 10, 1996 [16]. The consequences were severe. In the WSCC system, approximately 7.5 million customers were interrupted from continuous supply [16]; in the Sri Lanka event, it took about an hour to bring the system back to normal, following a nationwide 30 minute blackout. With ways of predicting and controlling Hopf bifurcations, the above incidents conceivably could have been avoided.

This thesis addresses the issues of predicting, mitigating and avoiding Hopf bifurcations in power systems. The presented Hopf bifurcation examples are low

frequency phenomena (0.1-3 Hz i.e. electromechanical oscillations) which are more commonly observed than at subsynchronous torsional frequencies. They appear due to onerous developing active and reactive power load profiles and are usually triggered by line outages, as will be demonstrated in this thesis.

1.2 Literature Review

Power systems are generally modeled by means of highly nonlinear dynamical systems of equations and a variety of control and independent parameters. In critical circumstances, variations of a parameter may cause unstable oscillations. For example in [13, 20, 21], oscillatory behavior of the power system was identified using Hopf bifurcation theory. In [22], two qualitatively different system instabilities due to bifurcations were observed. The possibility was raised of the coexistence of oscillatory instabilities and voltage collapse, depending on the value of the causal parameter under consideration. Another study [23] shows the occurrence of two Hopf bifurcations prior to a saddle node bifurcation, as is also reported in [11]. The first Hopf bifurcation was unstable ("subcritical") whereas the second one was stable ("supercritical"). Also [23] shows the occurrence of a cyclic fold (two limit cycles of different stability approach one another and collide at a saddle-node bifurcation) bifurcation and two period doubling (a stable limit cycle losses its stability, while another closed orbit starts with twice the period as the original cycle) bifurcations at different parameter values for the same system.

The attention in the literature has been to reveal the presence of Hopf bifurcations, rather than suggesting means of their prediction. An index to determine the proximity of a system to a Hopf bifurcation with respect to a given system parameter would be beneficial, either as a tool in system operation or in planning

studies. While there has been some work done in this area using optimization techniques [24], extensive computations and optimizations are needed every time the topology of the system changes. Methods to detect so-called transcritical and Hopf bifurcations in power systems are discussed in [12], based on what is used in general dynamical systems [25]; thus the real part of the critical eigenvalue can be used as an index to detect Hopf bifurcation in a dynamical system. However, its non-linearity indices makes it impractical for power system applications.

A closed-loop monitoring system for detecting impending instability related to Hopf bifurcations in uncertain nonlinear plants is proposed in [26]. A benefit of this methodology is that it gives a warning at a point close to the instability even when no accurate system model is available. However, earlier prediction of such an event is not possible, as the index is not continuous or smooth. A predictable index with linear or quadratic shape is useful in projecting the problematic loading levels, for a given generation and load directions, both in planning and operation stages. By predicting a problem (e.g. Hopf bifurcation) well in advance, a measure can be deviced (e.g. tuning of appropriate controller gain) to mitigate the problem. In this thesis, a predictable index is proposed and its practical benefits are demonstrated.

The various bifurcations, and the associated rich dynamical behavior that a power system can exhibit, lead to the question of whether instability problems induced by Hopf bifurcations can be predicted and avoided, and, specifically, the possible role of feedback control. Some positive results in this direction are reported in [23, 27, 28] where the issues of bifurcation control through feedback stabilization techniques are addressed. A technique to eliminate a Hopf bifurcation by introducing a "reverse" Hopf bifurcation through an optimal change of parameters is presented in [29].

Alternatively, Hopf bifurcation can be viewed as an oscillatory problem, and

there is a vast amount of work reported in the literature in the area of power system oscillation damping. One of the pioneering works in this area deals with appropriate setting of excitation control parameters for improvement in damping and stability of synchronous generators [30]. Given the characteristics and nature of their oscillations, Hopf bifurcation theory can be used to study them as proposed in [31]. Hence, in this thesis, typical oscillation control techniques are studied in the context of Hopf bifurcations, as an efficient way of controlling the associated instability problems.

Of the range of power system controllers either available or being considered for damping oscillations the Power System Stabilizer (PSS), as applied to generators, is the most widely applied. More recently, Flexible Alternating Current Transmission System (FACTS) controllers have been developed and they can be also exploited for oscillation damping purposes. While a FACTS controller may well be applied in practice to achieve a particular local system objective such as voltage control and enhancement of power flow capability, in principle it can be placed at a strategic location with suitable control signals to enhance damping. FACTS controller placement and selection of the best control input signal for oscillation damping, based on mode controllability and observability concepts, are discussed in [32, 33]. In [34], control of Hopf bifurcations is studied by means of a Static Var Compensator (SVC) on a generator-infinite bus test system and on a three machine test system by placing the SVC between two generators. Hopf bifurcation control using PSS and SVC on a 16 bus test system are discussed in [31]. Other FACTS controllers, i.e. Thyristor Controlled Series Compensator (TCSC), Static Synchronous Compensator (STATCOM), Static Synchronous Series Compensator (SSSC) and Unified Power Flow Controller (UPFC), with suitable input control signals have also been studied for the control of electromechanical oscillations (Hopf bifurcation), so that

the pair of purely imaginary eigenvalues, associated with the Hopf bifurcation can be moved into the left half plane, thus damping the oscillations.

In this thesis, the PSS and several FACTS controllers, i.e. SVC, TCSC, and STATCOM are analyzed and compared from the point of view of Hopf bifurcation control. A new technique is introduced for the best placement of shunt FACTS controllers to control Hopf bifurcation. Attention is also made to the selection of the best input signals, to obtain maximum oscillation damping in the system.

The increasing trend in the use of FACTS controllers in power systems could lead to some undesirable interactions between FACTS and power system controllers or among FACTS controllers as reported in [35]. The interactions could exhibit serious instability problems in some cases, which can be triggered by not only interactions among FACTS controllers located in a given area, but also due to interactions among PSSs and FACTS controllers used throughout the system, as demonstrated in this thesis.

1.3 Research Objectives

The following outstanding areas of current interest will be addressed in Hopf bifurcation studies and control as they pertain to in power systems:

1. Development of a simple index to predict Hopf bifurcations. For on-line or off-line monitoring, it should present a predictably linear or at least quadratic behavior with respect to parameter changes in the system.

2. The study of several power system controllers, specially PSSs and various FACTS controllers in the control of Hopf bifurcations.

3. Analysis of performance and interactions of various controllers under a wide range of operating and fault conditions.

Thus, this thesis concentrates on the detection and prediction of Hopf bifurcations, their control through PSS and FACTS controllers with the most suitable placements and control signals, and the performance and interactions of these controllers for a variety of system conditions.

1.4 Outline of the Thesis

This thesis is organized as follows: Chapter 2 introduces the modeling of PSS and the FACTS controllers that are used in this thesis, i.e. SVC, TCSC and STATCOM. In this chapter, the analysis techniques, analytical tools and test systems used in this thesis are also discussed.

The theory behind Hopf bifurcations, the effect of Hopf bifurcation of dynamic behavior on the system following a disturbance, and the proposed Hopf bifurcation indices, along with several numerical examples of their application are presented in Chapter 3. The effect of different nonlinear static load models on Hopf bifurcations is also discussed in this chapter.

Hopf bifurcation control using PSS and shunt and series FACTS controllers, including a new placement technique for shunt FACTS controllers are discussed in Chapter 4. The performance of the controllers under a wide variety of system operating and fault conditions, as well as possible interactions between PSS and FACTS, or between FACTS controllers, are discussed in Chapter 5. Finally, concluding observations together with possible future research directions are presented in Chapter 6.

Static and dynamic data of all the small test systems utilized in this thesis are given in Appendices A, B and C. The SVC and STATCOM controller parameters used in the two-area and the IEEE 50-machine test systems are given in Appendix D.

Chapter 2

MODELING, TOOLS AND TEST SYSTEMS

2.1 Introduction

Mathematical models of a power system for stability analysis (eigenvalue or time domain analysis) consist of differential and algebraic equations representing the models of system components, including generators, transformers, buses, lines (ac and dc), loads and FACTS controllers. A brief description of the models, especially the basic structure and terminal characteristics of PSS, SVC, TCSC and STATCOM controllers, are briefly discussed in this chapter. The basic analysis techniques, analytical tools and the test systems utilized for the research are also presented.

2.2 Power System Models

Mathematical models of a synchronous machine vary from the elementary classical to a detailed one. In the former, the machine is represented by two ordinary differential equations related to the mechanical motions. The basic mechanical motion of a generator is characterized by the so called swing equations (2.1).

$$\begin{aligned} \frac{d\delta}{dt} &= \omega \\ M_g \frac{d\omega}{dt} &= P_M - P_{ge} - D\omega \end{aligned} \tag{2.1}$$

where δ is generator internal bus voltage angle, ω is angular speed, M_g is moment of inertia of generator, P_{ge} electrical output of the generator, D is damping constant, and P_M is the mechanical power input to the generator.

In more detailed models, transient and subtransient behaviors are considered [18, 36]. In this research work, classical and detailed models were used to represent the machines in various test systems.

For eigenvalue or time domain simulation studies, it is necessary to include the effects of the excitation and prime mover controllers. They indirectly influence the reactive and active power outputs of a generator respectively. IEEE Type 1 or WSCC Type A, IEEE S1a, AC4a, and simple exciter models are used in this thesis, to represent the excitation control of generators, and hydraulic and simple turbine governor models are used to represent the prime mover controllers of various generators in some test systems as in [18].

The modeling of loads is often complicated by the unpredictability of the compounding of devices (e.g. Fluorescent, Compact Fluorescent and Incandescent

lamps, Refrigerators, Heater, Motor, Oven and Furnace). However, load models are traditionally classified into two broad categories: static and dynamic. In this research work, the influence of three basic static load models, namely constant impedance, constant current and constant power, on the system Hopf bifurcation point has been studied. Their definitions are as follows [37]:

1. *Constant Impedance Load Model (constant Z)*: A static load model where the real and reactive power varies with the square of the voltage magnitude. It also referred to as constant admittance load model.

2. *Constant Current Load Model (constant I)*: A static load model where the real and reactive power varies directly with voltage magnitude.

3. *Constant Power Load Model (constant PQ)*: A static load model where the real and reactive power does not vary with changes in voltage magnitude. It is also known as constant MVA load model.

All these load models can be described by an equation of a polynomial load model:

$$\begin{aligned} P &= P_0 \left(\frac{V}{V_0}\right)^a \\ Q &= Q_0 \left(\frac{V}{V_0}\right)^b \end{aligned} \tag{2.2}$$

where P_0 and Q_0 stand for the real and reactive powers consumed at a reference voltage V_0. The exponents a and b depend on the type of load that is being represented, e.g. for constant power load models $a = b = 0$, for constant current load models $a = b = 1$ and for constant impedance load models $a = b = 2$.

In load flow studies, in order to obtain P-V curves of various test systems, the loads were represented as constant PQ, and increased according to (2.3), i.e. both real and reactive power consumptions were increased by the same ratio by keeping a constant power factor at each load.

$$\begin{aligned} P_L &= P_{Lo}(1+\lambda) \\ Q_L &= Q_{Lo}(1+\lambda) \end{aligned} \tag{2.3}$$

where P_{Lo} and Q_{Lo} are the initial real and reactive power respectively and λ is the loading factor, which represents the slow varying parameter used in bifurcation studies.

2.3 Power System Stabilizer

A PSS can be viewed as an additional block of a generator excitation control or Automatic Voltage Regulator (AVR), added to improve the overall power system dynamic performance, particularly to damp power/frequency oscillations. The PSS uses auxiliary stabilizing signals such as shaft speed, terminal frequency and/or power to change the input signal to the AVR. This is a very effective method of enhancing small-signal stability performance [18, 38].

The three basic blocks in a PSS are illustrated in Figure 2.1. The stabilizer Gain block determines the amount of damping. Next, the Washout block serves as a high-pass filter, with a time constant that allows the signal associated with oscillations in rotor speed to pass unchanged; without this block, the steady state changes would modify the terminal voltages. Finally, the Phase-compensation block provides the appropriate phase-lead characteristic to compensate for the phase lag between the

exciter input and the generator electrical (air-gap) torque; in practice, two or more first-order blocks may be used to achieve the desired phase compensation.

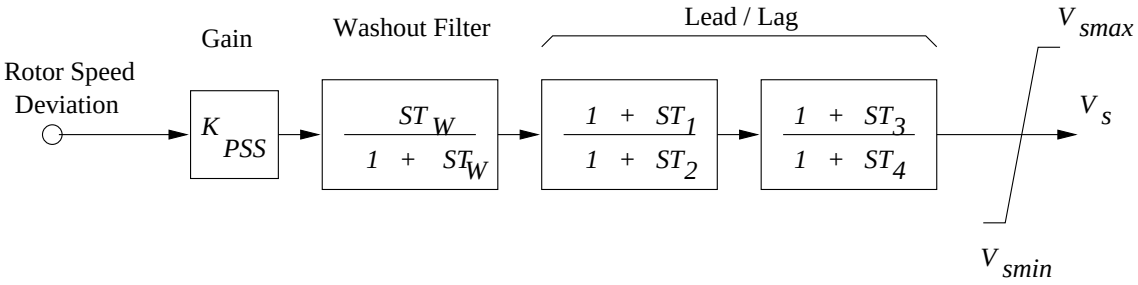

Figure 2.1: Basic block diagram of power system stabilizer.

In this research work, the PSS is considered as the first choice to ameliorate Hopf bifurcations triggered by line outages. FACTS controllers are also considered for this purpose.

2.4 FACTS controllers

FACTS controllers are a family of high-speed electronic controllers of increasing interest for enhancing power system performance [39]. They can significantly increase the utilization of installed capacity while reducing susceptibility to power disturbances through rapid automatic response and operator-initiated actions.

Certain FACTS controllers have already been applied and others are under development. SVC, TCSC, STATCOM, SSSC and UPFC (a combination of a SSSC and a STATCOM) are well known FACTS controllers [32, 34, 40, 41, 42, 43, 44].

This thesis concentrates on SVC, TCSC and STATCOM controllers as these have been already identified as feasible alternatives to PSS controller for the control of electromechanical oscillation in power system (whether as their principal

function or, more likely, as the supplementary dynamic capability to other strategic objectives). For exclusive oscillation control, a FACTS controller would be nevertheless more expensive than a PSS, as illustrated in the approximate cost comparison of these controllers shown in Table 2.1 [45, 46]. A brief description follows of the models of each of these FACTS controllers.

Table 2.1: Cost comparison of PSS and FACTS controllers

Controller	Cost (US)
PSS	\$30, 000
SVC	\$40/kvar (controlled portions)
TCSC	\$40/kvar (controlled portions)
STATCOM	\$50/kvar

2.4.1 SVC

A shunt connected SVC injects capacitive or inductive current so as to maintain or control a specific variable, typically bus voltage [39]. SVCs were first developed in the late 1960s for the compensation of large fluctuating industrial loads, such as electric arc furnaces. Thyristor-Switched Capacitors (TSCs) or a Fixed Capacitor (FC) with a Thyristor-Controlled Reactor (TCR) provide rapid and fine voltage control.

By the late 1970s SVC were applied to transmission systems to achieve improved dynamic voltage control. The two most popular configurations are the FC with TCR, and TSC with TCR. Figures 2.2 and 2.3 show a basic structure of a SVC with voltage control and its control characteristic, respectively, for a FC and TCR type SVC [47].

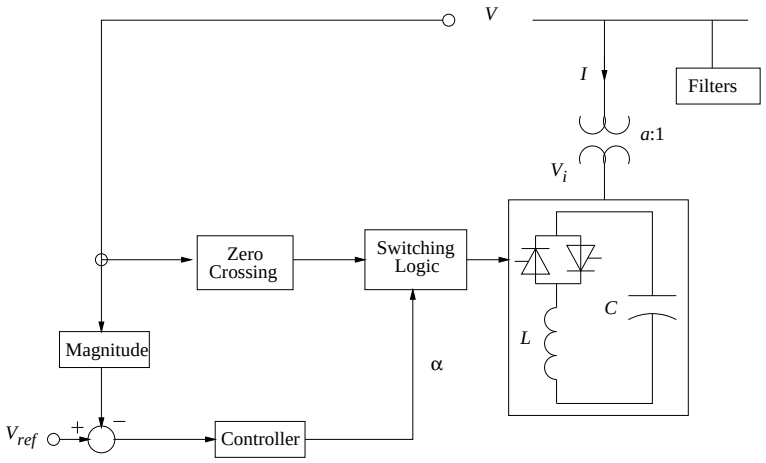

Figure 2.2: Basic SVC structure with voltage control.

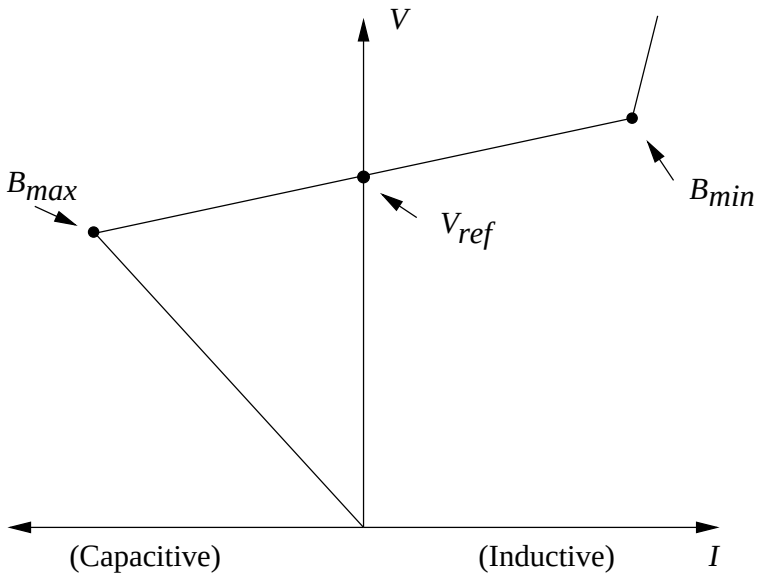

Figure 2.3: Typical steady-state voltage control strategy of an SVC.

Model and Controls

An additional stabilizing signal with a supplementary control superimposed on the voltage control loop of a SVC can also provide oscillation damping by moving critical eigenvalues to the open left-half plane as discussed in [31, 34, 48].

MASS and ETMSP modules of PSAPAC [49, 50], which are two of the analytical tools used in this thesis (section 2.6.2 and 2.6.3) allow the controller to be modeled as a voltage control device made up of a static Gain block, two Lead/Lag blocks, and an end-block (SD-2) as shown in Figure 2.4. The SD-2 end-block is a static device that represents the TCR and FC as an equivalent, nonlinear, controllable susceptance B_{SVC} [50]. A supplementary control input signal is also considered for the purpose of Hopf bifurcation control as also depicted in Figure 2.4. In another simulation tool, PST, used in this research work (section 2.6.2 and 2.6.3), the SVC is represented by a variable reactance with maximum inductive and capacitive limits, which directly correspond to the limits in the firing angles of the thyristors, as shown in Figure 2.3. This reactance is assumed to vary to control the SVC bus voltage, with a supplementary control block and input signals to damp oscillations as shown in Figure 2.5.

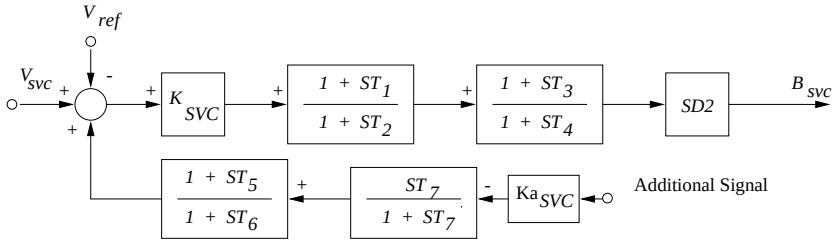

Figure 2.4: A Use Defined SVC used in MASS and ETMSP: UDSVC-1.

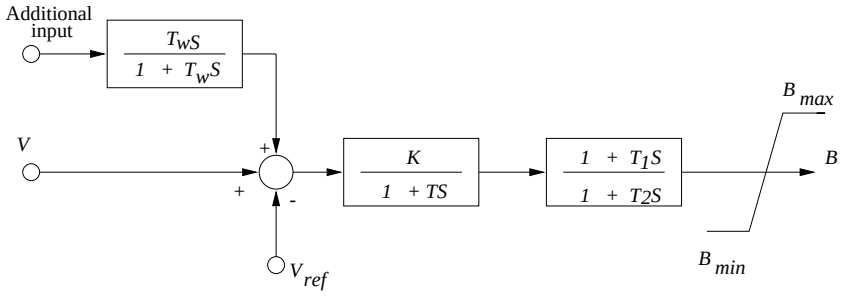

Figure 2.5: Block diagram of an SVC used in PST.

2.4.2 TCSC

The maximum power transfer capability of a transmission line is increased by series capacitor compensation of the series inductive reactance. The use of modular blocks of capacitors to provide, say, 30-40 % compensation is long established. However, the subsynchronous series resonant frequency so produced has been known to introduce negative damping of generator torsional modes. The dynamic capability of a TCSC can be used for oscillation damping (both subsynchronous and electromechanical) in addition to the steady state compensation of series reactance.

A TCSC controller is basically a Thyristor Controlled Reactor (TCR) in parallel with a bank of capacitors. A typical single module TCSC structure for current control and the steady state corresponding V-I characteristic curve are shown in Figures 2.6 and 2.7, respectively [47].

Model and Control

ETMSP and MASS allow the TCSC controller to be modeled as current, power, or voltage control device with a washout block with gain, lag, lead/lag block, gain block with limits, and an end block (SD2) as shown in Figures. 2.8 and 2.9. The SD-2 end block is basically a static device that represents the TCR and FC combination

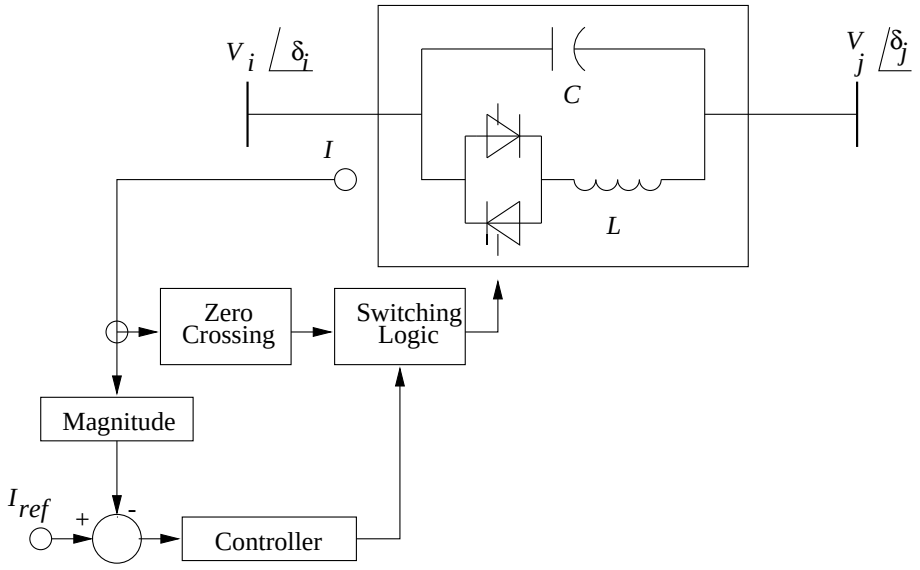

Figure 2.6: Basic TCSC structure with current control.

as an equivalent, nonlinear, controllable susceptance B_{SVC} with limits [50].

2.4.3 STATCOM

The STATCOM resembles in many respects a synchronous compensator, but without the inertia. The basic electronic block of a STATCOM is the Voltage-Sourced Converter (VSC), which in general converts an input dc voltage into a three-phase output voltage at fundamental frequency, with rapidly controllable amplitude and phase angle.

The basic structure of a STATCOM for either phase control or Pulse Width Modulation (PWM) control, and its V-I characteristic are depicted in Figures. 2.10 and 2.11, respectively [47]. As can be seen in Figure 2.10, a STATCOM is made up of a coupling transformer, a VSC and a dc capacitor. The control system can be designed to maintain the magnitude of the bus voltage constant by controlling the

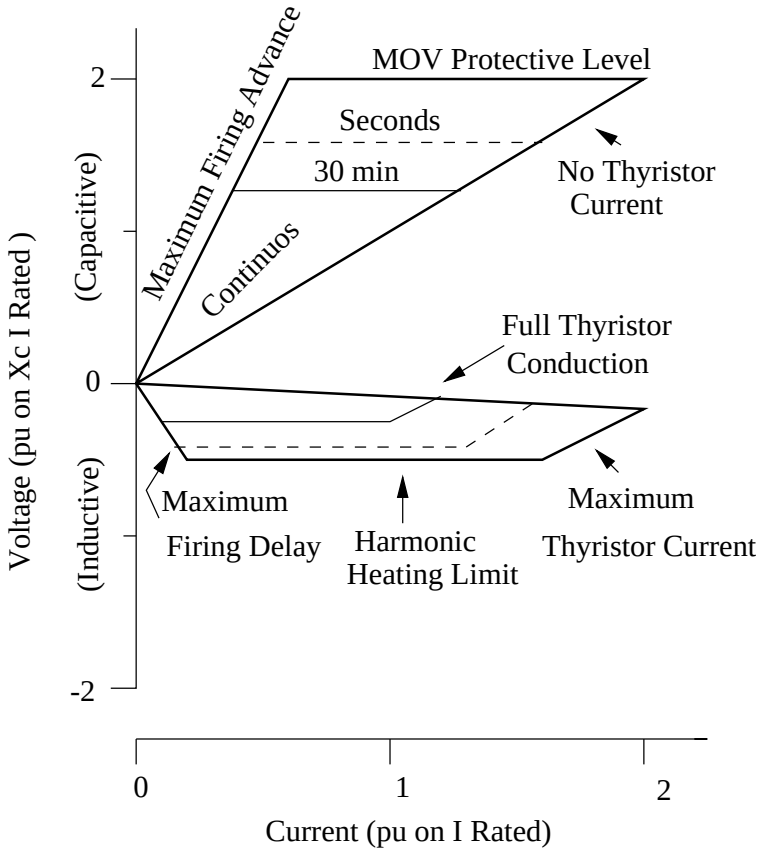

Figure 2.7: TCSC V-I steady state characteristics.

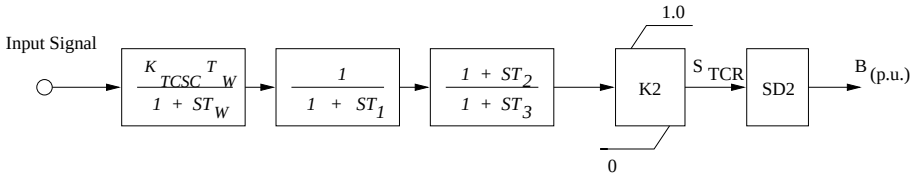

Figure 2.8: A User Defined TCSC used in MASS and ETMSP: UDTCSC-1.

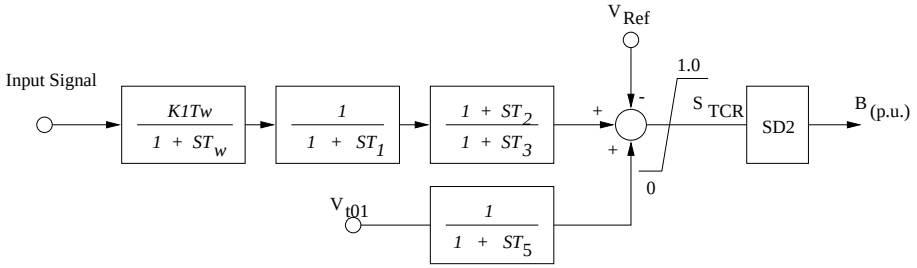

Figure 2.9: A User Defined TCSC used in MASS and ETMSP: UDTCSC-2.

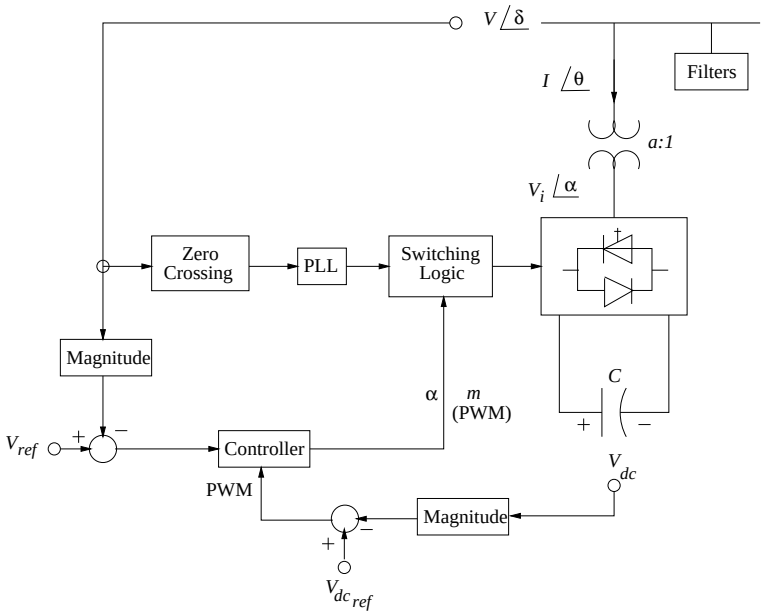

Figure 2.10: Basic STATCOM structure.

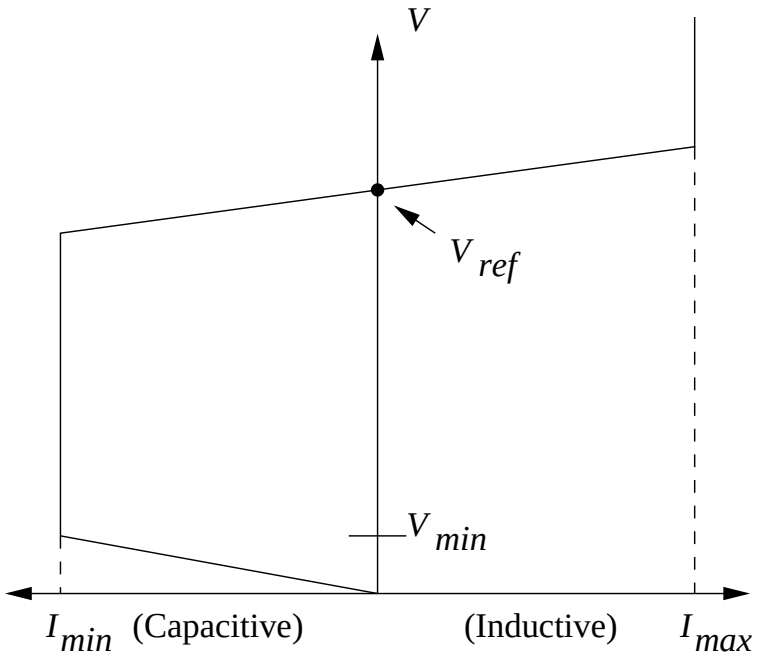

Figure 2.11: STATCOM V-I steady state characteristics.

magnitude and/or phase shift of the VSC output voltage. In steady state operation, the inverter voltage V_i is assumed to be in phase with the ac terminal voltage V, as there is practically no active power flowing from or to the VSC. The STATCOM supplies reactive power to the ac system if V_i is greater than V; it draws reactive power from the ac system if V is greater than V_i. The dc capacitor voltage V_{dc} is controlled through the phase angle α, which determines the transient active power flow between the system and the VSC, and hence the charging and discharging of C.

The STATCOM is represented using the fundamental frequency model described in [47], which represents the active and reactive power flows from and to the VSC. The model is basically a controllable voltage source behind an impedance with the representation of the charging and discharging dynamics, of the dc capacitor, as

well as the STATCOM ac and dc losses.

Model and Controls

A phase control strategy is assumed for the STATCOM bus voltage, and a supplementary control block and signal are added for Hopf bifurcation control, as depicted in Figure 2.12. The p.u. differential-algebraic equations (DAE) corresponding to this model are [47]:

$$\begin{bmatrix} \dot{x_c} \\ \dot{\alpha} \\ \dot{m} \end{bmatrix} = f(x_c, \alpha, m, V, V_{dc}, V_{ref}, V_{dc_{ref}}) \tag{2.4}$$

$$\dot{V_{dc}} = \frac{VI}{CV_{dc}}\cos(\delta - \theta) - \frac{V_{dc}}{R_c C} - \frac{R}{C}\frac{I^2}{V_{dc}}$$

$$0 = \underbrace{\begin{bmatrix} P - VI\cos(\delta-\theta) \\ Q - VI\sin(\delta-\theta) \\ P - V^2G + kV_{dc}VG\cos(\delta-\alpha) + kV_{dc}VB\sin(\delta-\alpha) \\ Q + V^2B - kV_{dc}VB\cos(\delta-\alpha) + kV_{dc}VG\sin(\delta-\alpha) \end{bmatrix}}_{g(\alpha,k,V,V_{dc},\delta,I,\theta,P,Q)}$$

where, $G + jB = (R + jX)^{-1}$, is used to represent the transformer impedance, any ac series filters, etc. ; $k = \sqrt{3/8}m$, P and Q are the real and reactive powers flowing into the VSI, $V < \delta$ is the terminal voltage, $V_i < \alpha$ is the inverter voltage and x_c stands for the internal control system variables.

The steady state model of the STATCOM can be obtained from (2.4) by replacing the differential equations with the steady state equations of the dc voltage and

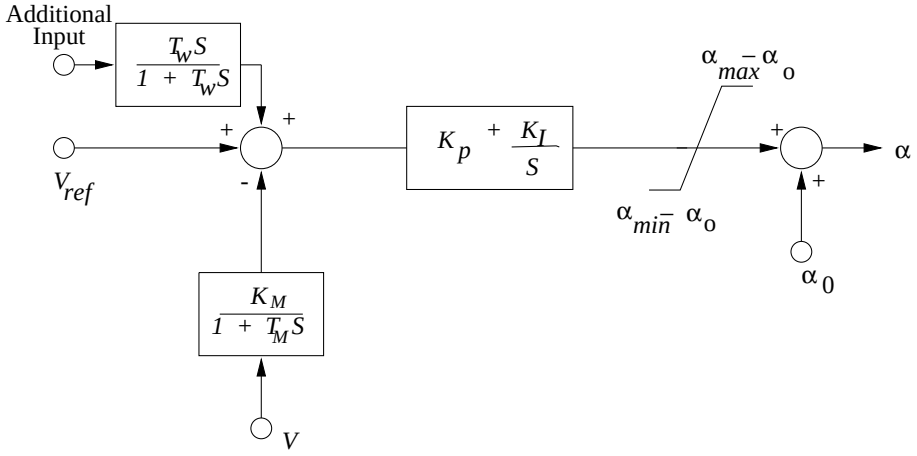

Figure 2.12: STATCOM phase control with oscillation damping.

the voltage control characteristics of the STATCOM. Notice that the controller droop is directly represented on the V-I characteristic curve, with the controller limits being defined by its ac current limits. Hence, the steady state equations for the phase controller are given by

$$0 = \begin{bmatrix} V - V_{ref} + X_{SL} I \\ 0 = k - 0.9 \\ P - {V_{dc}}^2 / R_c - R I^2 \\ g(\alpha, k, V, V_{dc}, \delta, I, \theta, P, Q) \end{bmatrix} \tag{2.5}$$

Since there is no STATCOM model available in the PSAPAC, complete static and dynamic models as described above with phase control is implemented in PST using the symbolic library and vectorized computation techniques in MATLAB.

2.5 General System Equations

Based on the equations of the various components and their control models described in sections 2.3 and 2.4, the power system can be represented for the problem in hand by the following set of differential and algebraic equations (DAE):

$$\begin{aligned} \dot{x} &= f(x, y, \lambda, p) \\ 0 &= g(x, y, \lambda, p) \end{aligned} \tag{2.6}$$

where $x \in \Re^n$ is a vector of state variables associate with dynamic states of generators, loads, and other system controllers; $y \in \Re^m$ is a vector of steady-state algebraic variables resulting from neglecting fast dynamics (e.g. some load voltage phasor magnitudes and angles); $\lambda \in \Re^\ell$ is a set of uncontrollable parameters, such as active and reactive power load variations, and in this thesis it is used to represent the loading factor (l=1) as previously defined in (2.3); and $p \in \Re^k$ is a set of controllable parameters such as tap settings, Automatic Voltage Regulator (AVR) and SVC reference voltages.

For eigenvalue analysis (small signal stability or steady state stability analysis), (2.6) can be linearized around an equilibrium operating point (x_o, y_o) for given values of the parameters (λ_o, p_o). Thus,

$$\begin{bmatrix} \Delta\dot{x} \\ 0 \end{bmatrix} = \underbrace{\begin{bmatrix} J_1 & J_2 \\ J_3 & J_4 \end{bmatrix}}_{J} \begin{bmatrix} \Delta x \\ \Delta y \end{bmatrix} \tag{2.7}$$

where, J is the system Jacobian, and $J_1 = \partial f/\partial x|_0$, $J_2 = \partial f/\partial y|_0$, $J_3 = \partial g/\partial x|_0$, $J_4 = \partial g/\partial y|_0$. If it is assumed that J_4 is nonsingular, which is a requirement for equations (2.6) to appropriately represent the system [51], the system eigenvalues

can be readily computed by eliminating the vector of algebraic variable Δy in (2.7), as follows:

$$\Delta \dot{x} = (J_1 - J_2\ J_4^{-1}\ J_3)\Delta x = A\ \Delta x \tag{2.8}$$

That is, the DAE system can be reduced to a set of ODE equations [51]. Then, bifurcations of the power system model, and particularly Hopf bifurcations which are the interest of this work, can be studied by monitoring the eigenvalues of matrix A in (2.8) as system parameters λ and P changes. Time domain simulations, on the other hand, which are used in this research to study the global stability of the system model, were obtained by numerically intergrating equations (2.6). More detailed descriptions follow of the various analysis techniques and tools used here.

2.6 Analysis Techniques

Full P-V or "nose curves" of the test systems used for bifurcation analyses were obtained using a Continuation Power Flow (CPF) technique. One advantage is that the algorithms are not prone to divergence problems at operating conditions near steady state stability limits. Furthermore, it yields additional information, such as sensitivities with respect to the parameter λ, that can be used to better understand the phenomenon under study [52].

In order to detect Hopf bifurcations on the P-V curves corresponding to the various test systems, the multiple power flow solutions generated by the CPF for the varying parameter λ, from the base load to the maximum loading conditions, were used to obtain the reduced system state matrix at each equilibrium point. Then eigenvalues were used to detect the various bifurcation points, especially Hopf bifurcation, which were combined with the time domain simulations to analyze the resulting system oscillations.

2.6.1 Continuation Power Flow (CPF)

CPF methods are typically employed to trace the P-V curve up to the maximum loading point (maximum loadability or steady state stability limit) of the system. While they are computationally demanding for larger systems [10, 18, 53], they provide additional information about the system behavior, such as sensitivity information with respect to parameter variations.

The CPF technique uses an iterative process involving predictor and corrector steps as shown in Figure 2.13. In some cases, an additional parameterization step, is used to avoid certain convergence problem. Thus, from a known initial point A, a tangent predictor step is used to estimate the solution point B for a given load direction defined by the parameter λ. A corrector step is then used to determine the exact solution C using a power flow with an additional equation to find the proper value of λ. This process is repeated until the desired bifurcation diagram or P-V curve is obtained. A parameterization step may be used to avoid convergence problems when the Jacobian becomes singular around the maximum loading point by simply exchanging the parameter λ with a variable with the largest change.

All P-V curves were obtained by the University of Waterloo Power Flow (UWPFLOW) [54]. It has been designed to calculate local fold bifurcations such as saddle node and limit induced bifurcations in power systems and is based on CPF and direct computational methods. A variety of output files permit further analyses, such as tangent vectors, left and right eigenvectors at the bifurcation point, power flow solutions at different loading levels, left and right eigenvectors associated with the smallest eigenvalue, and voltage stability indices, etc.

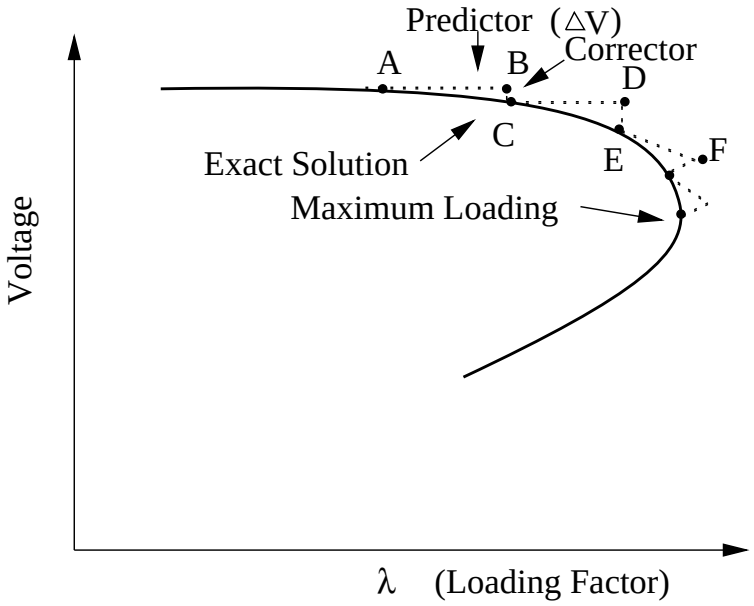

Figure 2.13: Illustration of Continuation Power Flow technique.

2.6.2 Eigenvalue Analysis

Bifurcation studies are based on eigenvalue analysis, also referred to as small signal stability, steady state stability or modal analysis [18]. Once the reduced system state matrix A (2.8) is determined at an equilibrium point along the P-V curve, the eigenvalues and eigenvectors are given by:

$$Av = \mu v \tag{2.9}$$

where μ is the eigenvalue, and v is the corresponding right eigenvector. The main drawback is the need for obtaining the inverse of J_4, and hence the associated loss of sparsity. However, the augmented system equations can be used directly, so that efficient sparsity-based algorithms can speed up the eigenvalue computation [55]; thus, the eigenvalue computation can be restated as

$$\begin{bmatrix} J_1 & J_2 \\ J_3 & J_4 \end{bmatrix} \begin{bmatrix} v_1 \\ v_2 \end{bmatrix} = \mu \begin{bmatrix} v_1 \\ 0 \end{bmatrix} \tag{2.10}$$

This is termed the generalized eigenvalue problem, where $[v_1\ v_2]^T$ are the augmented right eigenvectors of μ. By eliminating v_2 from (2.10), (2.9) can be readily obtained.

If the rotor angles (δ) are taken as state variables, there will be a null eigenvalue if the algebraic variables are eliminated. This is because of the fact that the sum of the columns corresponding to $\Delta\delta$ is zero [18]. In most of the commercially available small signal stability tools, an exact null eigenvalue does not appear because numerical techniques are used to obtain the system Jocobian and/or state matrix.

The eigenvalues of the test systems were calculated using the, Multi-Area Small-Signal program (MASS) from the Electric Power Research Institute (EPRI) program. The small signal stability module of the Power System Toolbox (PST) also was used to calculate the eigenvalues in some cases. MASS forms the state matrix A of a power system and determines all the eigenvalues and eigenvectors of the matrix by the QR algorithm. It also produces various outputs for further analysis such as participation factors, state matrix, and frequency response. However, it does not produce the full Jacobian which is necessary for one of the proposed indices and the new FACTS controller placement technique as described in the Chapters 3 and 4. For this reason the PST software tool was used.

PST is a MATLAB based power system analysis tool [56, 57]. It was developed to perform power system analysis with user defined models. This program contains several graphic tools, namely Voltage Stability, Transient Stability and Small Signal Stability. The program code can be modified to accommodate user-defined power system controller models.

2.6.3 Time Domain Analysis

Time domain analysis is valuable not only for verifying and benchmarking the small signal response but also for assessing the effects of the nonlinearities on dynamic damping. Time domain simulations are the available practical method of transient stability analysis to date, in which a set of nonlinear differential equations representing machines and controllers are simultaneously solved using step-by-step numerical intergration techniques, such as trapezoidal or predictor corrector methods.

For the time domain simulation in this thesis, the Extended Transient-Midterm Stability Program (ETMSP) of EPRI and the transient stability analysis module of PST were used. ETMSP combines multiple numerical intergration methods and advanced modeling of variety of devices and controllers for transient and mid-term stability analyses. MASS and ETMSP share common data files, representing the static and dynamic power system data. The programs can read static network data from BPA, PTI, WSCC, IEEE and EPRI power flows format, and dynamic generator plant data from PTI format. The transient stability analysis module of PST uses a predictor corrector method in solving the differential equations. This module also accommodates any user defined models and reads the static and dynamic data in matrix format as shown in Appendices B and C.

2.7 Test Systems

The various proposed methodologies have been applied to a number of test systems, ranging from 2 machines (3 buses) to 50 machines (145 buses). A brief description of each of these systems follows.

2.7.1 Three-bus Test System

A one line diagram of the simplest test system is shown in Figure 2.14 [56]. Both of the generators were modeled in detail, assuming an exciter (AC4a) and hydraulic governor. The nominal load is 900 MW, and 300 Mvar. Static and dynamic data of the test system are given in Appendix B, as relevant to software package.

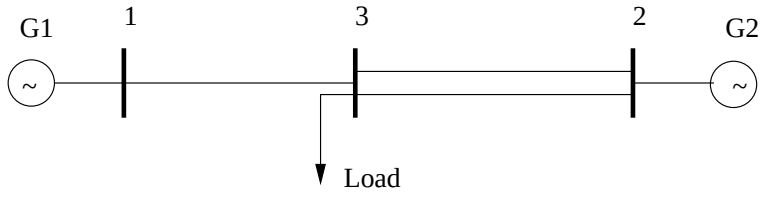

Figure 2.14: Three-bus test system.

2.7.2 Two-area Test System

Figure 2.15 is the one-line diagram of a two-area system proposed in [18] for oscillation studies. The topology of the system is symmetrical with respect to bus 8, however the loads and the limits of individual generator are not equal in both areas. All of the generators were modeled in detail with a simple exciter except G2. A simple turbine governor also considered in each of the generators, except G3. The total system load is 2734 MW and 200 Mvar. Static and dynamic data are given in Appendix C.

2.7.3 IEEE 14-bus Test System

A single line diagram of the IEEE 14-bus test system [58] is shown in Figure 2.16. It consists of five synchronous machines with IEEE type-1 exciters, three of which

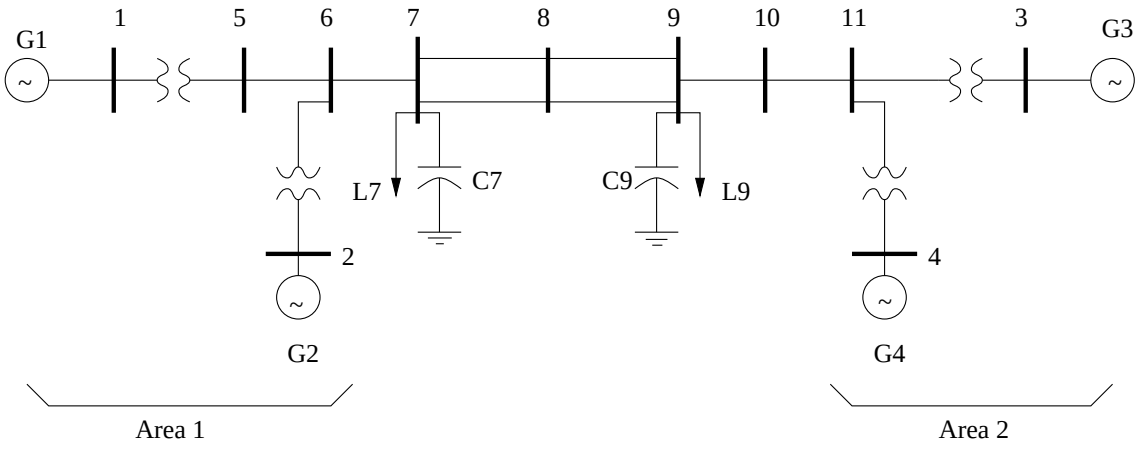

Figure 2.15: Two-area test system.

are synchronous compensators used only for reactive power support. There are 11 loads in the system totaling 259 MW and 81.3 Mvar. The dynamic data for the generators and exciters were selected from [59]. The static and dynamic data are given in the Appendix D in a format appropriate for the ETMSP and MASS packages.

2.7.4 IEEE 50-machine Test System

The IEEE 50 machine system shown in Figure 2.17 is an approximated model of an actual power system, and was developed for stability studies in 1990 [60]. It consists of 145 buses and 453 lines including 52 fixed tap transformers. Two dynamic data sets were used for this test system for this thesis. In the first, seven of the generators were modeled in detail with exciters (IEEE S1a), whereas the rest were represented using just their swing equations [56]. This case is referred to as Case I. It is important to mention that the original inertia values in some of the generators were reduced to allow for the appearance of Hopf bifurcations. In the second data set, six of the generators were modeled in detail with simple exciters

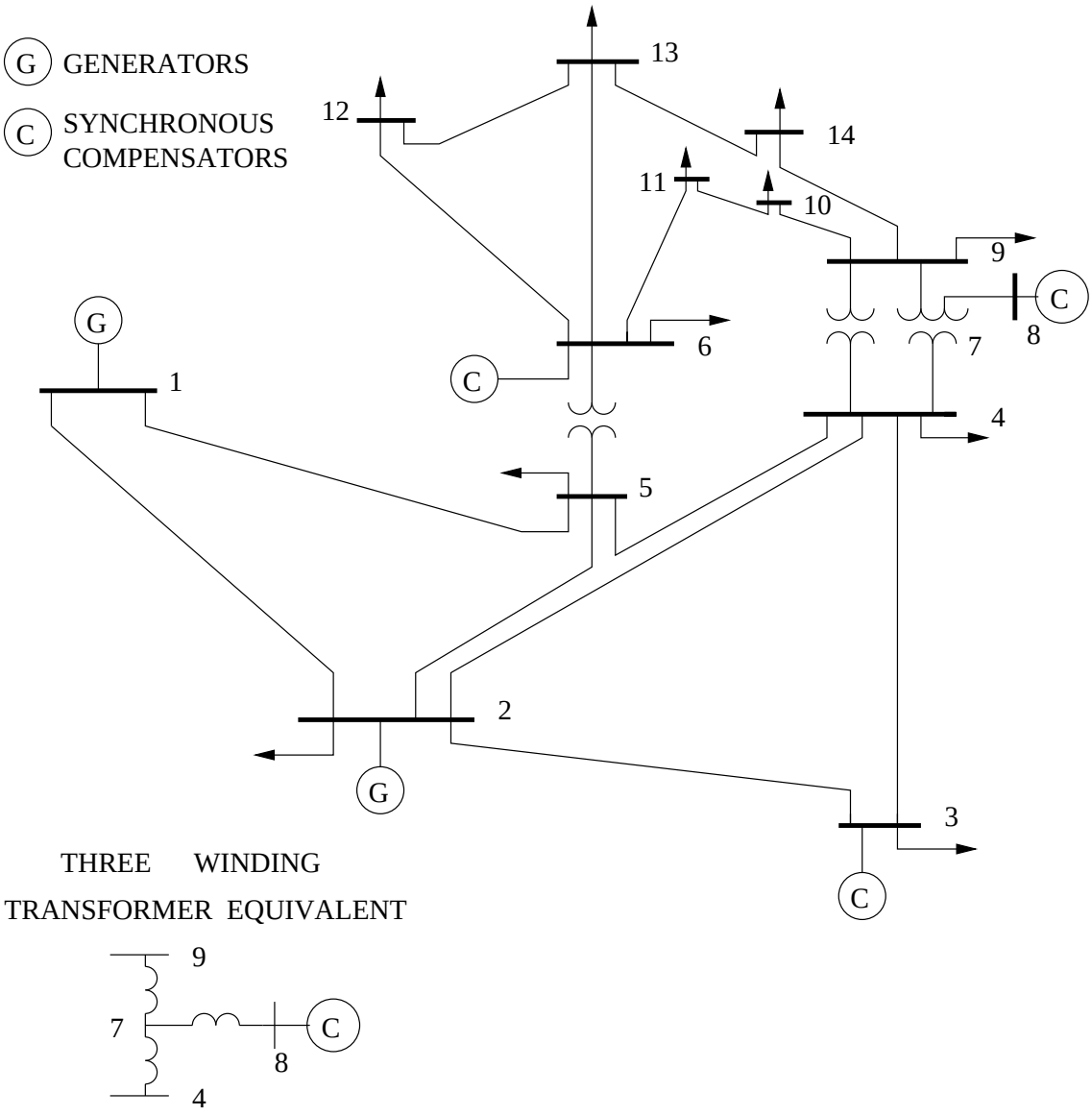

Figure 2.16: IEEE 14-bus test system.

[60]. This second case is referred to as Case II. There are 60 loads for a total of 2.83 GW and 0.80 Gvar.

2.8 Summary

This chapter has described a number of Flexible AC Transmission System (FACTS) controllers as will be incorporated into test system in the exploration of Hopf bifurcation control. Following a description of the adopted analysis techniques, analytical tools and software, the test systems have been presented.

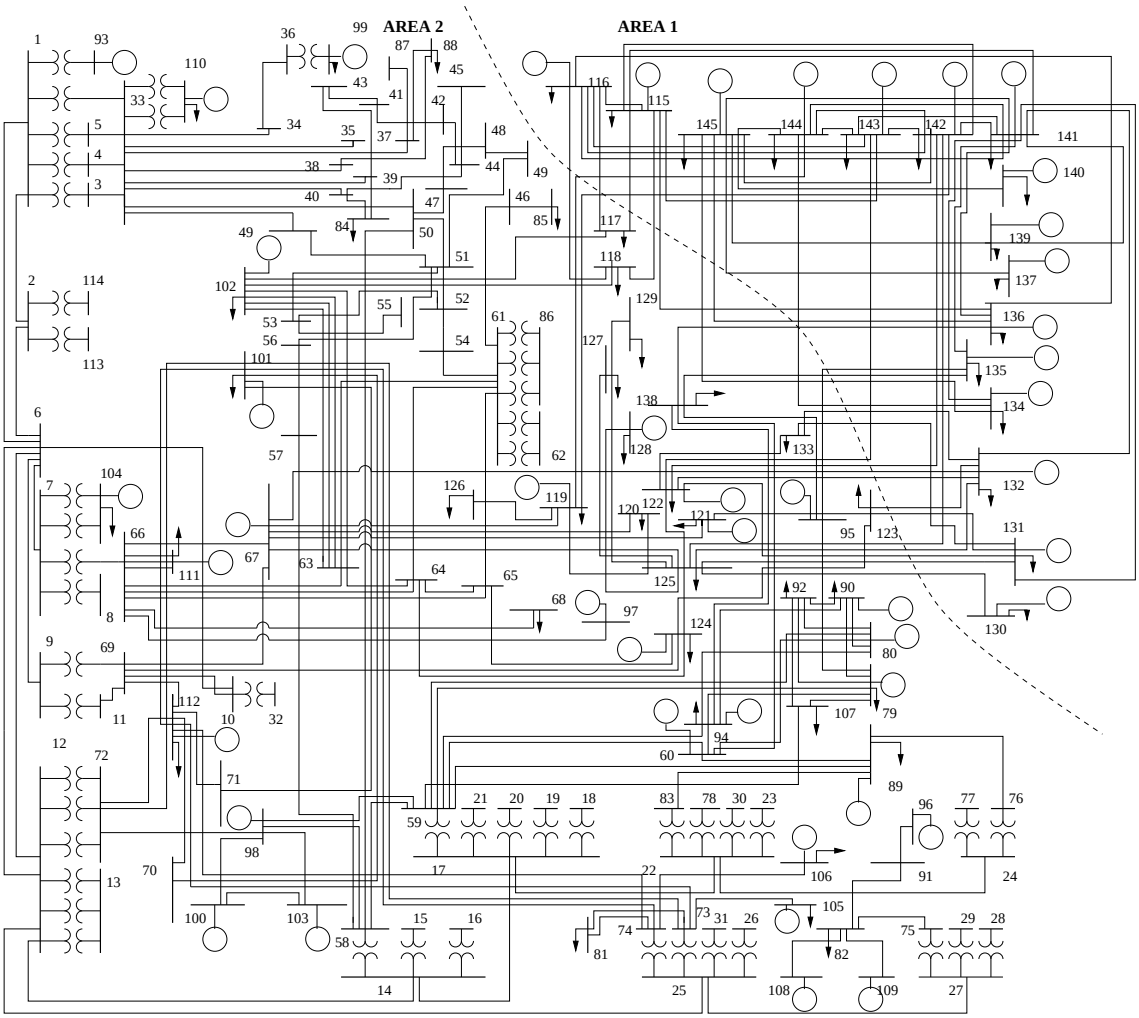

Figure 2.17: IEEE 50-machine test system.

Chapter 3

HOPF BIFURCATIONS AND INDICES

3.1 Introduction

Power system oscillations associated with Hopf bifurcations, which are typically triggered by line outages, could lead to partial or full power interruptions. Hence, with ways of predicting or detecting, in advance, these types of bifurcations possible power outages could be avoided.

Following, for reference, a brief summary of the theorem underlying Hopf bifurcations, two alternative indices are introduced for off-line or on-line prediction of oscillatory problems associated with these bifurcations. A methodology to linearize the indices is presented, together with the application of these indices to several test systems as well as to other types of nonlinear systems. The effect of nonlinear static load models on Hopf bifurcations is also discussed in this chapter.

3.2 Hopf Bifurcations

In 1942, E. Hopf observed the bifurcation from an equilibrium point to a family of periodic solutions in non-linear systems of dimension greater than or equal to two. Hopf bifurcations are characterized by periodic orbits (limit cycles) emerging around an equilibrium point. They can be studied by linearized analysis, as at the bifurcation points the system Jacobian has a pair of purely imaginary eigenvalues [25].

Consider the dynamical power system modeled by (2.6). When the parameters λ and/or p vary, the equilibrium points (x_o, y_o) change, and so do the eigenvalues of the corresponding system state matrix. The equilibrium points are asymptotically stable if all the eigenvalues of the system state matrix have negative real parts. The point where a complex conjugate pair of eigenvalues reach the imaginary axis with respect to the changes in (λ, p), say $(x_o, y_o, \lambda_o, p_o)$, is known as a Hopf bifurcation point. This phenomenon is illustrated in Figure 3.1 using the locus of the critical eigenvalues in the complex plane, i.e. the bifurcating complex conjugate pair of eigenvalues.

At a Hopf bifurcation point $(x_o, y_o, \lambda_o, p_o)$, the following transversality conditions are satisfied [25]:

1. $[f(x_o, y_o, \lambda_o, p_o)\ g(x_o, y_o, \lambda_o, p_o)]^T = 0$.

2. The Jacobian matrix evaluated at $(x_o, y_o, \lambda_o, p_o)$ should only have a simple pair of purely imaginary eigenvalues $\mu = \pm j\beta$.

3. The rate of change of the real part of the critical eigenvalues with respect to

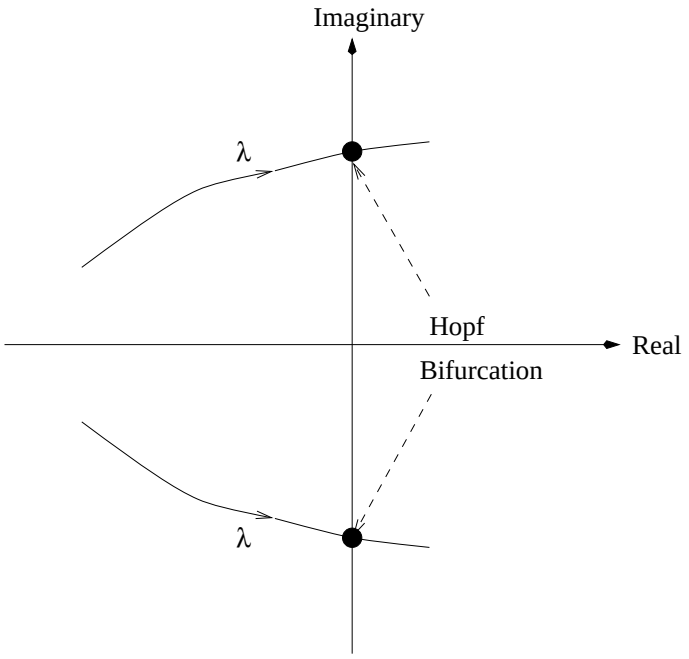

Figure 3.1: Locus of the critical eigenvalues on a Hopf bifurcation.

a varying system parameter, say λ_i, should be nonzero, i.e.

$$\left.\frac{d\mathrm{Re}\{\mu\}}{d\lambda}\right|_o \neq 0$$

If this is the case, a limit cycle appear at $(x_o, y_o, \lambda_o, p_o)$ with an initial period of

$$T_o = \frac{2\pi}{\beta}$$

These conditions imply that a Hopf bifurcation corresponds to a system equilibrium state with a pair of purely imaginary eigenvalues with all other eigenvalues having non-zero real parts, and that the pair of bifurcating or critical eigenvalues cross the imaginary axis as the parameters (λ, p) change, yielding oscillations in the system.

Power system oscillations are associated with a pair of complex eigenvalues of system equilibria (operating points) crossing the imaginary axis of the complex

plane, from the left half-plane to the right half-plane, when the system undergoes sudden changes (e.g. line outages). If this particular oscillatory problem is studied using more gradual changes in the system as proposed here, such as slowly varying parameters like system loading, it can be directly viewed as a Hopf bifurcation problem. Thus, by predicting or detecting these types of bifurcations well in advance, a possible oscillatory instability problem may be avoided. In the following section, Hopf bifurcation induced oscillatory instability, and the effect of nonlinear static load models on Hopf bifurcations are demonstrated in a test power system.

3.3 Hopf Bifurcation and Results with Alternative Load Models

Load variations are the main driving forces that may stress the system into Hopf bifurcations. The influence of different static load models on Hopf bifurcations and the corresponding dynamic response to the system are discussed here. The dynamic loading margin (DLM) of a power system, where DLM is defined as the separation distance of λ between the base load operating point (λ=0) to the closest Hopf bifurcation point for a given load and generation directions, is used as the measure to compare the effect of the different load models on the system dynamics.

Figures 3.2, 3.3 and 3.4 show the P-V curves and Hopf bifurcation (HB) points for the base case and two line outages (2-3 and 2-4) for constant PQ, current, and impedance load models respectively. In each figure, load lines were drawn according to (2.2), to illustrate the modified operating points due to line outages. In Figure 3.2, the vertical line with operating points A and B corresponds to the constant PQ load line, the inclined line in Figure 3.3 corresponds to a constant current load line

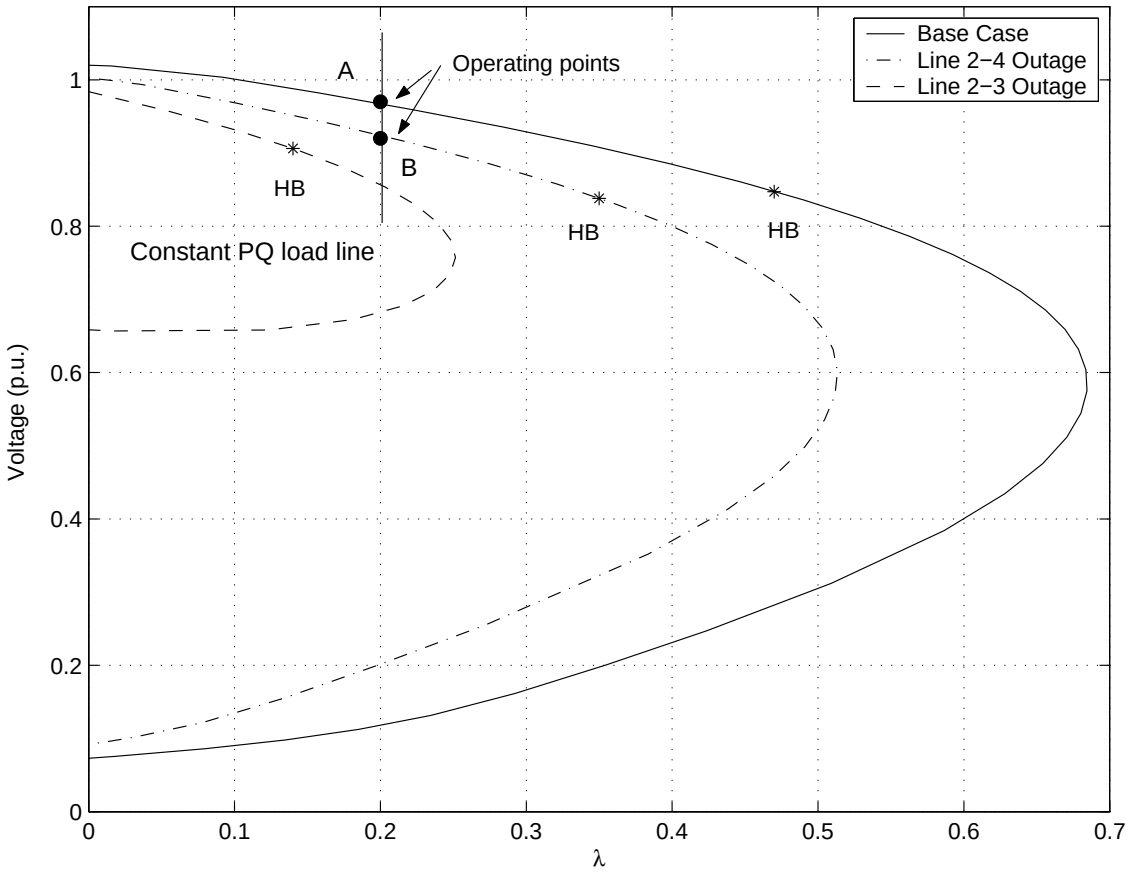

Figure 3.2: P-V curves at bus 14 for different contingencies for the IEEE 14-bus test system with constant PQ load line.

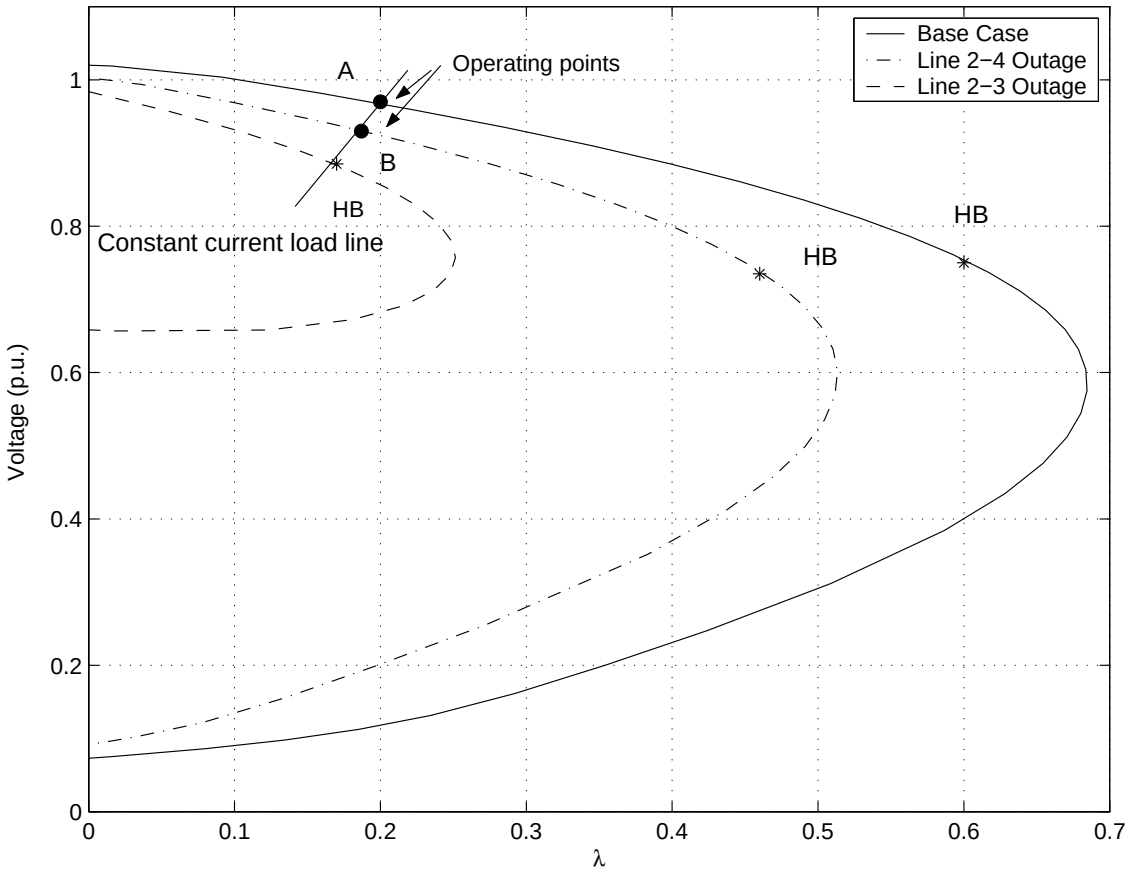

Figure 3.3: P-V curves at bus 14 for different contingencies for the IEEE 14-bus test system with constant current load line.

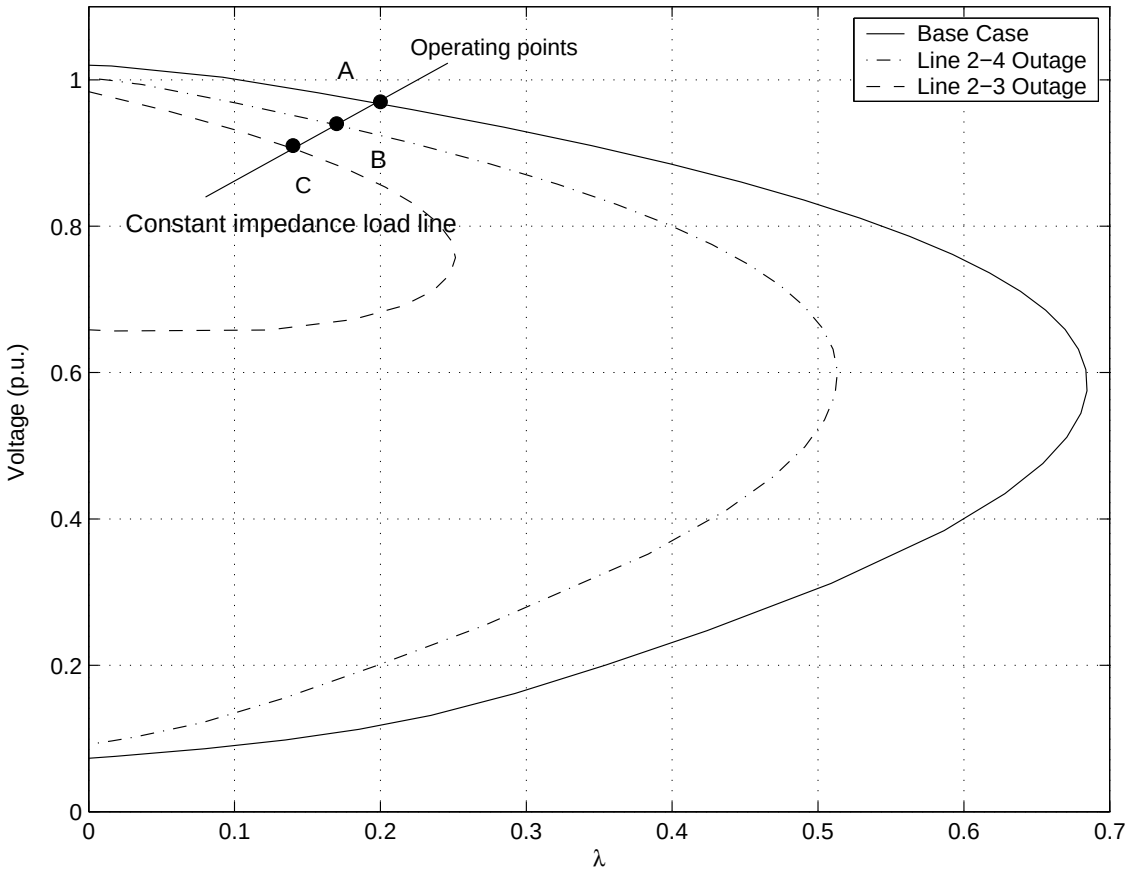

Figure 3.4: P-V curves at bus 14 for different contingencies for the IEEE 14-bus test system with constant impedance load line.

and the inclined line with less slope correspond to the constant impedance load line in Figure 3.4. All these P-V curves were plotted at the weakest bus of the system (the bus closest to experiencing voltage collapse). In obtaining the P-V curves, all the loads in the system were increased according to (2.3) and real power needed was dispatched by generator 1 (swing bus). For line outage studies, lines 2-3 and 2-4 were the most heavily loaded lines in the system.

Table 3.1 shows the dynamic loading margins (DLM) corresponding to Figures 3.2, 3.3 and 3.4. The lowest DLM values were observed when all the loads were modeled as constant PQ. In other words, this load model could be considered as the most onerous load to the system. However, no Hopf bifurcation point was detected in the system with constant impedance load models. Thus, the dynamic loading margin in this case was equal to the static loading margin (SLM) or the maximum loadability point on the P-V curves.

Table 3.1: Hopf bifurcation point for different static load models

	Dynamic Loading Margins (p.u.)		
	Const. PQ	Const. I	Const. Z
Base case	0.47	0.60	0.68*
Line 2-4 outage	0.35	0.46	0.51*
Line 2-3 outage	0.14	0.17	0.25*

*Equal to the maximum static loading margin

For the same test system, Figure 3.5 shows some eigenvalues for the base case at the Hopf bifurcation point, with all the loads modeled as constant PQ. A pair of purely imaginary eigenvalues appears on the imaginary axis at the Hopf bifurcation point. A participation factor analysis reveals that the dominant state variable

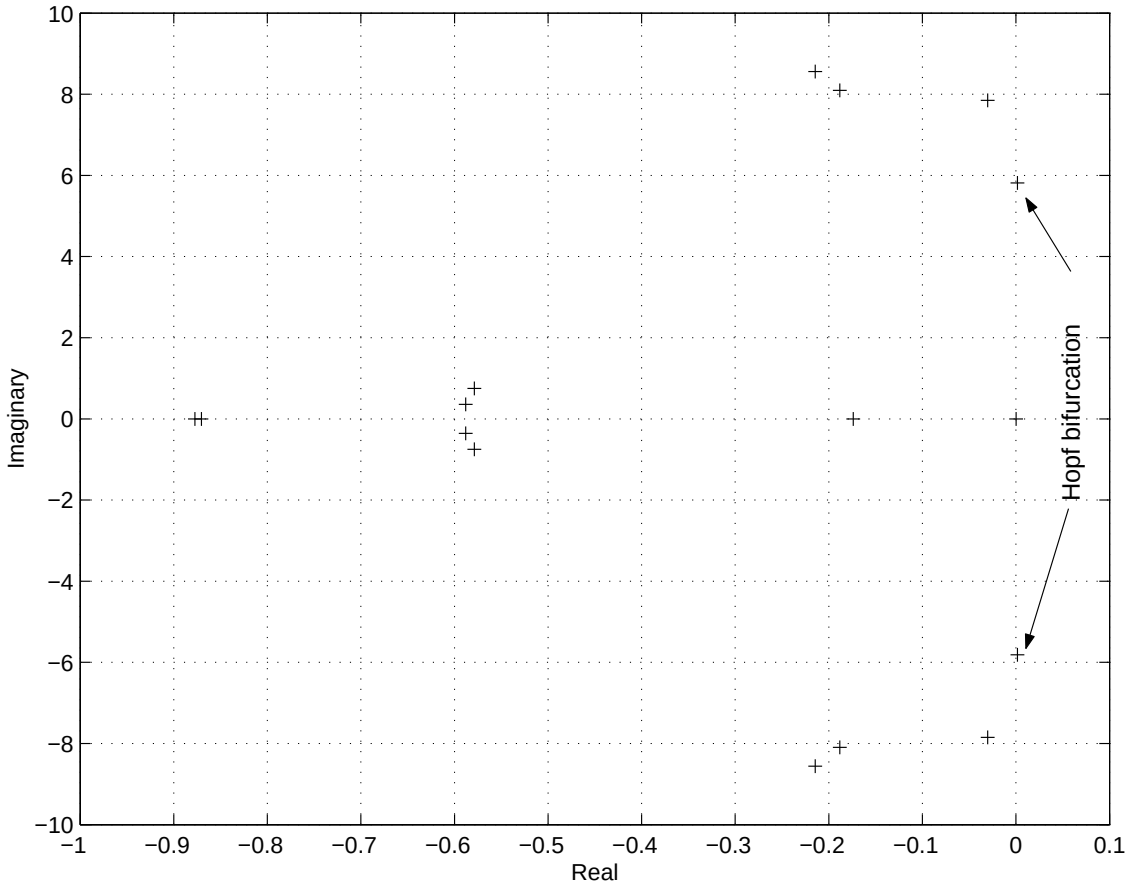

Figure 3.5: Some eigenvalues plot at the Hopf bifurcation point for the IEEE 14-bus test system base case.

associated with the critical mode (Hopf bifurcation mode) are the machine modes δ and ω at bus 3. In order to study the effect of Hopf bifurcation on the system dynamic performance due to the line outages, two time domain simulations were carried out at λ=0.2 p.u. (Figure 3.2, operating point A) with all the loads modeled as constant PQ.

According to Figure 3.2, in the case of a line 2-4 outage, there is a stable operating point (B); this is clear from Figure 3.6 as generator frequencies resume

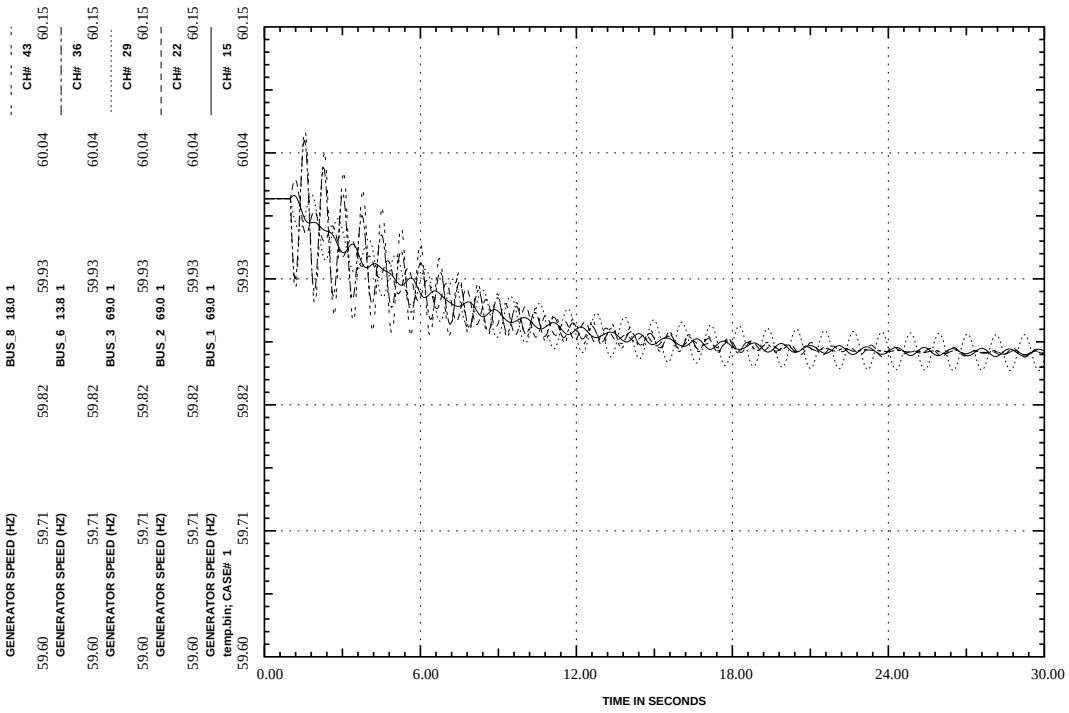

Figure 3.6: Generator frequency plot for a line 2-4 outage in the IEEE 14-bus test system (λ=0.2).

steady state after the line outage. However, an oscillation with decreasing amplitude in the time domain simulation indicates operation close to Hopf bifurcation. A line 2-3 outage produces instability due to a Hopf bifurcation. This can be observed in Figure 3.7.

Prediction and control of the Hopf bifurcation can avoid the above instability. In section 3.4, two Hopf bifurcation indices are proposed for prediction. Control strategies to avoid instability are discussed in detail in the Chapter 4.

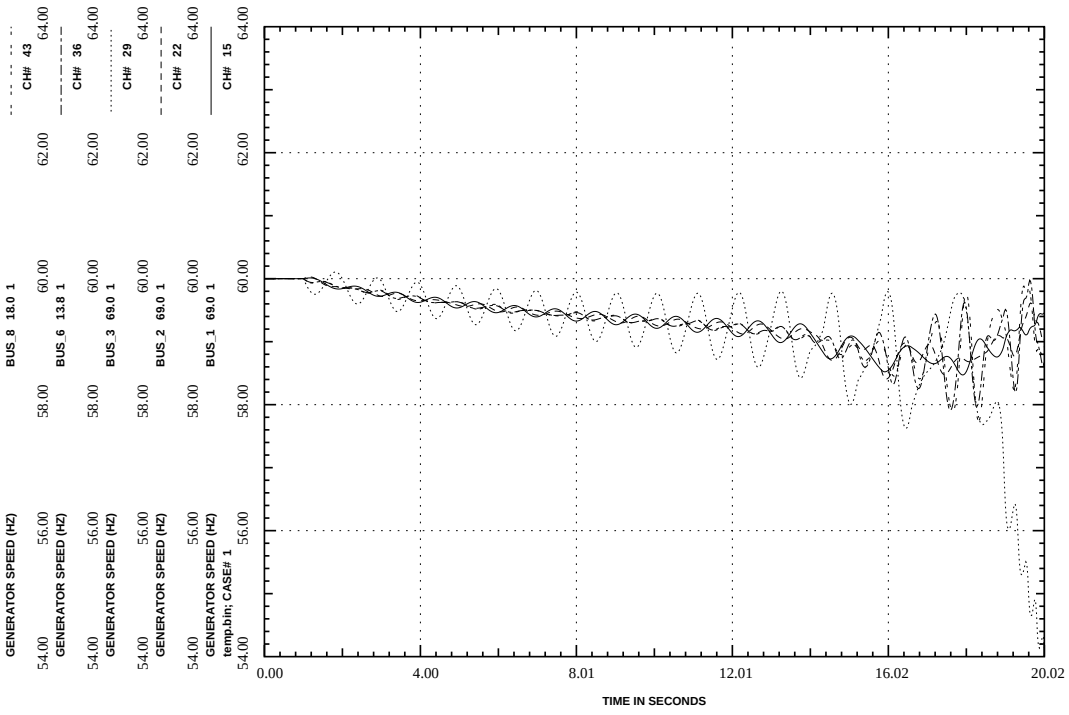

Figure 3.7: Generator frequency oscillation due Hopf bifurcation triggered by a line 2-3 outage in the IEEE 14-bus test system (λ=0.2).

3.4 Hopf Bifurcation Indices

Since at a Hopf bifurcation point the system Jacobian has a simple pair of purely imaginary eigenvalues, the problem can be restated as follows: For the system state matrix A, a complex pair of eigenvalues can be rewritten as

$$A\,[v_R \pm jv_I] = [\alpha \pm j\beta]\,[v_R \pm jv_I] \tag{3.1}$$

where α and β are the real and imaginary parts of the eigenvalue μ, respectively, and $v_R \pm jv_I$ is the associated eigenvector. If real and imaginary parts are separated from equation (3.1), it follows that

$$\begin{aligned} (A-\alpha I_n)v_R + \beta v_I &= 0 \\ (A-\alpha I_n)v_I - \beta v_R &= 0 \end{aligned} \tag{3.2}$$

$$\Rightarrow \quad \begin{bmatrix} A-\alpha I_n & \beta I_n \\ -\beta I_n & A-\alpha I_n \end{bmatrix} \begin{bmatrix} v_R \\ v_I \end{bmatrix} = 0$$

$$\left[\underbrace{\begin{bmatrix} A & +\beta I_n \\ -\beta I_n & A \end{bmatrix}}_{A_m} - \alpha I_{2n} \right] \begin{bmatrix} v_R \\ v_I \end{bmatrix} = 0 \tag{3.3}$$

Since $[v_R\ v_I]^T \neq 0$, at a Hopf bifurcation where $\alpha = 0$,

$$\det\{\ A_m - \alpha I_{2n}\ \} = 0$$

That is, the modified matrix A_m becomes singular at this point. Observe that this matrix is also singular at a saddle-node bifurcation, as $\alpha = \beta = 0$ in this case.

Following the same criteria previously proposed to define indices for saddle-node bifurcations [10], the singular value of the modified state matrix is used here as an index for detecting Hopf bifurcations.

3.4.1 The First Proposed Index (HBI_1)

The first Hopf bifurcation index (HBI) is defined as follows:

$$HBI_1 = \sigma_{min}(A_m) \tag{3.4}$$

where σ_{min} is the minimum singular value of the modified state matrix A_m, which becomes zero at a Hopf or saddle-node bifurcation point.

The HBI_1 index has the problem that it requires the state matrix A which is computationally demanding, as previously discussed in section 2.6.2. This problem can be avoided if the full system matrix (2.10) is used. Then for a complex pair of eigenvalues, the eigenvalue problem can be rewritten as:

$$\begin{bmatrix} J_1 & J_2 \\ J_3 & J_4 \end{bmatrix} \begin{bmatrix} v_{1_R} \pm j v_{1_I} \\ v_{2_R} \pm j v_{2_I} \end{bmatrix} = [\alpha \pm j\beta] \begin{bmatrix} v_{1_R} \pm j v_{1_I} \\ 0 \end{bmatrix} \tag{3.5}$$

By separating the real and imaginary parts and rearranging these equations:

$$\begin{bmatrix} J_1 - \alpha I & J_2 & \beta I & 0 \\ J_3 & J_4 & 0 & 0 \\ -\beta I & 0 & J_1 - \alpha I & J_2 \\ 0 & 0 & J_3 & J_4 \end{bmatrix} \begin{bmatrix} v_{1_R} \\ v_{2_R} \\ v_{1_I} \\ v_{2_I} \end{bmatrix} = 0 \tag{3.6}$$

$$\left[\underbrace{\begin{bmatrix} J_1 & J_2 & \beta I & 0 \\ J_3 & J_4 & 0 & 0 \\ -\beta I & 0 & J_1 & J_2 \\ 0 & 0 & J_3 & J_4 \end{bmatrix}}_{J_m} - \alpha \begin{bmatrix} I & 0 & 0 & 0 \\ 0 & 0 & 0 & 0 \\ 0 & 0 & I & 0 \\ 0 & 0 & 0 & 0 \end{bmatrix} \right] \begin{bmatrix} v_{1_R} \\ v_{2_R} \\ v_{1_I} \\ v_{2_I} \end{bmatrix} = 0 \tag{3.7}$$

Since at a Hopf bifurcation $\alpha = 0$, the matrix J_m becomes singular; notice that this also holds at a saddle-node bifurcation point. Therefore, the minimum singular value of the modified full Jacobian matrix J_m can be used as another index to indicate proximity to a Hopf or a saddle-node bifurcation. Consequently, a second HBI is proposed.

3.4.2 The Second Proposed Index (HBI_2)

This index is defined as:

$$HBI_2 = \sigma_{min}(J_m) \tag{3.8}$$

It is computationally less involved than HBI_1, as full advantage can be taken of the sparsity of J_m.

Both indices, HBI_1 and HBI_2, behave similarly to the singular value index of A and J respectively when the critical eigenvalue is real (the critical eigenvalue can be defined here as the eigenvalue closest to the imaginary axis and moving with a change in parameter). Thus, for β=0:

$$A_m = \begin{bmatrix} A & 0 \\ 0 & A \end{bmatrix} \tag{3.9}$$
$$\Rightarrow HBI_1 = \sigma_{min}(A_m) = \sigma_{min}(A)$$

Similarly, for $\beta = 0$,

$$J_m = \begin{bmatrix} J_1 & J_2 & 0 & 0 \\ J_3 & J_4 & 0 & 0 \\ 0 & 0 & J_1 & J_2 \\ 0 & 0 & J_3 & J_4 \end{bmatrix} = \begin{bmatrix} J & 0 \\ 0 & J \end{bmatrix} \tag{3.10}$$

$$\Rightarrow HBI_2 = \sigma_{min}(J_m) = \sigma_{min}(J)$$

3.4.3 Linearization of the Two Proposed Indices

Indices based on first order information such as minimum singular values, or critical eigenvalues, may be inadequate to predict possible instabilities in practical power systems, which may exhibit large discontinuities in the presence of system control limits (e.g. generator Q limits). Improvement is made by considering a "second order" index (i.e. an index divided by its gradient with respect to the parameter under study) that exploits additional embedded information as suggested in [61]. Thus, it has been observed that minimum singular value of a power system Jacobian can be approximated using the following equation [10]:

$$\sigma_{min} = (a - b\lambda)^{1/c} \tag{3.11}$$

with suitable values of the scalar positive constants a, b and c; and λ being the loading factor. As shown in [10], these functions can be linearized by dividing the function by its gradient at each point, since

$$\frac{\sigma_{min}}{d\sigma_{min}/d\lambda} = c\lambda - \frac{ac}{b} \tag{3.12}$$

A new proposal is to adopt the principle of 3.12 to the linearization of Hopf bifurcation indices, HBI_1 and HBI_2. The linearized indices are:

$$LHBI_1 = \frac{HBI_1}{|dHBI_1/d\lambda|} \tag{3.13}$$

and

$$LHBI_2 = \frac{HBI_2}{|dHBI_2/d\lambda|} \tag{3.14}$$

While these indices, especially HBI_1 and the linearization as $LHBI_1$, can be applied to any nonlinear dynamical system, the application to power systems is the primary concern for this thesis.

3.5 Test System Examples

The proposed Hopf bifurcation indices were applied to several power system examples. The results are presented bellow. Loads were modeled conservatively throughout as constant impedance loads, Any Hopf bifurcation appearing for this type of load would certainly appear for more onerous load models. Furthermore, most of the commercial power system analytical tools use this as a default load model in the dynamic analysis.

3.5.1 Three-bus Test System

The proposed indices were applied to the three-bus power system depicted in Figure 2.14. Figures 3.8 shows the P-V curves at bus 3, for the base case and also for a line 2-3 outage. The real and reactive power required by the system are shared equally by both generators as the system load increases up to the nose point.

Figures 3.9 shows the locus of the critical eigenvalue. Some eigenvalues plot at the Hopf bifurcation for the base case are shown in Figure 3.10. A participation factor analysis indicates that the dominate state variables associated with the

critical mode (Hopf bifurcation modes) are the δ and ω (electromechanical modes) of generator 2. Hopf bifurcations were detected in both cases by monitoring the system eigenvalues as the system loading changes.

Figure 3.11 indicates that HBI_1 and HBI_2, have almost linear profiles with respect to the loading factor λ, becoming zero at the Hopf bifurcation point, as expected. According to the indices, loading the system beyond 0.45 p.u. is problematic and also a line 2-3 outage could lead to an oscillatory unstable condition when the system operates beyond 0.2 p.u. loading factor, in the base case.

A time domain simulation was performed for the line 2-3 outage at λ=0.30 p.u. The system is unstable following the line outage, as shown in Figure 3.12.

3.5.2 Two-area Test System

The proposed Hopf bifurcation indices HBI_1 and HBI_2 were also applied to the two-area system given in Figure 2.15. Figures 3.13 and 3.14 show the corresponding P-V curves and indices for the base case and for a line 9-10 outage, respectively. The results for line 7-8 and 8-9 outages did not differ from the base case. Also, line 9-10 was modified to two identical parallel lines, so that the outage of one of them did not lead to islanding.

As shown in Figure 3.14, Hopf bifurcations were detected in both cases. This is confirmed by the locus of the critical eigenvalue in Figure 3.15 for the base case for which loading the system beyond 0.08 p.u. is not feasible. A participation factor analysis indicates that the dominant state variables associated with the critical (Hopf bifurcation) mode are δ and ω of generator 3. Once again the Hopf bifurcation indices show a smooth profile and predictable behavior with respect to the load changes in the system.

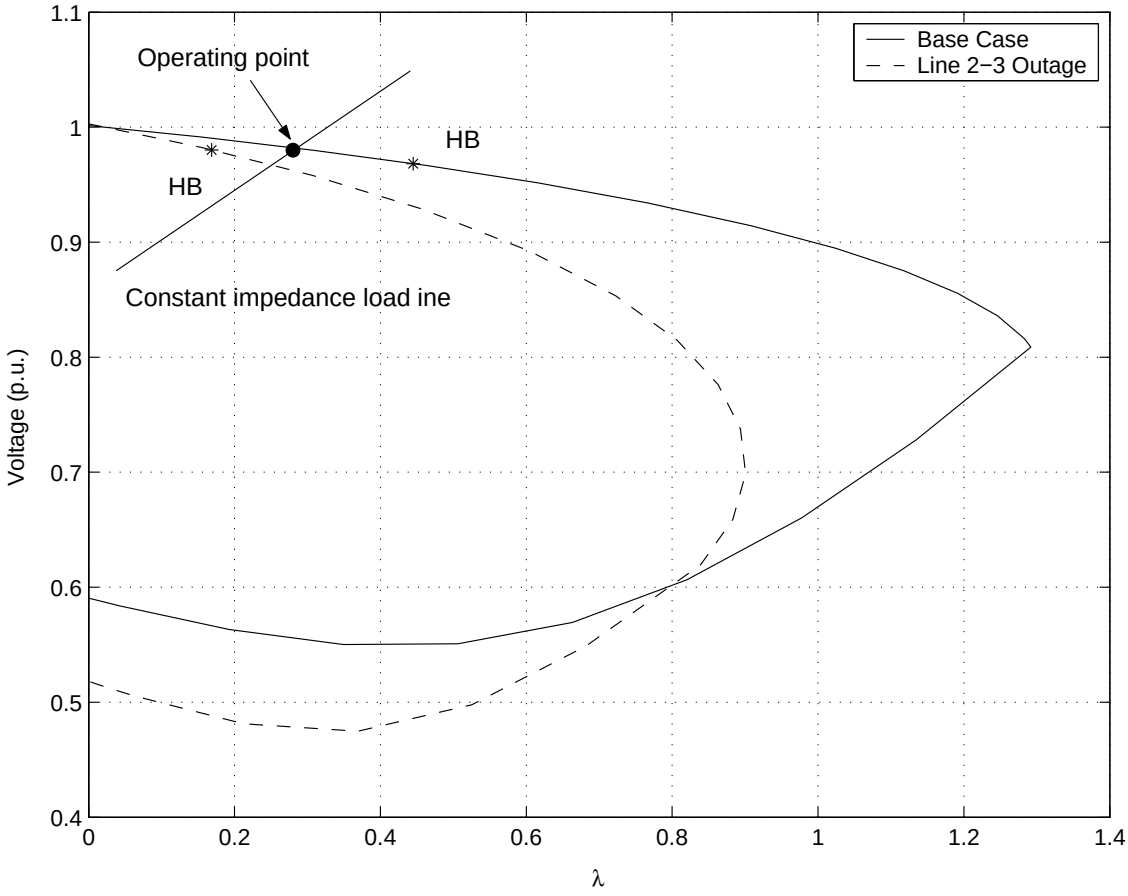

Figure 3.8: P-V curves at bus 3 for the three-bus system.

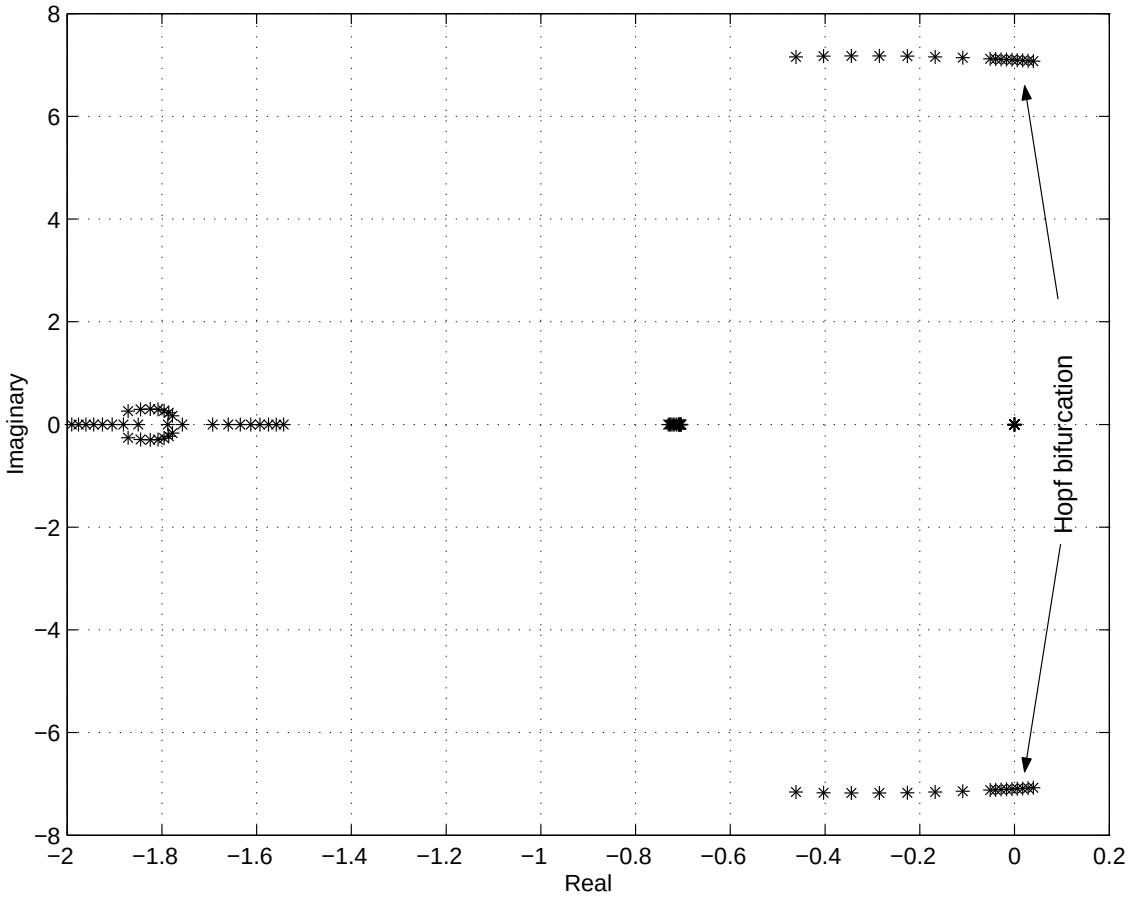

Figure 3.9: Locus of the critical eigenvalue for base case for the three-bus system.

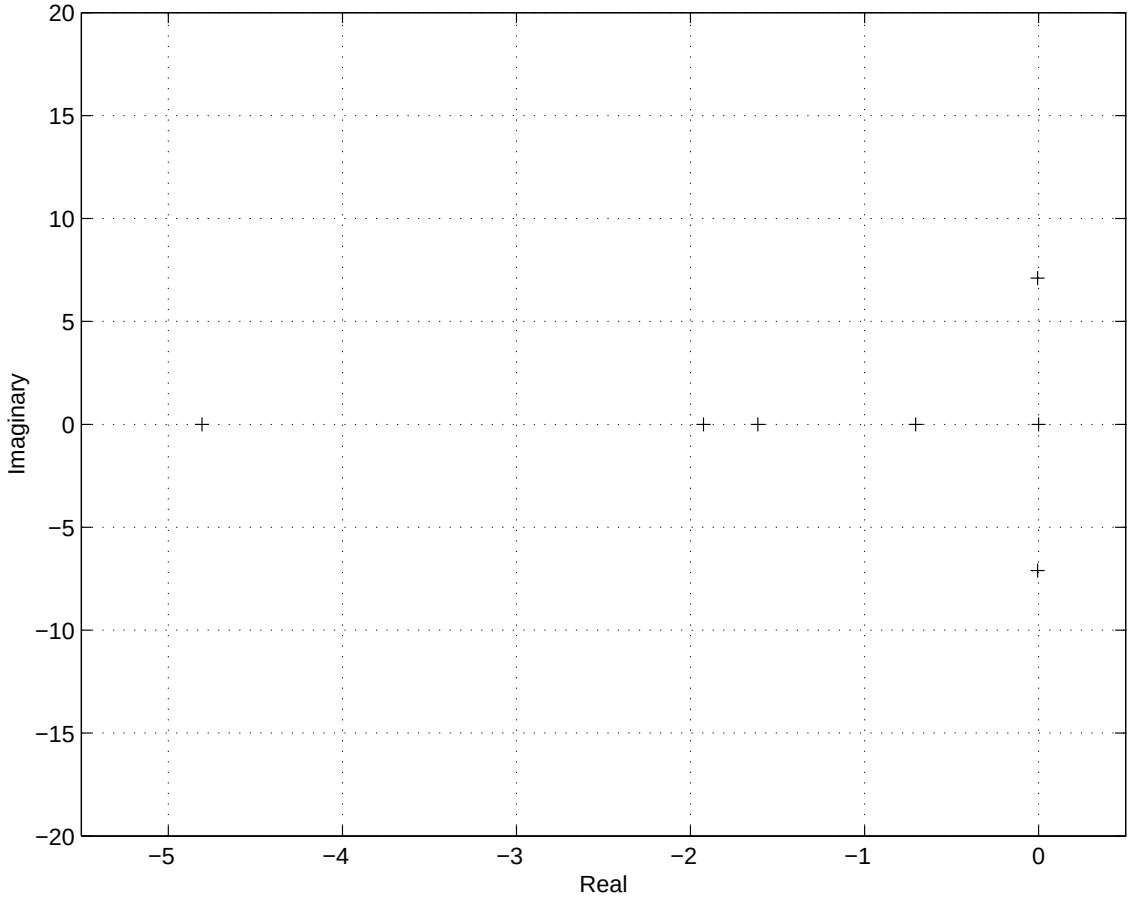

Figure 3.10: Some eigenvalues plot at the Hopf bifurcation point for base case for the three-bus system.

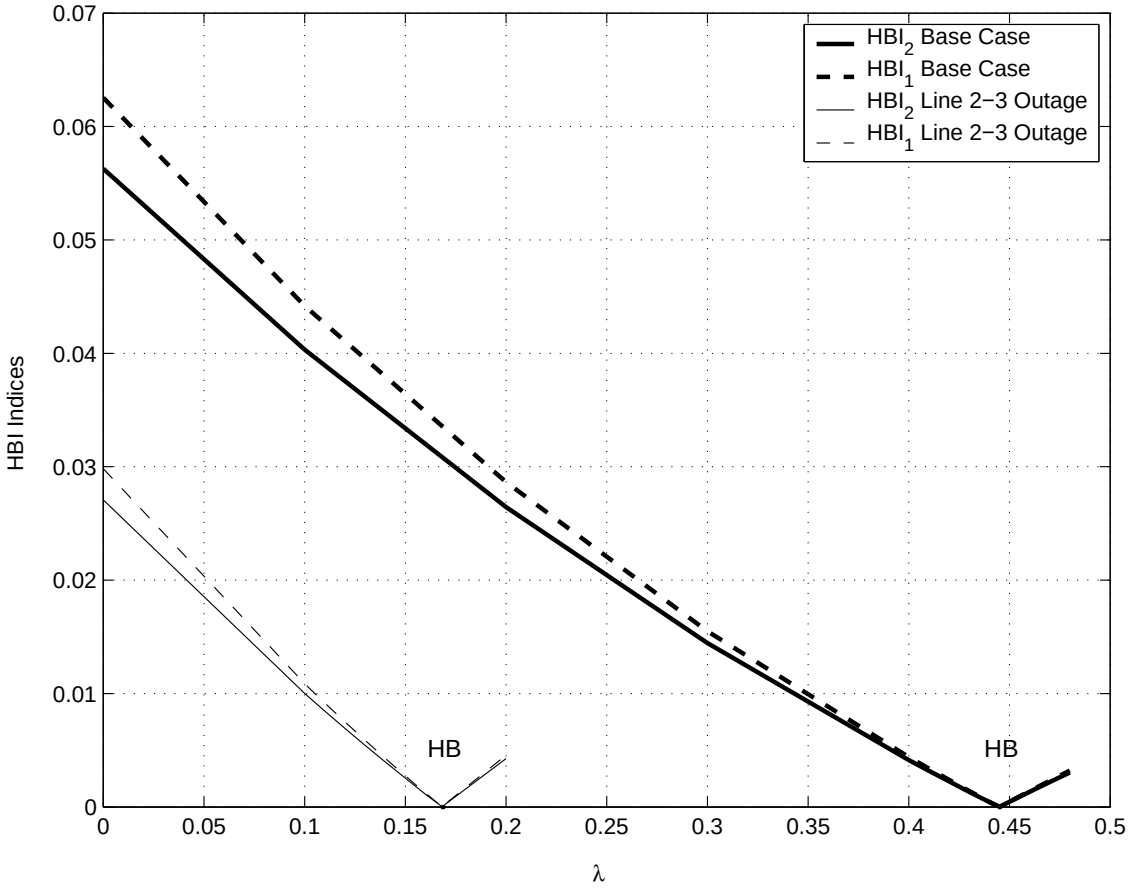

Figure 3.11: Hopf bifurcation indices for the three-bus system.

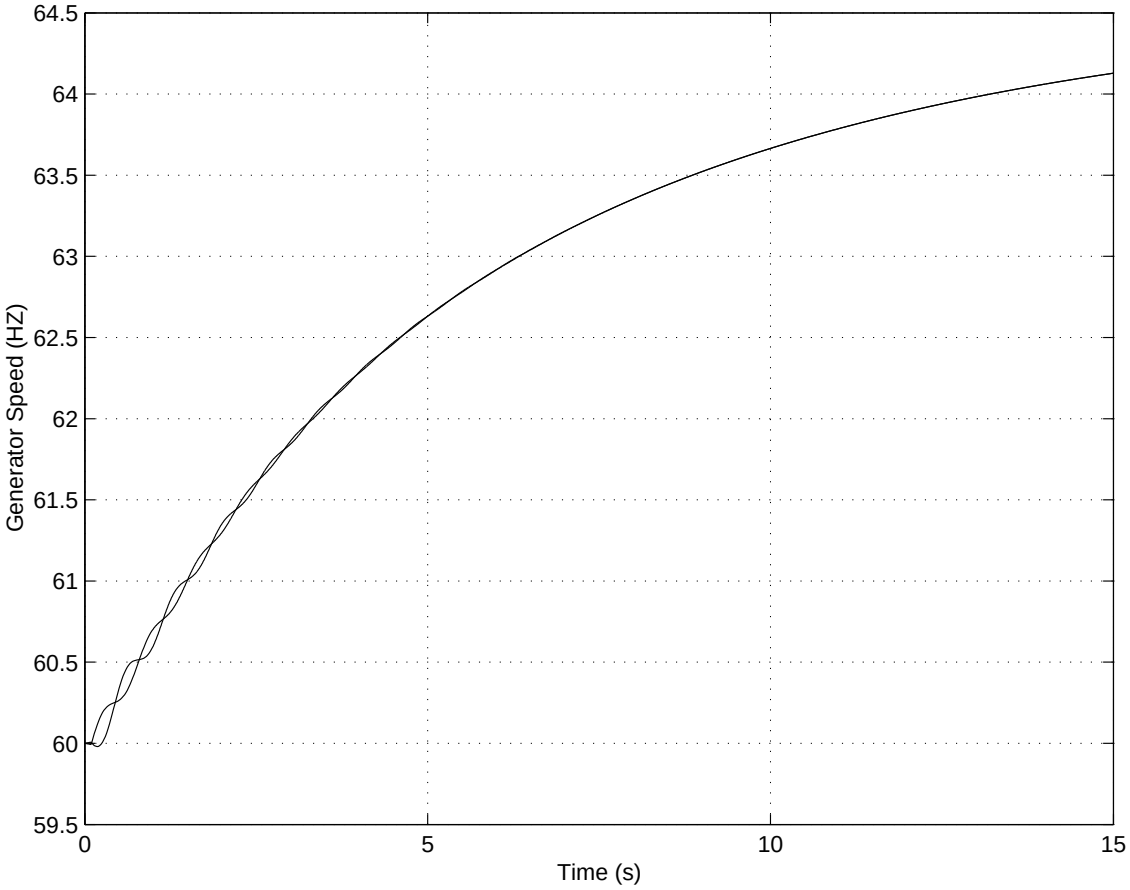

Figure 3.12: Generator frequency oscillation due to a Hopf bifurcation triggered by a line 2-3 outage in the three-bus test system.

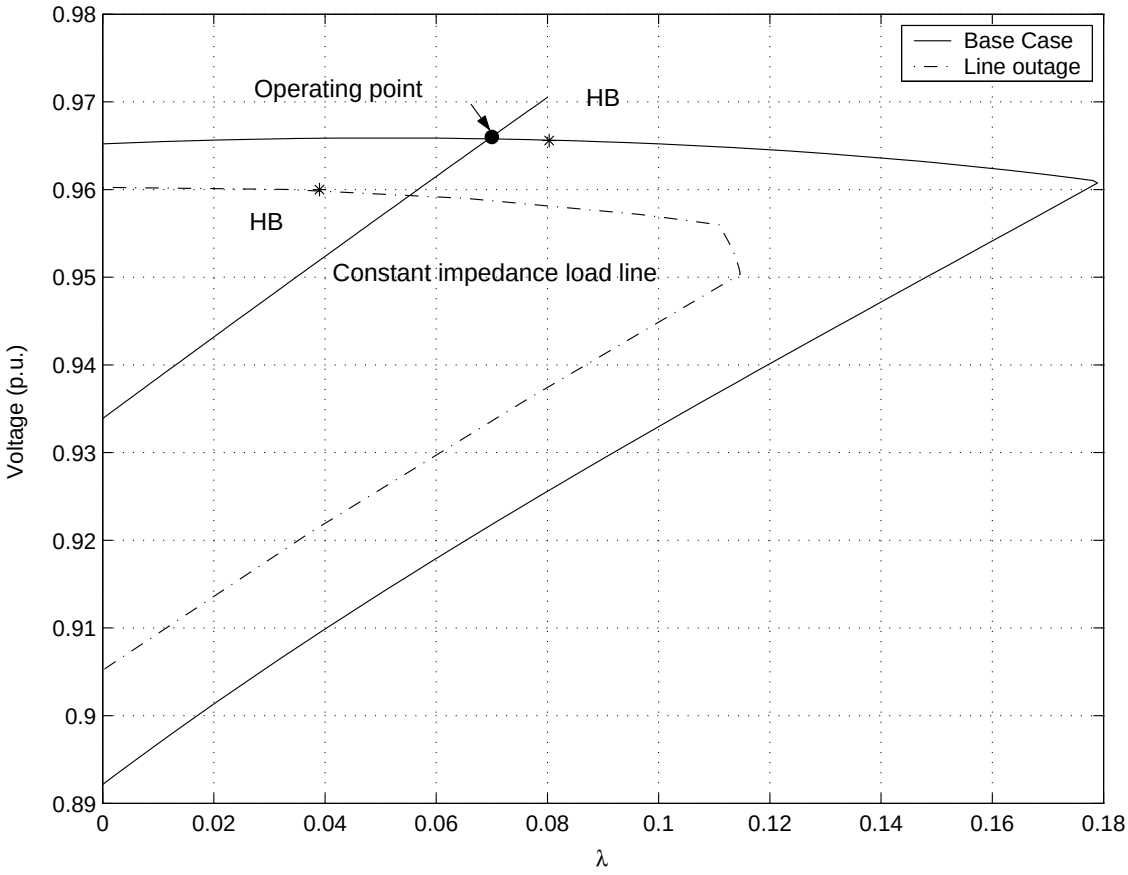

Figure 3.13: P-V curves at bus 11 for the two-area system.

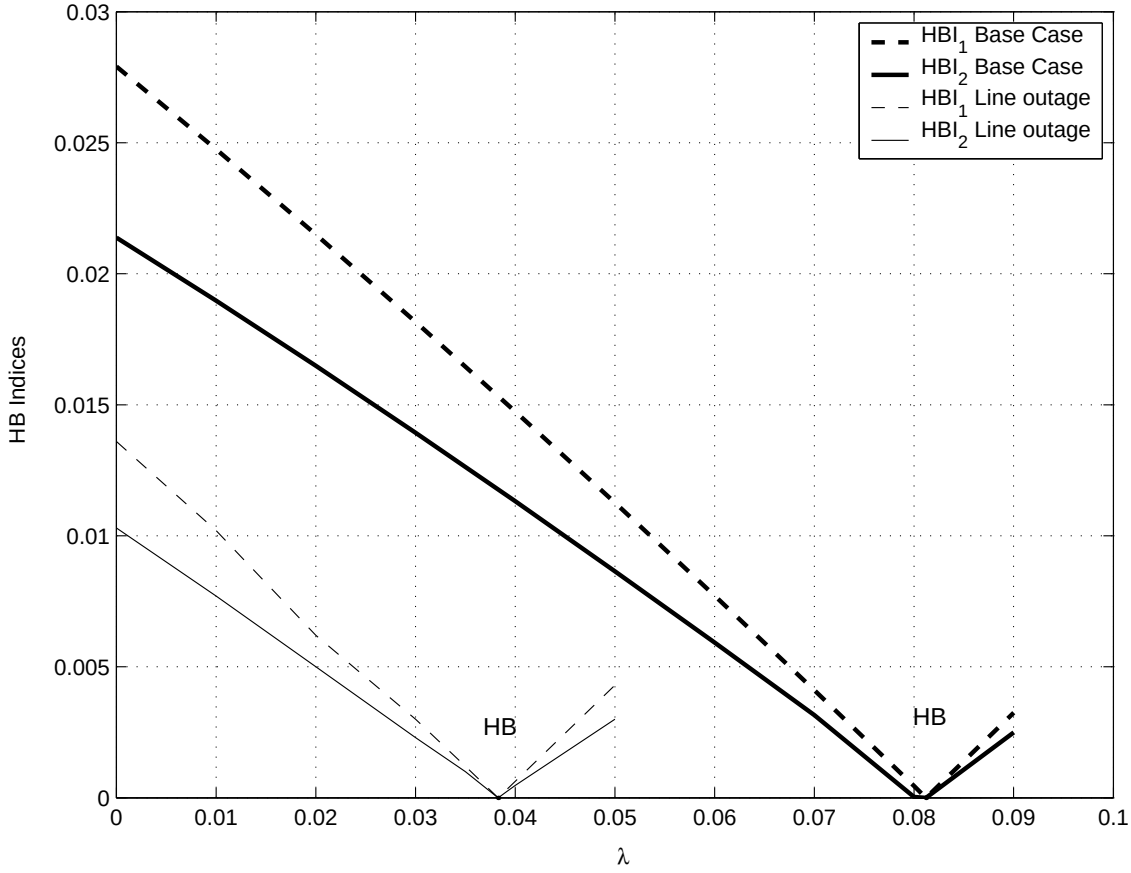

Figure 3.14: Hopf bifurcation indices for the two-area system.

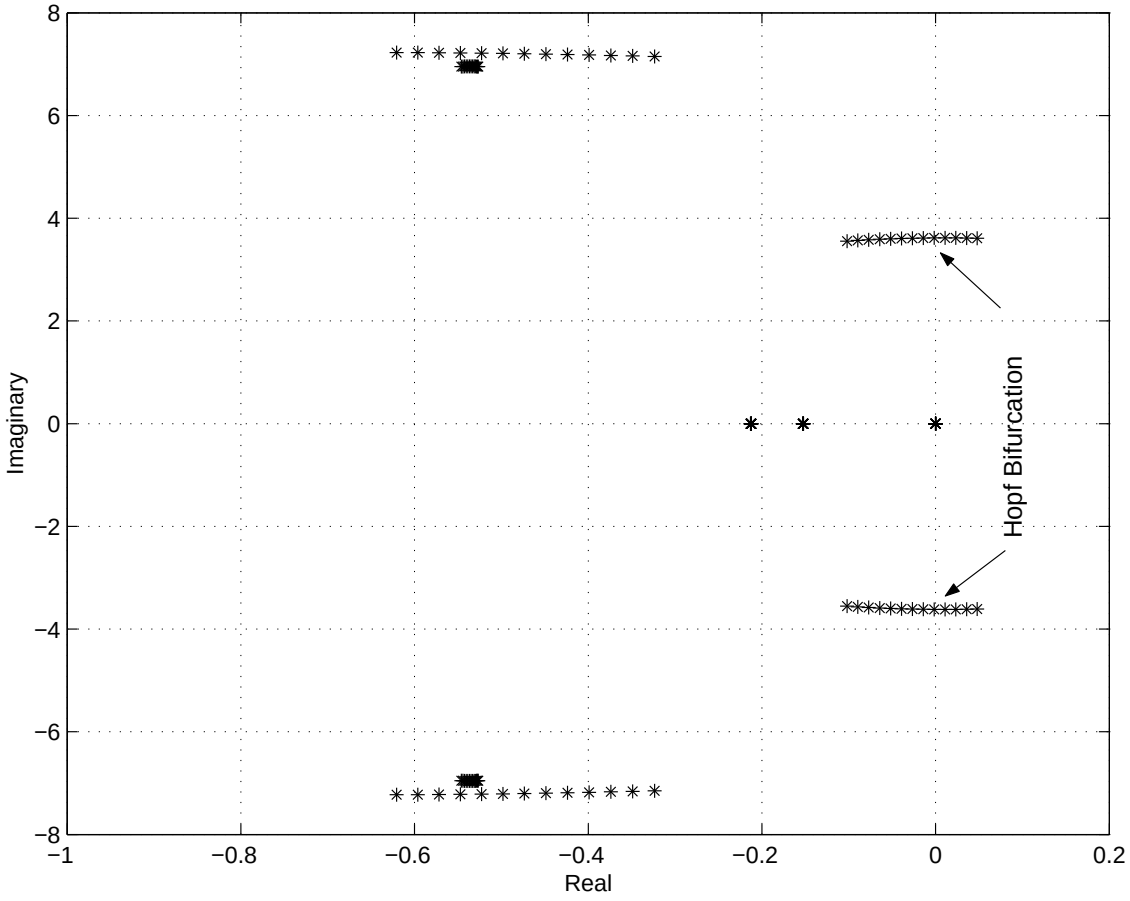

Figure 3.15: Locus of the critical eigenvalue for the base case for the two-area system.

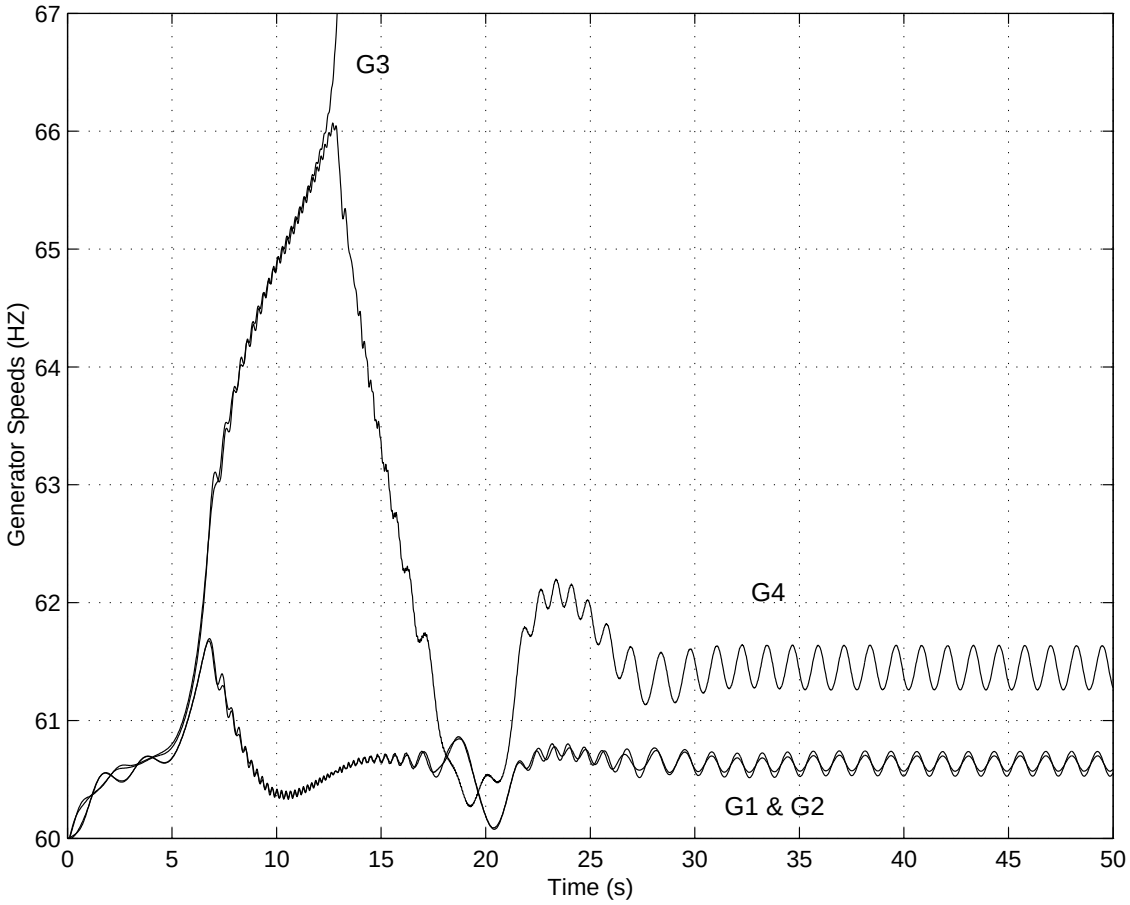

Figure 3.16: Generator frequency oscillation due to Hopf bifurcation triggered by line 9-10 outage in the two-area system.

A time domain simulation was carried out for the line outage at λ=0.070 p.u. to see the effect of the Hopf bifurcation on the system. The system became oscillatory unstable as shown in Figure 3.16.

3.5.3 IEEE 14-bus Test System

There was no Hopf bifurcation detected in the IEEE 14-bus test system with all the loads represented as constant impedance, for the base case or other line outages, as previously discussed in section 3.3.

3.5.4 IEEE 50-machine Test System

Case I

The proposed indices are applied to the much larger IEEE 50-machine test system shown in Figure 2.17. The P-V curves and Hopf bifurcation indices for the base case and for a line 79-90 outage are shown in Figures 3.17 and 3.18, respectively, and designated as CASE I. The P-V curves are shown at bus 92 for a specific load and generation direction (i.e. only positive loads in the system were increased and all the generators were allowed to dispatch the power needed). The line 79-90 was chosen for the outage as this is one of the most heavily loaded lines in the weakest area of the system.

According to the Hopf bifurcation indices in Figure 3.18, loading the base system beyond 0.009 p.u. is not feasible. Again, observe the indices vary almost linearly with respect to the load parameter (λ). A participation factor analysis indicates that the dominant state variable associated with the Hopf bifurcation mode are δ and ω of the generator located at bus 93.

A time domain simulation for a line 79-90 outage at λ=0.0060 p.u. is depicted in Figure 3.19. It is clear that the system becomes oscillatory unstable due to the Hopf bifurcation triggered by the line outage.

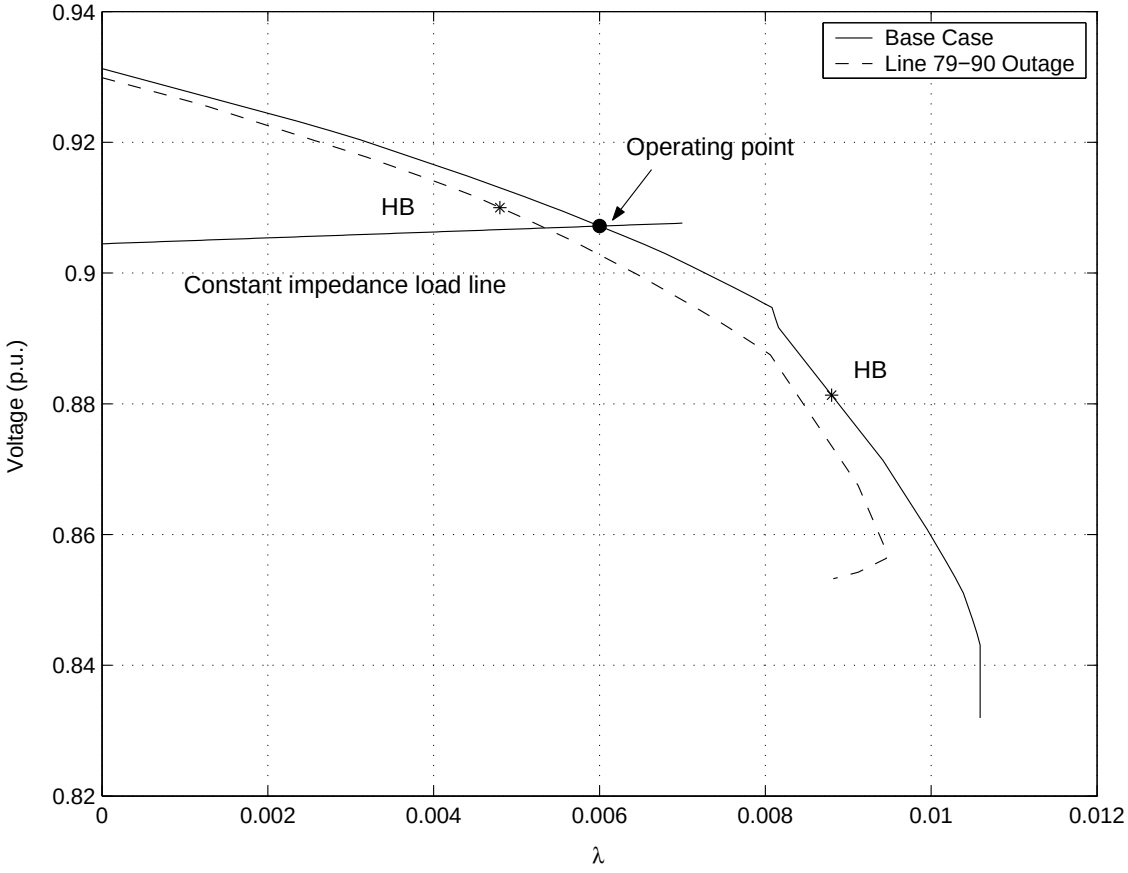

Figure 3.17: P-V curve at bus 92 for the IEEE 50-machine system (Case I).

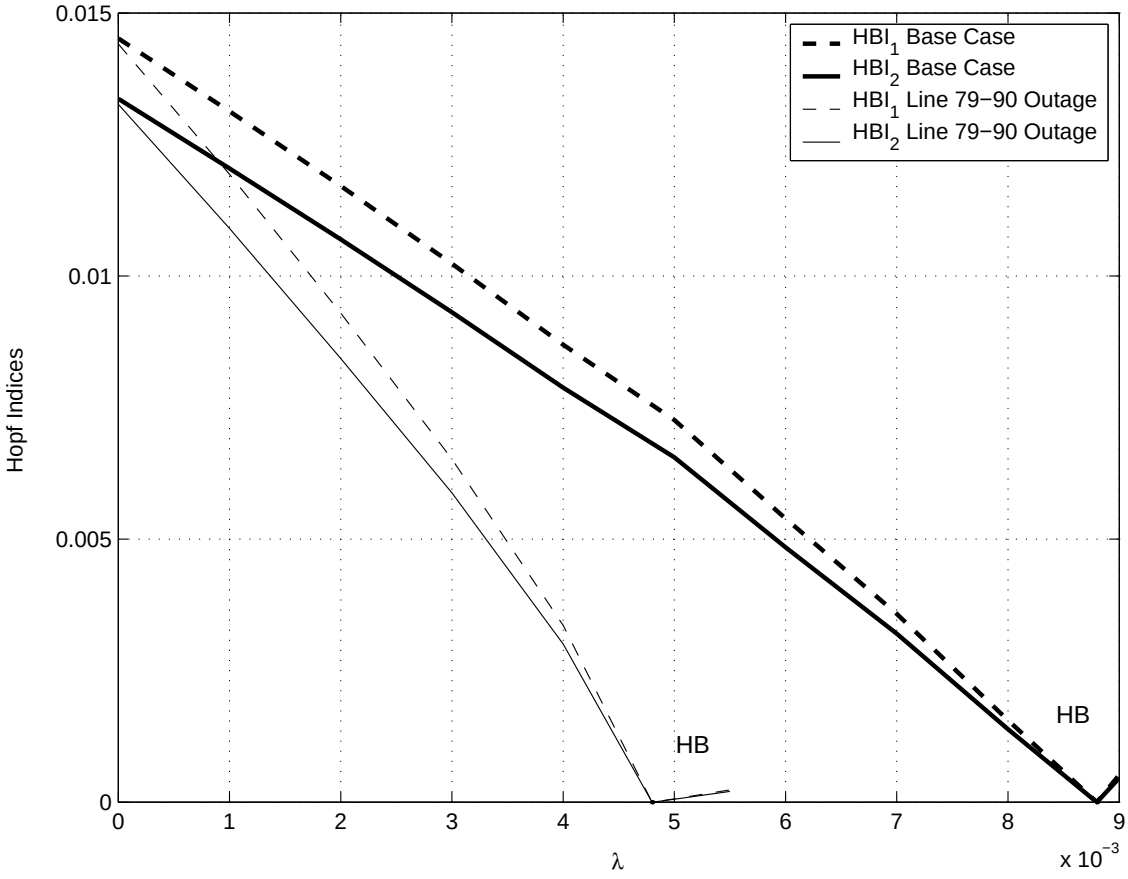

Figure 3.18: Hopf bifurcation indices for the IEEE 50-machine system (Case I).

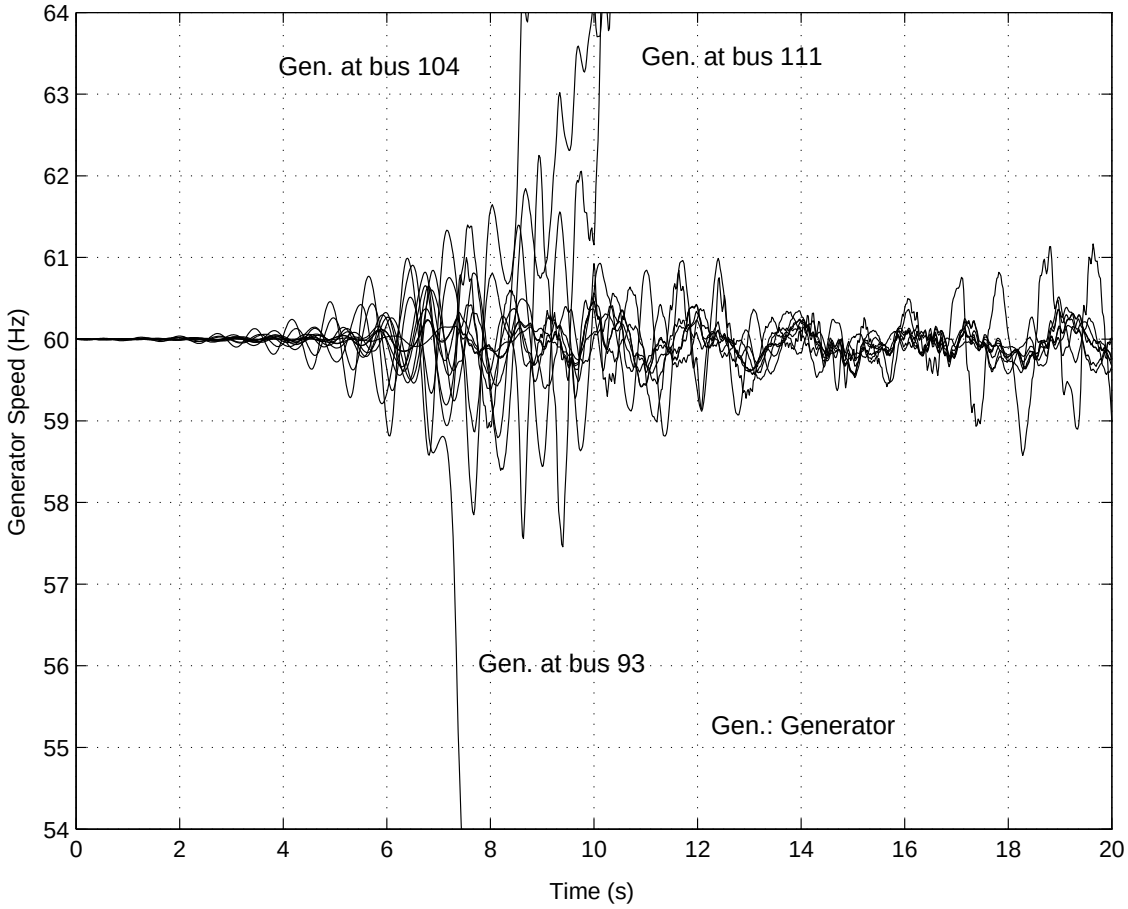

Figure 3.19: Generator frequency oscillation due to a Hopf bifurcation triggered by the line 79-90 outage in the IEEE 50-machine system (Case I).

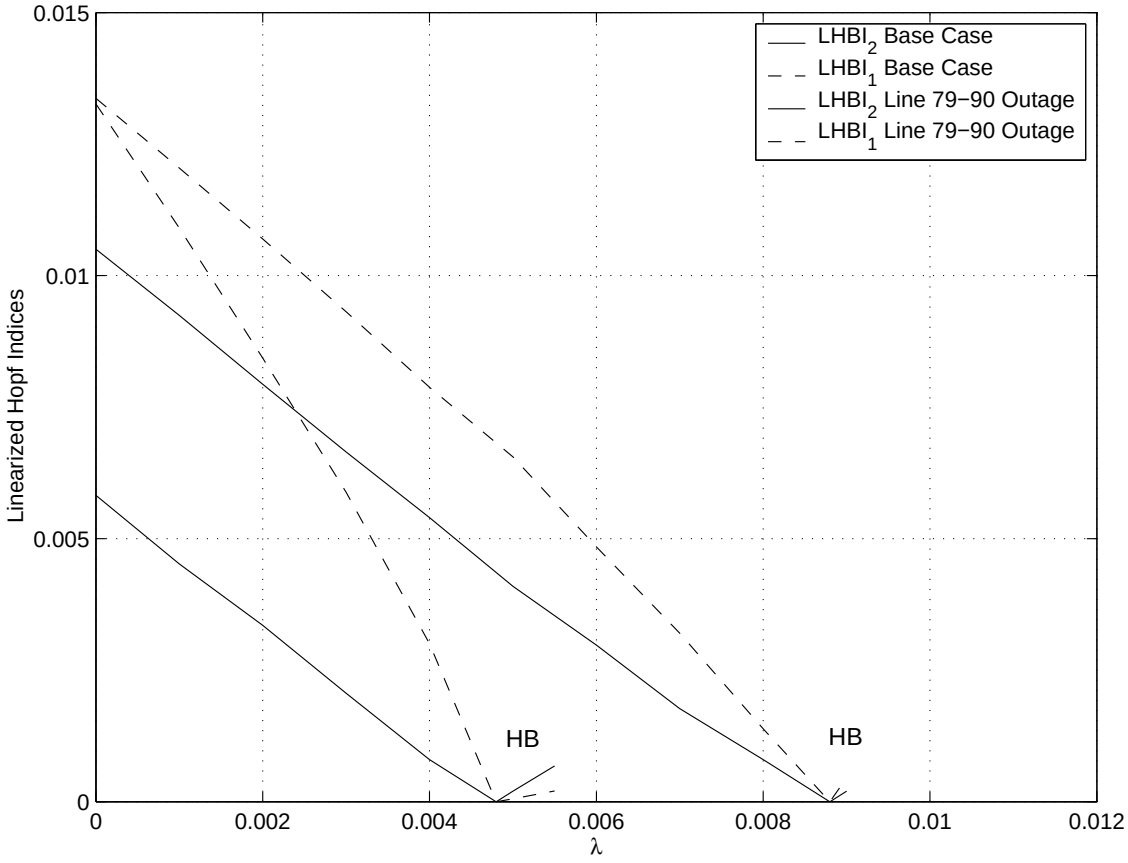

Figure 3.20: Linearized Hopf bifurcation indices for the IEEE 50-machine system (Case I).

As can been seen in all the examples, the Hopf bifurcation indices show almost a linear behavior with respect to the load changes. However, in this particular example, limits of the generators lead to a nonlinear behavior of the indices, as shown in Figure 3.18. However, by using the linearization technique proposed in section 3.3, it is possible to obtain a linear profile, especially around the bifurcation point as shown in Figure 3.20. Here, the sensitivity or gradient of Hopf bifurcation indices with respect to loading factor λ was calculated numerically.

Case II

The P-V curves and corresponding HBI_1 plots are given in Figures 3.21 and 3.22, for the base case and for a line 79-90 outage, for the IEEE 50-machine system Case II. In this case, MASS was used to produce the system state matrix and only HBI_1 was calculated due to the software limitations (i.e. MASS does not produce the full system matrix, as necessary for the HBI_2 calculation). As shown in Figure 3.22, the index plots are not smooth and not linear. In order to make the index linear, sensitivity of the singular value of the modified matrix was considered as described in (3.13). In this case too, the sensitivity or the gradient of the Hopf bifurcation index (HBI_1) with respect to the loading factor λ was calculated numerically.

Observe in Figure 3.23 that the LHBI shows a linear profile, especially closer to the Hopf bifurcation point. This Hopf bifurcation point was confirmed by performing a time domain simulation.

3.6 Comparison of Indices

3.6.1 Computational Time Comparison

The derivation of HBI_2 is computationally less demanding than HBI_1 as explained in Chapter 2. Table 3.2 shows the time saved when computing the HBI_2, instead of HBI_1. The savings increase with the size of the power system, due to the fact that the calculation of the inverse of the matrix J_4 (which has a dimension of twice the size as the number of buses in the system) is avoided by exploiting the sparsity of the jacobian in the HBI_2 calculations.

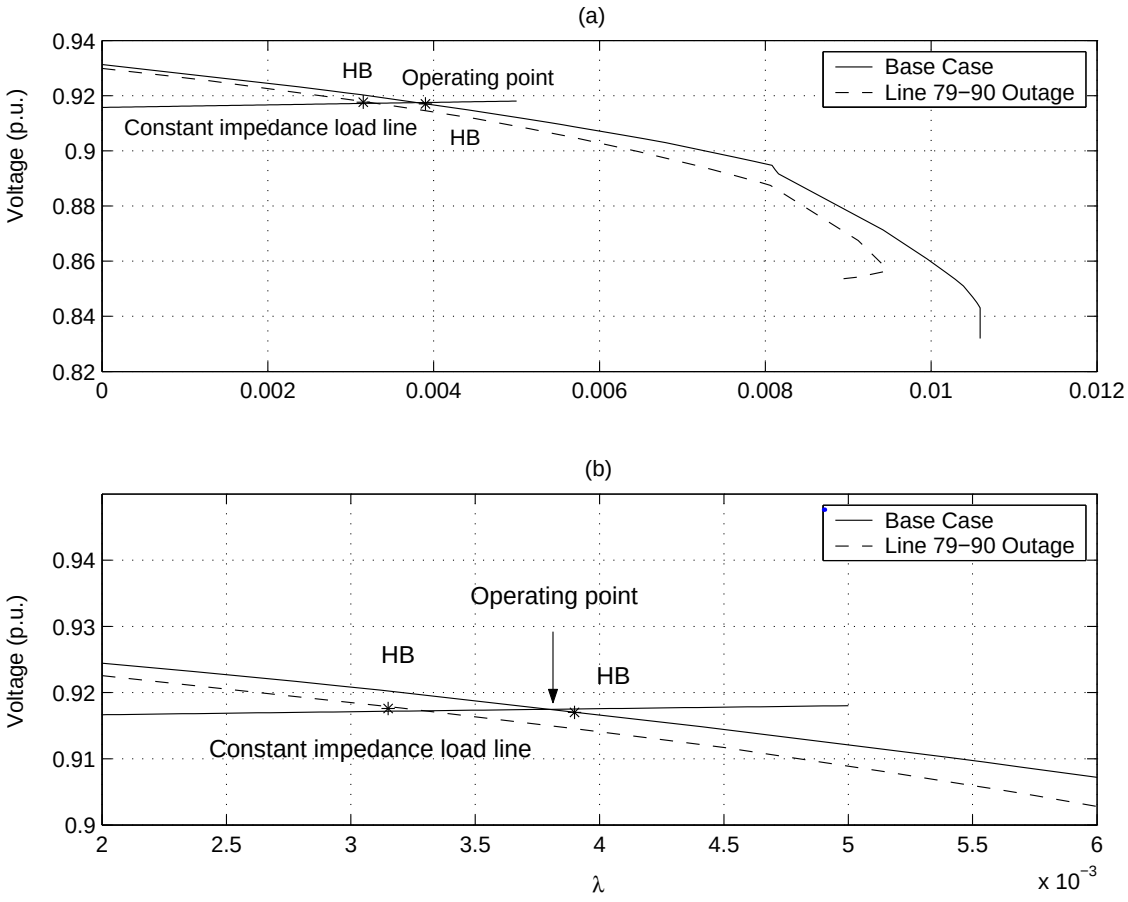

Figure 3.21: IEEE 50-machine system (case II): (a) P-V curves at bus 92; (b) enlargement around the operating point.

Table 3.2: Time Savings for computing HBI_2 with respect to HBI_1

System Name	Buses	Machines	Time Saving (%)
Three-bus	3	2	no saving
Two-area	11	4	4
IEEE 50-machine	145	50	20

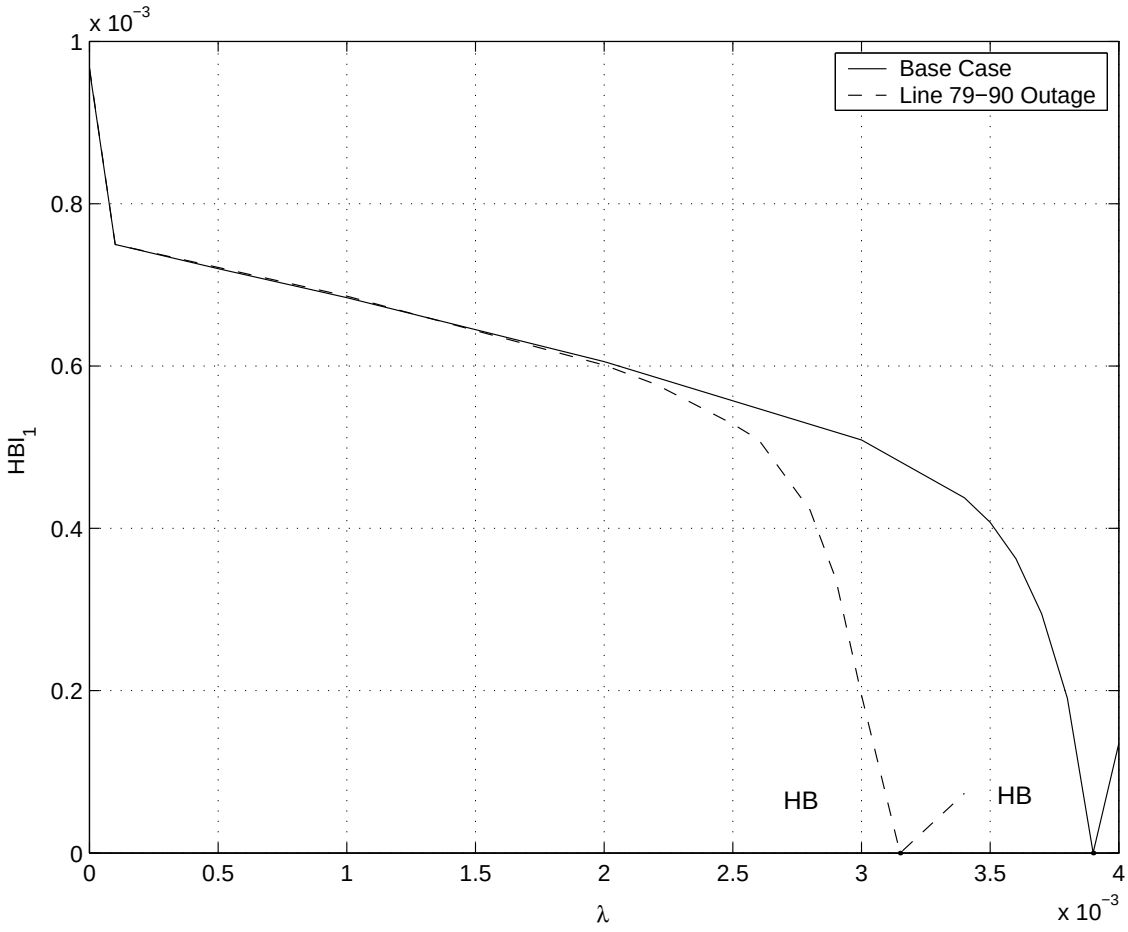

Figure 3.22: HBI_1 for the IEEE 50-machine system (Case II).

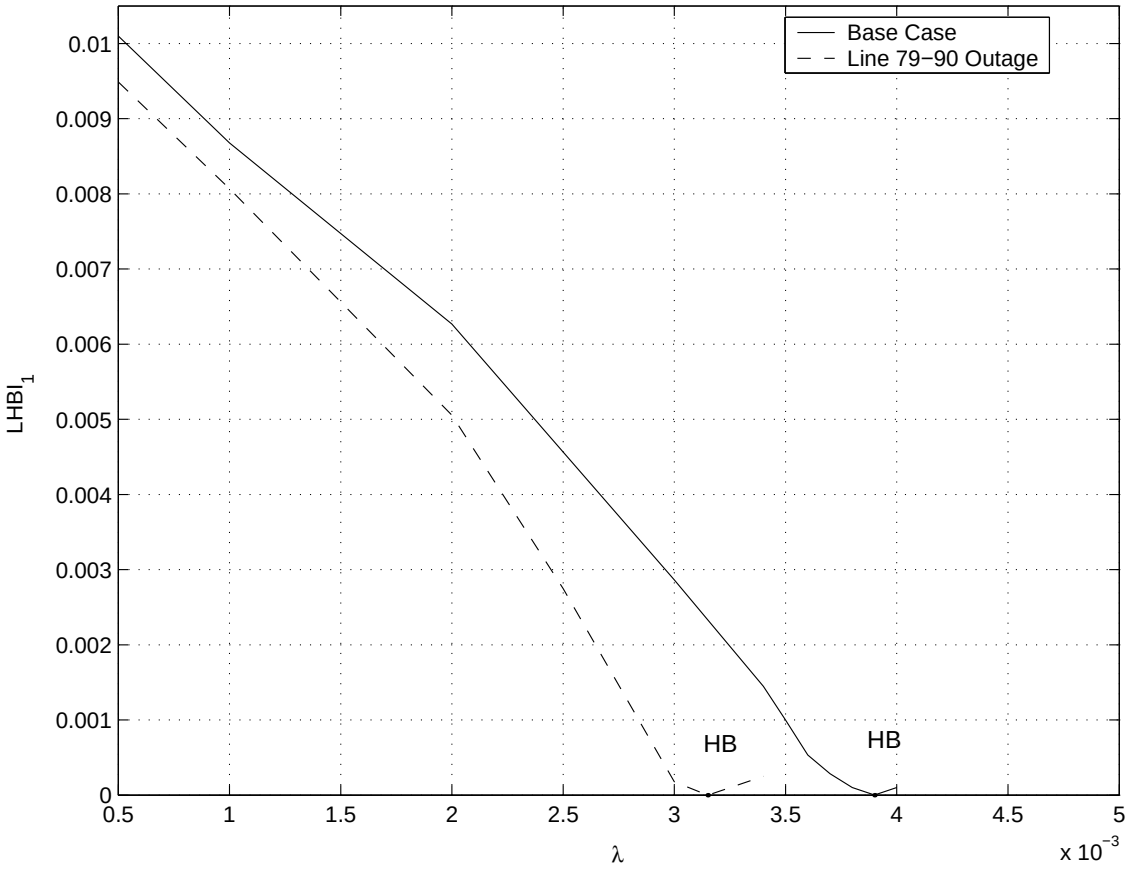

Figure 3.23: Linearized HBI_1 index for the IEEE 50-machine system (Case II).

3.6.2 Effectiveness for Reliable Detections

The calculation of the proposed indices, HBI_1 and HBI_2, on-line, requires the system state matrix A and full system matrix J, respectively, and the imaginary part of the critical eigenvalue (β). The information needed for the construction of the matrices are a fast load flow solution, along with the system topology update, models and data of machines and other controllers of interest. Typically, these system data (both static and dynamic) are available in a modern system control center, and getting a fast (or multiple) load flow solution is not an issue nowadays. Once the matrices are constructed, any efficient eigenvalue algorithm can be used to calculate β, which is the frequency of the critical mode in rad/s. Thus, the feasibility for reliable detection using these indices is promising.

As seen in several examples in section 3.5, HBI_1 or HBI_2 is adequate for a prediction or detection, as they behave in a predictable way with respect to loading factor λ. However, these indices could lose smoothness and behave in a nonlinear fashion due to controller limits or eigenvalues near resonance (e.g. Section 3.7.2). These could be considered as some of the limitations of these indices. Nevertheless, if these indices present nonlinear profile, the linearized indices $LHBI_1$ or $LHBI_2$ can be used to reduce the nonlinearity. In this case, the gradient information required for linearization may be obtained numerically.

3.6.3 Application to Practical Power Systems

The range of examples presented here, with different dynamic charteristics with varying size and complexity, suggest that the application of the indices to a practical power system is feasible. Furthermore, in certain systems, information of β or the frequency of the problematic modes (e.g. WSCC inter-area mode, Ontario Hydro

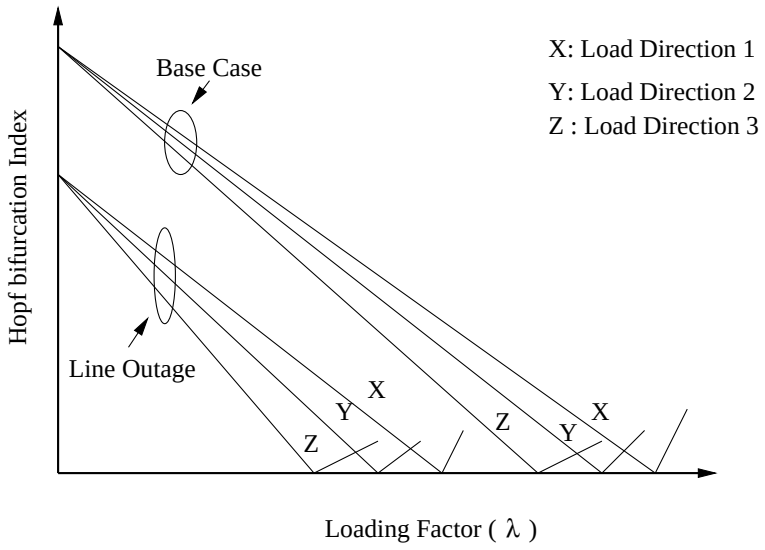

Figure 3.24: Sketches of Hopf bifurcation index for various cases.

local modes) are known. By inserting in the β in the state matrices, the index can be calculated without actually computing the critical eigenvalue, and thus predict the problematic load levels at which the indices become critical. However, for a practical power system HBI_2 (and $LHBI_2$) is preferred for on-line applications due the higher computational speed compared with HBI_1 (and $LHBI_1$).

In a real scenario, a power system faces varying operation conditions (e.g. load increase with different directions, line outages). Figure 3.24 illustrates possible profiles of Hopf bifurcation indices for various system conditions , i.e. base case and a line outage case with different load directions. In the case of a change in operating condition, the Hopf bifurcation indices follow a different profile. A possible profile of the Hopf bifurcation indices as an operator would see it in real time is depicted in Figure 3.25. By monitoring the index on-line, a remedial measure, such as load shedding, can be deviced when the indices hit a given threshold value, which is defined based on predictions made by extrapolating the index.

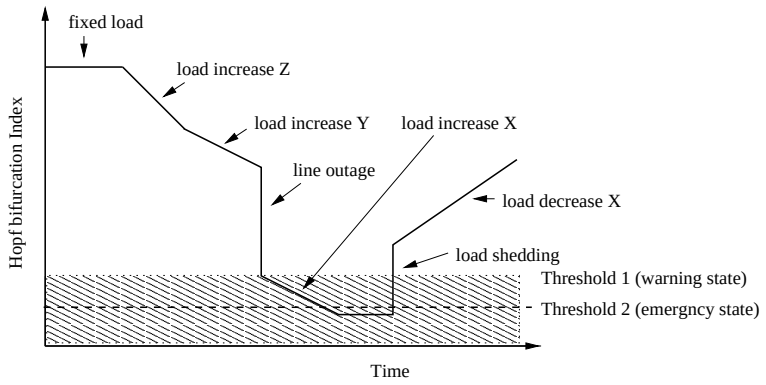

Figure 3.25: Hopf bifurcation index profile as an on-line operating tool.

3.7 Nonlinear Systems Examples

While this thesis is primarily concerned with enhancement of power system performance, it is of more general interest to note that the proposed Hopf bifurcation indices can be readily applied to any nonlinear system for predicting and/or detecting Hopf bifurcations. The results of applying these indices to two examples of nonlinear systems are discussed in this section.

3.7.1 Lorenz's equation

Lorenz's equations characterize a certain nonlinear system and can be expressed in the following form [25]:

$$\begin{aligned} \dot{y_1} &= P(y_1 - y_2) \\ \dot{y_2} &= -y_1 y_3 + R y_1 - y_2 \\ \dot{y_3} &= y_1 y_2 - b y_3 \end{aligned} \tag{3.15}$$

where b and P are positive constants and R is the bifurcation parameter. For $R \geq 1$ the system presents the following equilibria: $(\pm\sqrt{R-1}, \pm\sqrt{R-1}, R-1)$. For the equilibrium point $(\sqrt{R-1}, \sqrt{R-1}, R-1)$, the system has a Hopf bifurcation for b=1, P=4 and a given value of R. Figure 3.26 shows the movement of the eigenvalues for variations of the parameter R from a value of 1 to 40. As λ changes, the critical eigenvalue moves from the left-half plane to the right-half plane, crossing the imaginary axis at $R = 36$. The corresponding HBI_1 and $LHBI_1$ are given in Figures 3.27 and 3.28, respectively. Observe the smoothness and predictable behavior of these indices, especially close to the bifurcation point.

3.7.2 Two coupled linear oscillators

The following equation represents two linear oscillators mutually coupled by the term $b\dot{y}$ and $a\dot{x}$ [62]:

$$\begin{aligned} b\dot{y} &= \ddot{x} + \dot{x} + r^2 x \\ a\dot{x} &= \ddot{y} + \delta\dot{y} + 100y \end{aligned} \tag{3.16}$$

In this example, a case of mutual coupling, for a=b=1 and damping δ=0.91, is considered to evaluate HBI and LHBI. This case is characterized by two Hopf bifurcations and a strong resonance; the first one is a subcritical Hopf and the other one is a supercritical Hopf [62].

Figure 3.29 shows the movement of the eigenvalues with respect to changes in the value of r from 8 to 12. Observe that, there are two pairs of complex eigenvalues in the system, and one of them crosses the imaginary axis twice, near r=10. Furthermore, the eigenvalues show a strong resonance at $r \approx 11$.

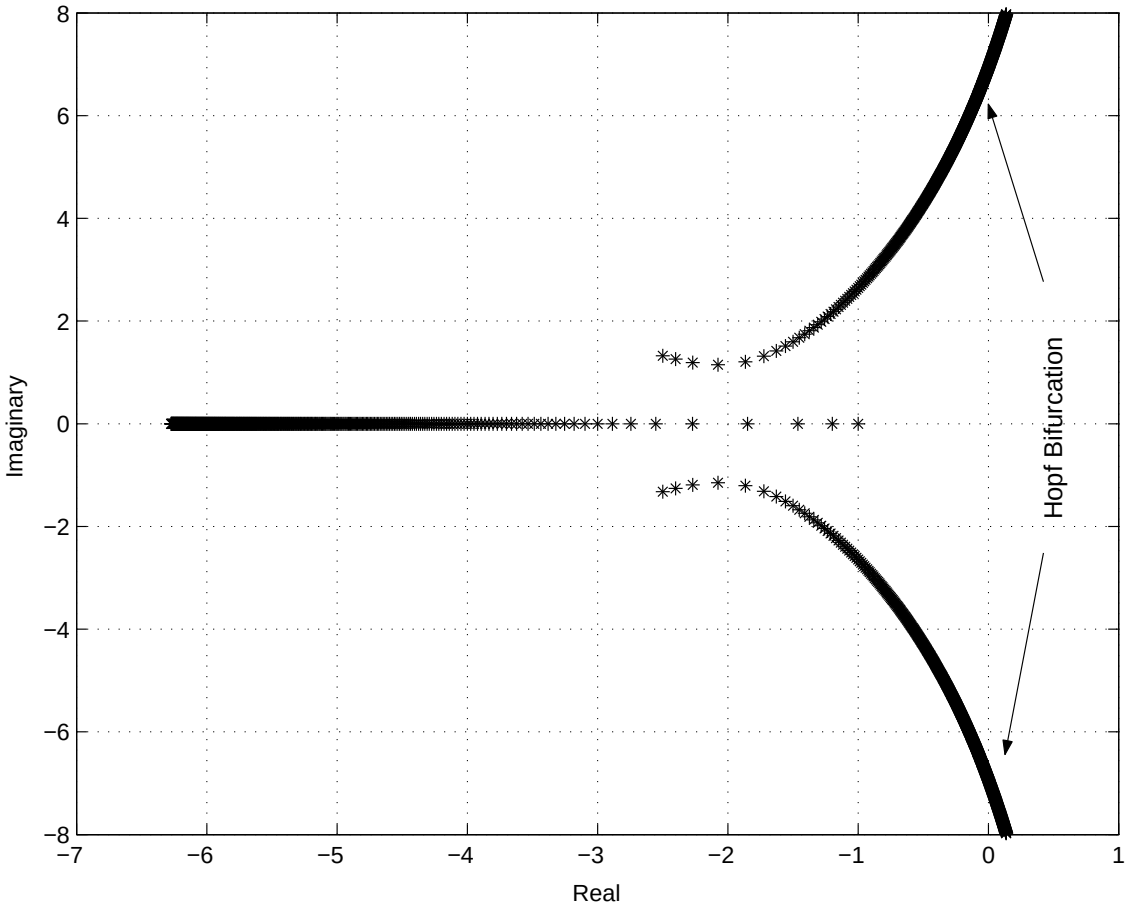

Figure 3.26: Movement of the eigenvalues with respect to the parameter R for Lorenz's equations.

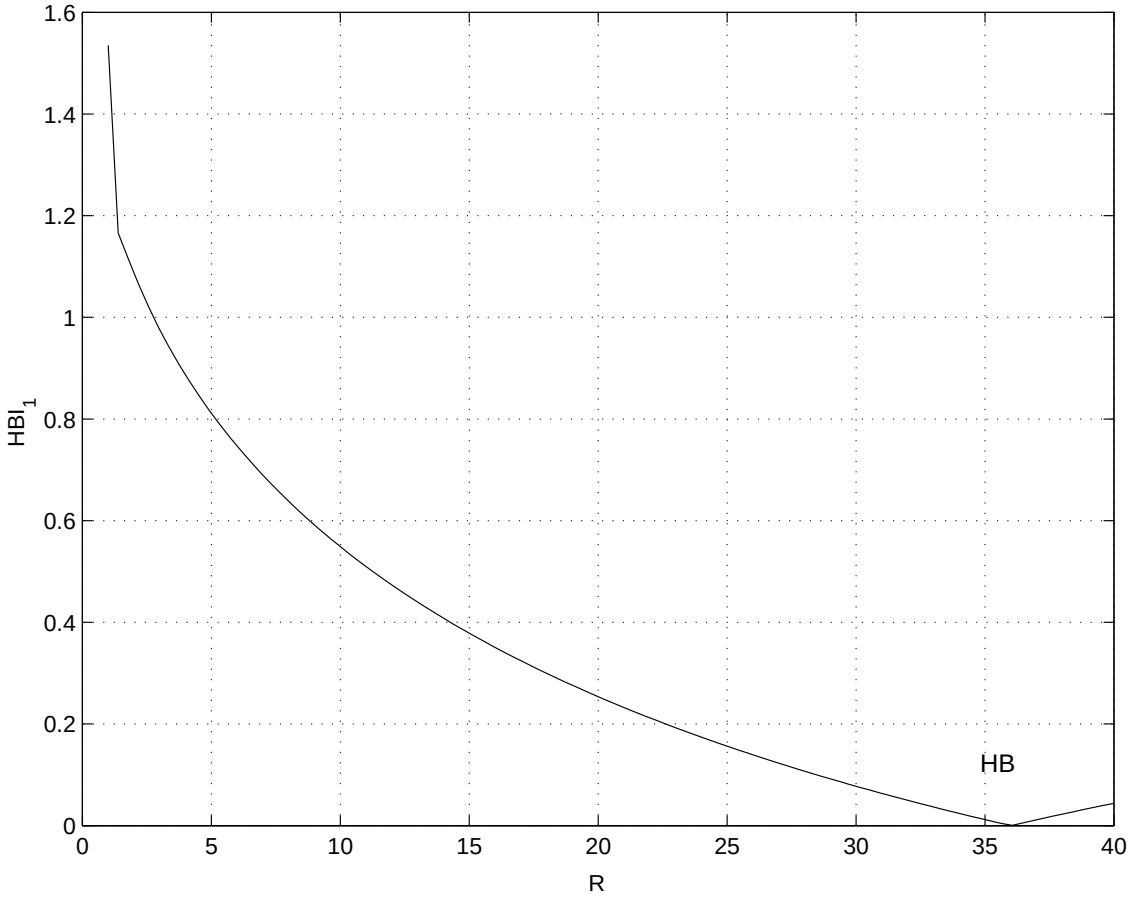

Figure 3.27: HBI_1 for Lorenz's equations.

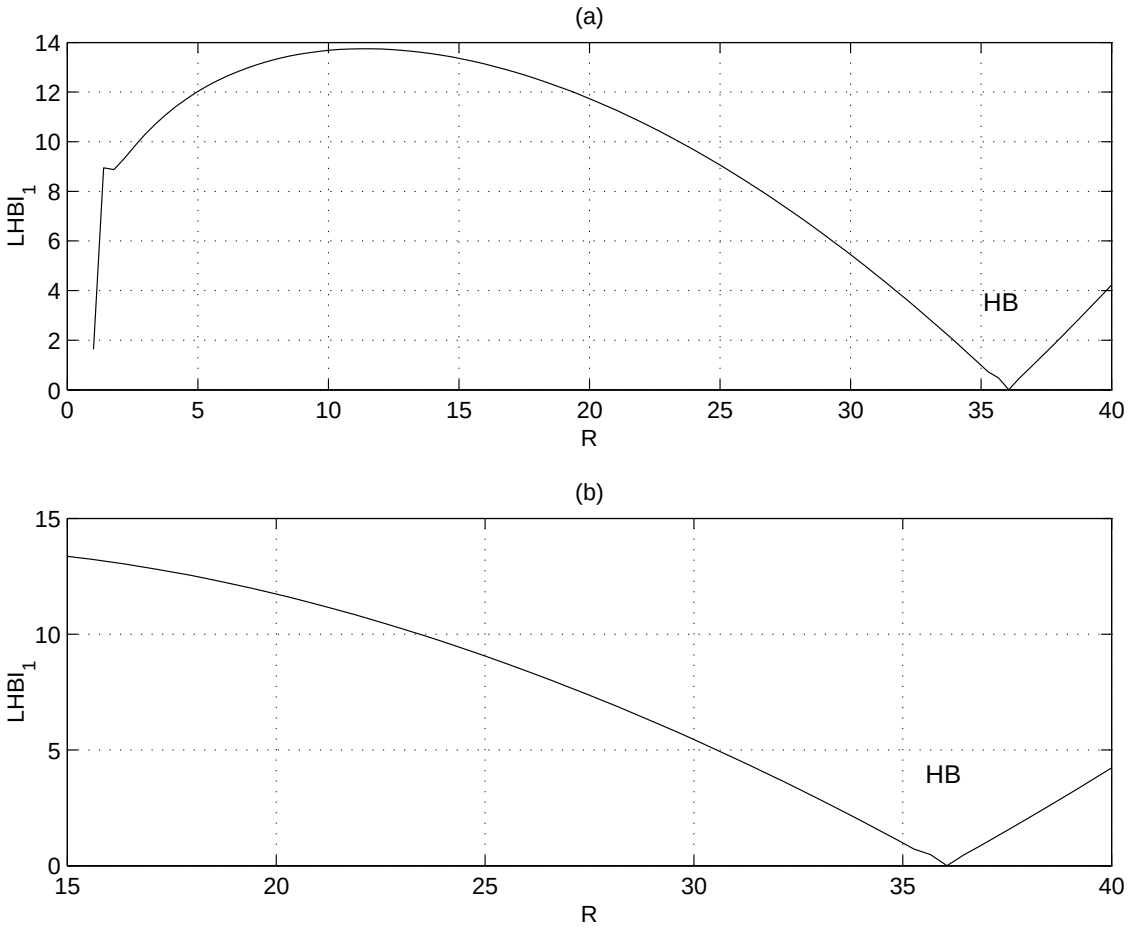

Figure 3.28: (a) $LHBI_1$ and (b) enlargement of $LHBI_1$ around the bifurcation point for Lorenz's equations.

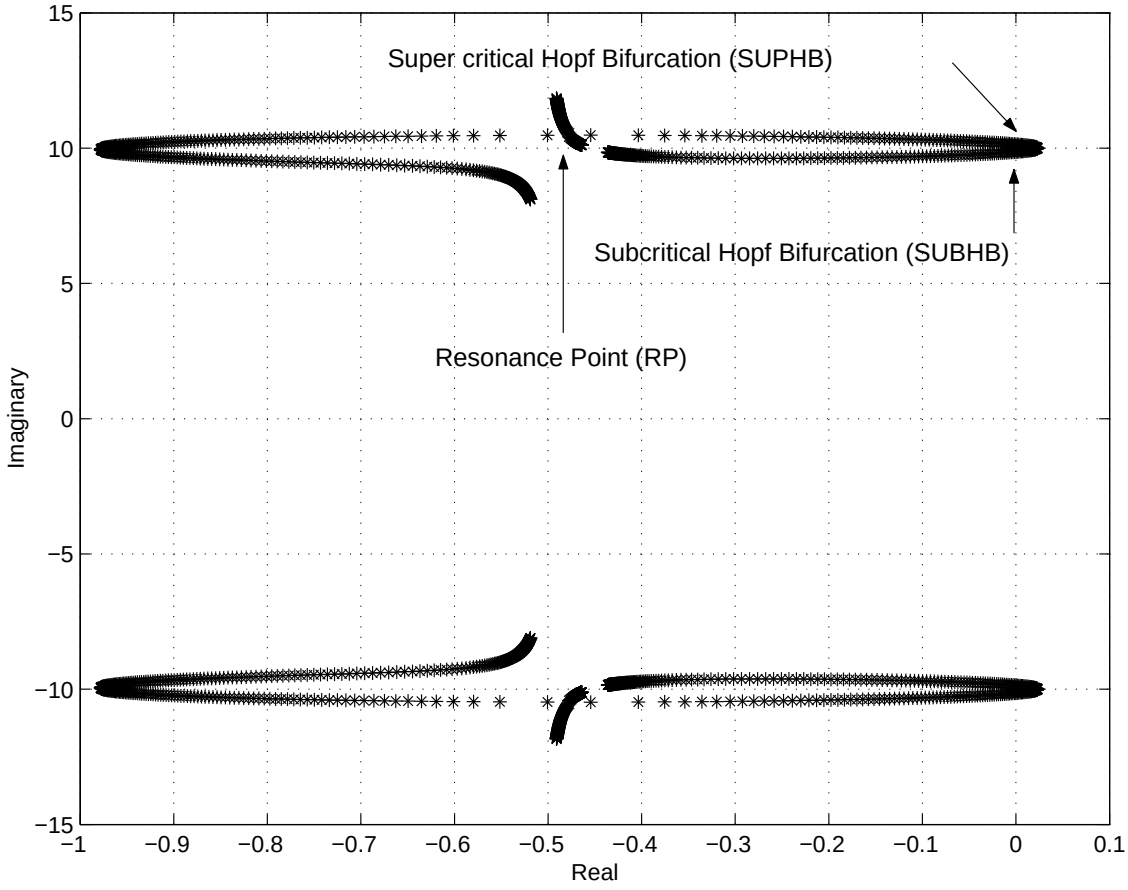

Figure 3.29: Movement of the eigenvalues with respect to the parameter r for the two coupled linear oscillators.

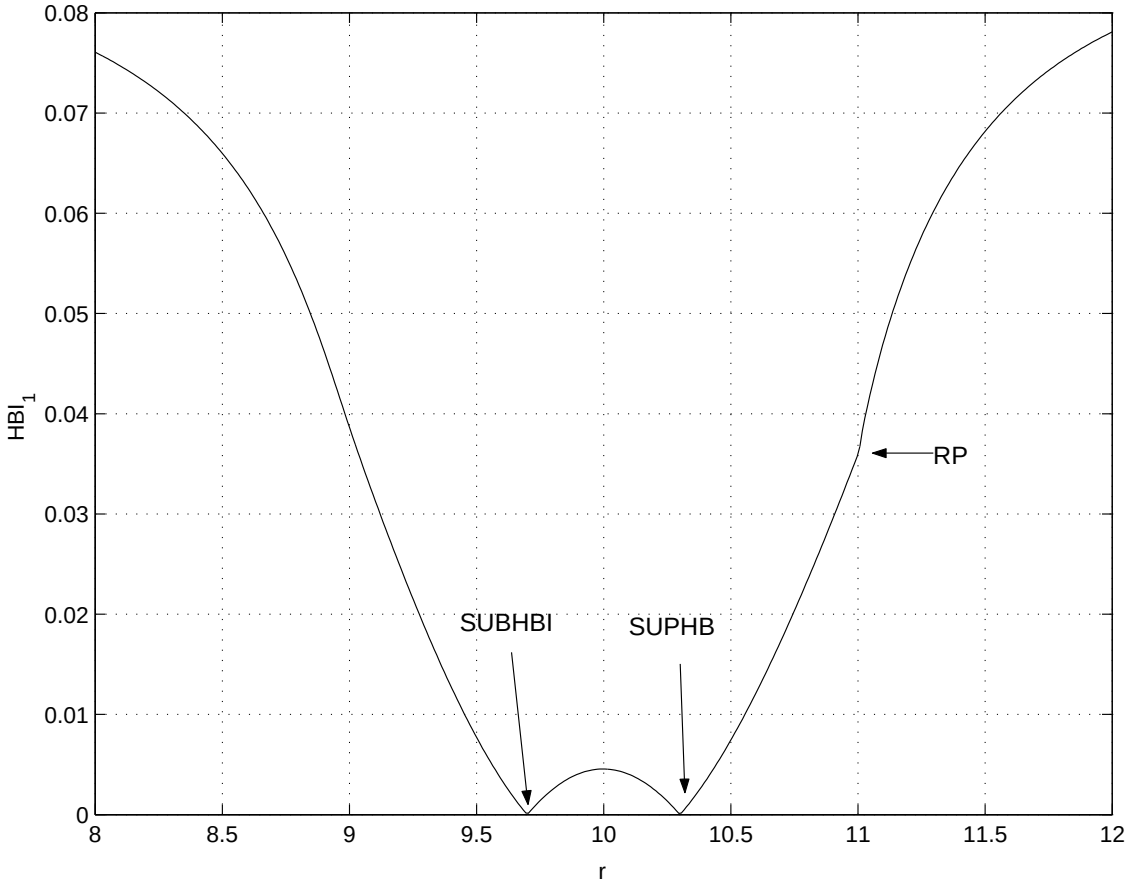

Figure 3.30: HBI_1 for the two coupled linear oscillators.

Figures 3.30 and 3.31 show HBI_1 and $LHBI_1$, respectively, for the coupled linear oscillators. The indices are smooth and predictable, especially close to the bifurcation point. As well, each index, $LHBI_1$ in particular, can predict a resonance point when there is a sudden change in the $LHBI_1$ due to the change in the critical eigenvalue.

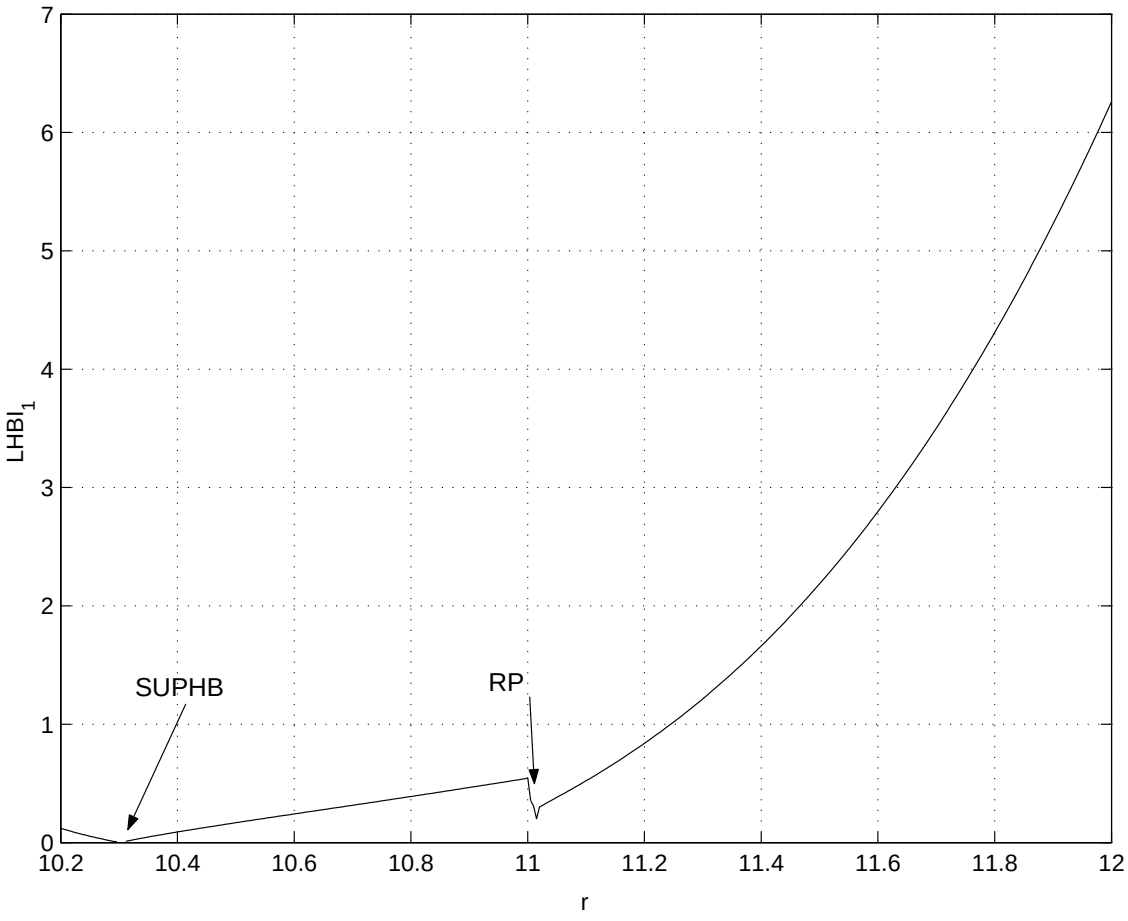

Figure 3.31: $LHBI_1$ for the two coupled linear oscillators.

3.8 Summary

Following the review and discussion of the theoretical background, an innovative approach is introduced in the form of two alternative indices for predicting or detecting Hopf bifurcations. Further enhancement is made through linearization of each index.

Three test systems of increasing size and complexity have been used to demonstrate the relevant system behavior and the significance of the proposed indices in power systems.

As a subsidiary issue, the benefit of the indices for assessment of non-linear systems in general has been demonstrated in two examples.

Chapter 4

HOPF BIFURCATION CONTROL

4.1 Introduction

Chapter 3 was concerned with indices for detection and prediction of Hopf instability. The consequential correction would be by system design changes in system planning or by the introduction of special controllers with damping capability. For this purpose, power system stabilizers (PSS) are well established, while newer FACTS controllers also have supplementary capability for oscillation control.

Even though PSS is very effective in enhancing the dynamic performance, its placement may be an issue nowadays due to diverse generator ownership in a deregulated environment. Hence, FACTS controllers, which have been shown to be also effective in the control of oscillatory problem, have become an attractive alternative. FACTS controllers can be designed to use a variety of control signals and, in principle, be placed at any location in the transmission system to achieve the

best possible damping. However, these controllers are certainly more expensive than PSS, and their location may well be determined by their primary functions such as increasing system loadability rather than for optimized damping. Such trade-offs will be made on a case-by-case basis. However, locations are selected in the presented results to demonstrate the possible effectiveness for Hopf oscillation control.

In this chapter, Hopf bifurcation control in the IEEE 14-bus test system is presented first, as a preliminary trial, to showcase the various alternatives (e.g. different controllers, controller placement, best control input signal). A new placement technique of shunt FACTS controllers is introduced together with application examples. Also, a methodology to select the best local control input signal using Mode Observability Index is presented. Finally, Hopf bifurcation control using the IEEE 50-machine test system is presented, together with the application of the placement and control input signal techniques.

4.2 Preliminary Example

For the IEEE 14-bus test system of Figure 2.16, Figure 3.2 shows the presence of Hopf bifurcations for the base case and the line outages, for the assumed load and generation directions. The loads were modeled as constant PQ in load flow and stability studies.

P-V curves for various cases, with and without different FACTS controllers, were obtained using UWPFLOW. The eigenvalue and time domain analyses were carried out using MASS and ETMSP, respectively. Figure 4.1 shows the P-V curves for the test system for the base case, line 2-4, and line 2-3 outages. Hopf bifurcation points are also indicated in these plots. In order to see the effect of the bifurcation, a time

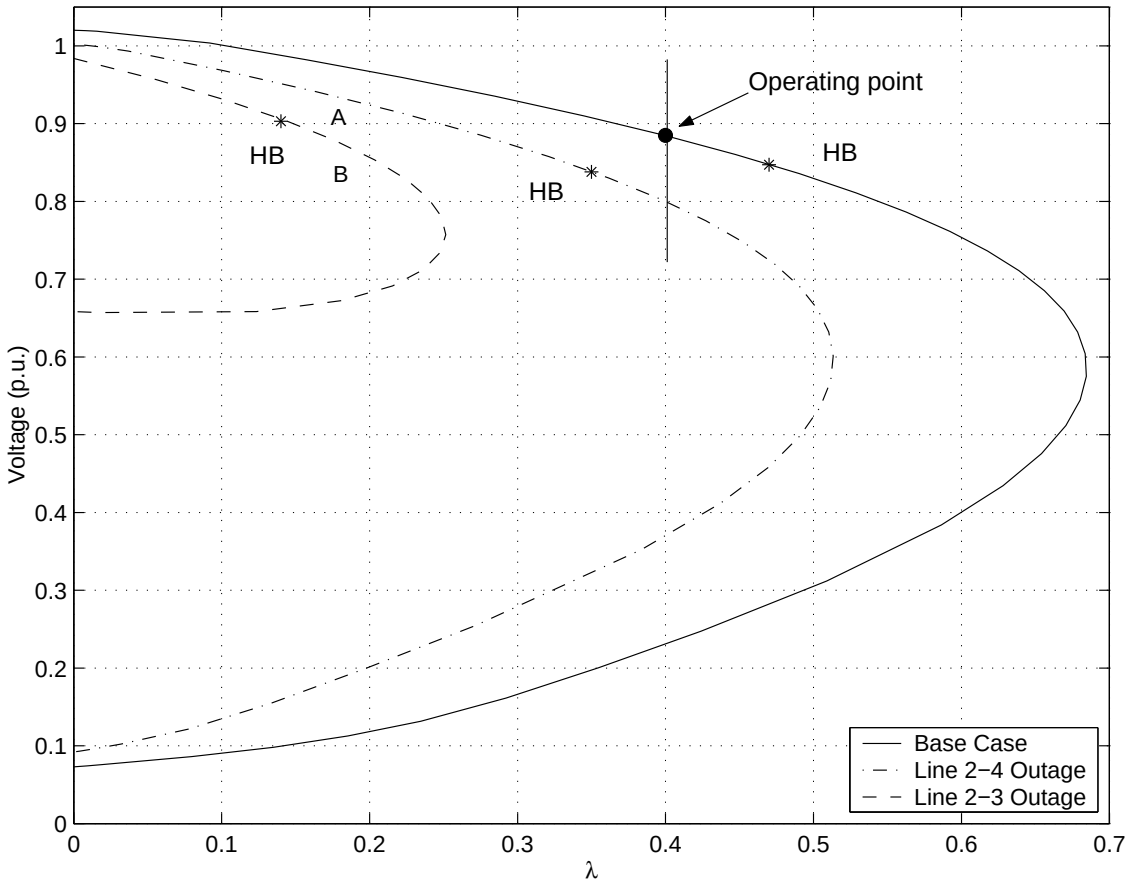

Figure 4.1: P-V curves at bus 14 for different contingencies for the IEEE 14-bus test system.

domain simulation was performed for the line 2-4 outage at the given operating point, which is depicted with a vertical line for λ=0.4 p.u. Thus, Figures 4.2 and 4.3 show how the Hopf bifurcation leads the system to an oscillatory unstable condition.

In order to control the oscillatory problem associated with the Hopf bifurcation, various power system controllers were used, namely PSS, SVC and TCSC. The detail results of the system with each of the controllers, including controller

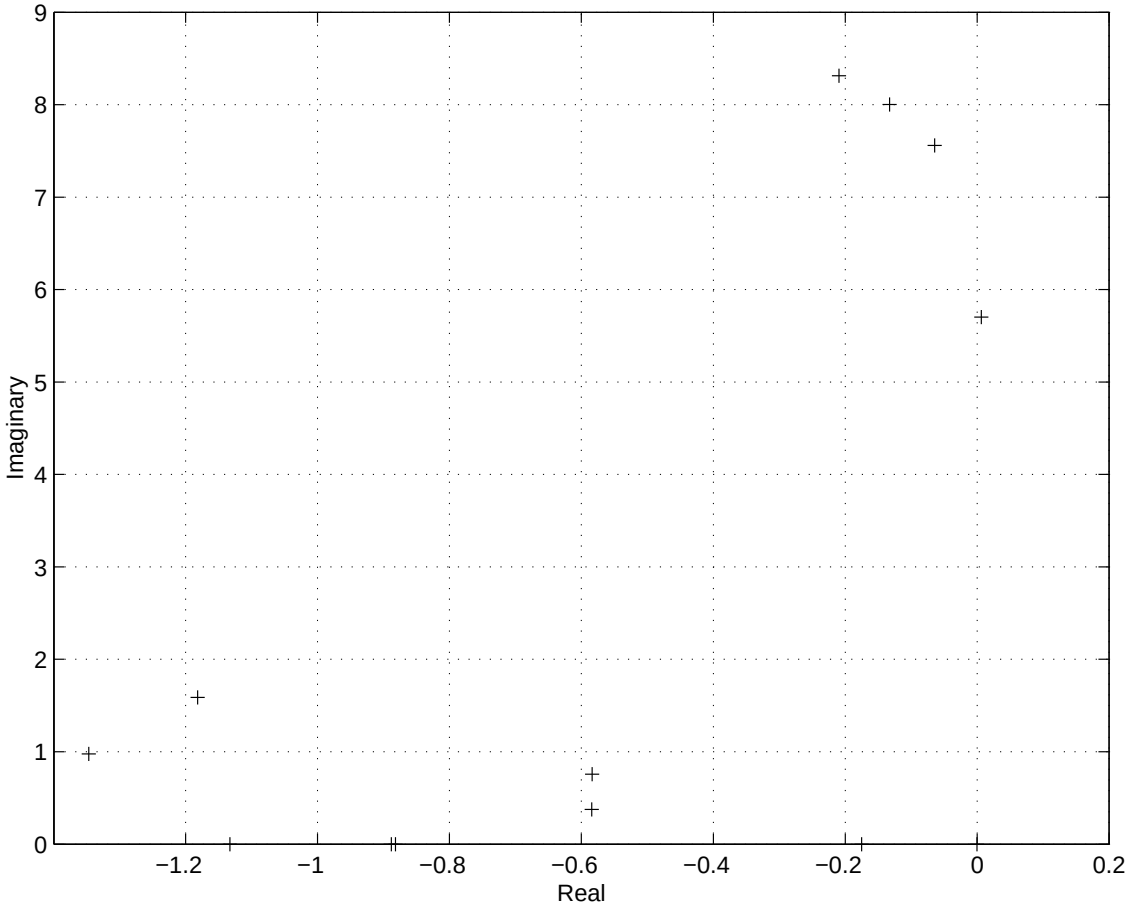

Figure 4.2: Some eigenvalues for the line 2-4 outage in the IEEE 14-bus test system at the operating point (λ=0.4).

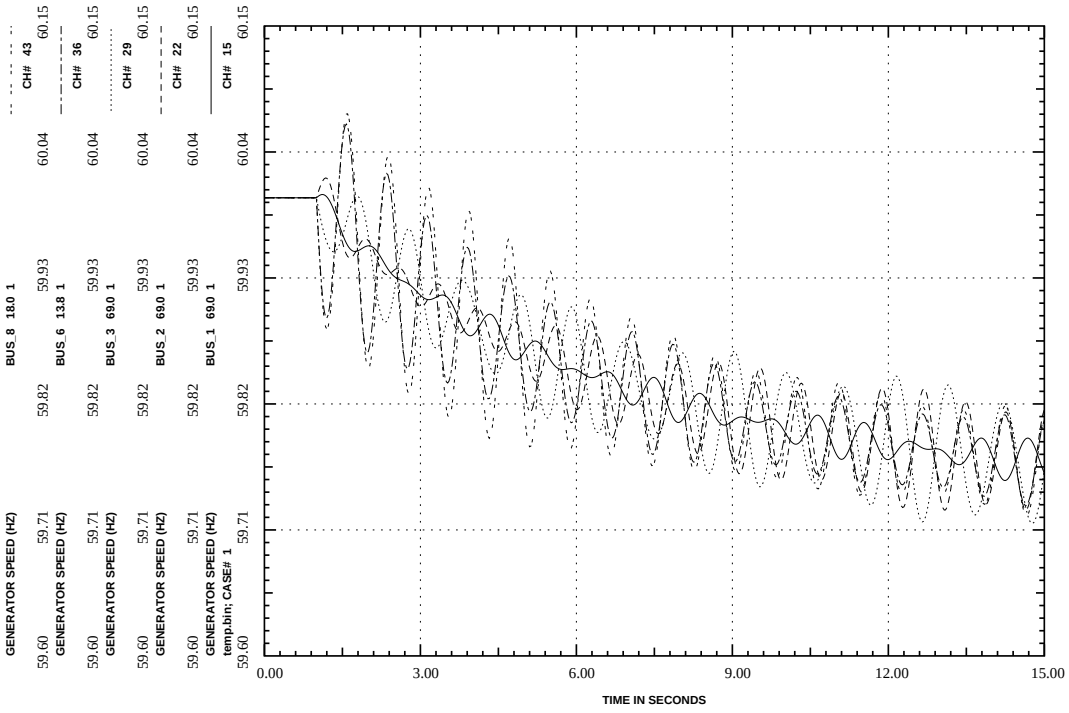

Figure 4.3: Generator frequency oscillation due to Hopf bifurcation triggered by line 2-4 outage at λ=0.4 for the IEEE 14-bus test system

placement and control input signal issues are discussed below.

4.2.1 PSS Controller Design

The dominant state variables associated with the Hopf bifurcation which are responsible for the oscillations were identified through a participation factor analysis [18]. A participation factor matrix is defined as the combination of left (w) and the right (v) eigenvectors associated with different modes of a system state matrix A. This identifies the dominant state variables associated with different modes or eigenvalues. Table 4.1 shows the state variables and associated participation factor of the critical mode at the Hopf bifurcation point for the base case. Observe that δ and ω of generator 3 are the dominant state variables associated with the Hopf bifurcation.

Table 4.1: Participation factors of the critical mode at the Hopf Bifurcation for the IEEE 14-bus test system

State Variable	Part. Factor	State Variable	Part. Factor
δ_3	1.0000	ω_1	0.1628
ω_3	1.0000	δ_2	0.0086
δ_1	0.1625	ω_2	0.0086

The PSS controller model used in this case is shown in Figure 2.1. The gain and various time constants of the PSS were selected from [59] based on the rating of the machine. Complete static and dynamic data of the system, including the PSS controller parameters are given in Appendix C.

A PSS installed at bus 3 was unable to damp the oscillations, because PSS con-

trol of a synchronous compensator produces little or no damping torque. The PSS was then introduced to the next generator location, i.e. generator 1, which successfully removed the Hopf bifurcation in all the cases as shown in Figure 4.4. Notice that there is no change in the maximum loading margin with a PSS controller, but this is not the case when the SVC or TCSC is introduced in the system as will be seen next. Figures 4.5 and 4.6 show an eigenvalue plot and the generator frequency plot for the line 2-4 outage, respectively, at the operating point (λ=0.4 p.u.). The PSS removes the instability due to the Hopf bifurcation by moving the critical complex mode into the open left-half plane. Damping on the other electromechanical modes (machines at bus 2 and 8) is also increased by the PSS.

4.2.2 SVC Controller Design

An SVC is considered as other possible alternative to remove or control the Hopf bifurcation. The model with supplementary control input signal as depicted in Figure 2.4 is used for all the simulations. With regards to the SVC location, only load buses were considered as suitable candidates. Since the system has only eight load buses, each possible location was tested with SVC. The SVC is rated at $\pm$ 100 Mvar. The controller parameter values are given in Appendix C. These data were taken from [50]. Table 4.2 shows the SVC location, the critical eigenvalue and associated damping of the system, for the first four locations. These results were obtained for the SVC without the supplementary control input signal and at the Hopf bifurcation point for the base case.

According to the results, bus number 4 is the best location for an SVC to control the oscillation due to the Hopf bifurcation. The placement plays a major role in adding damping to the critical mode. The loadability analyses yield bus 14 as the

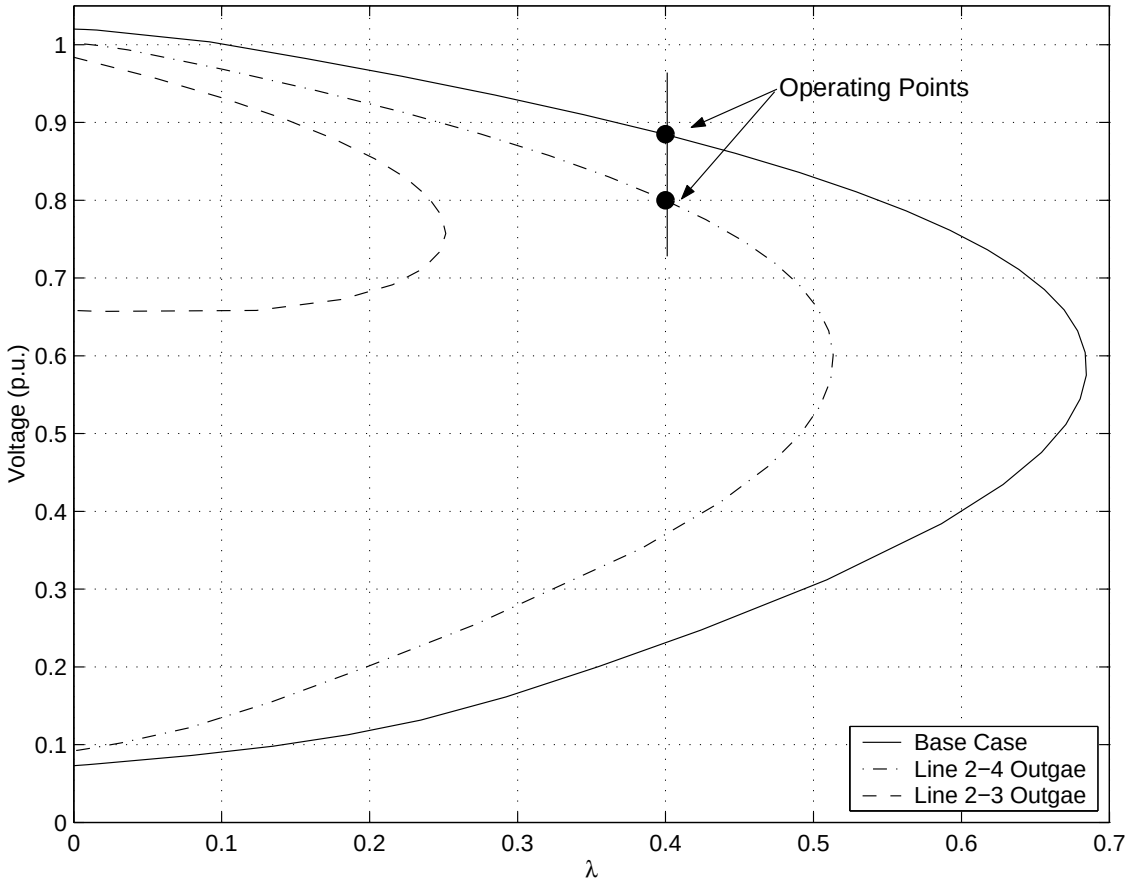

Figure 4.4: P-V curves at bus 14 for different contingencies for the IEEE 14-bus test system with a PSS at bus 1.

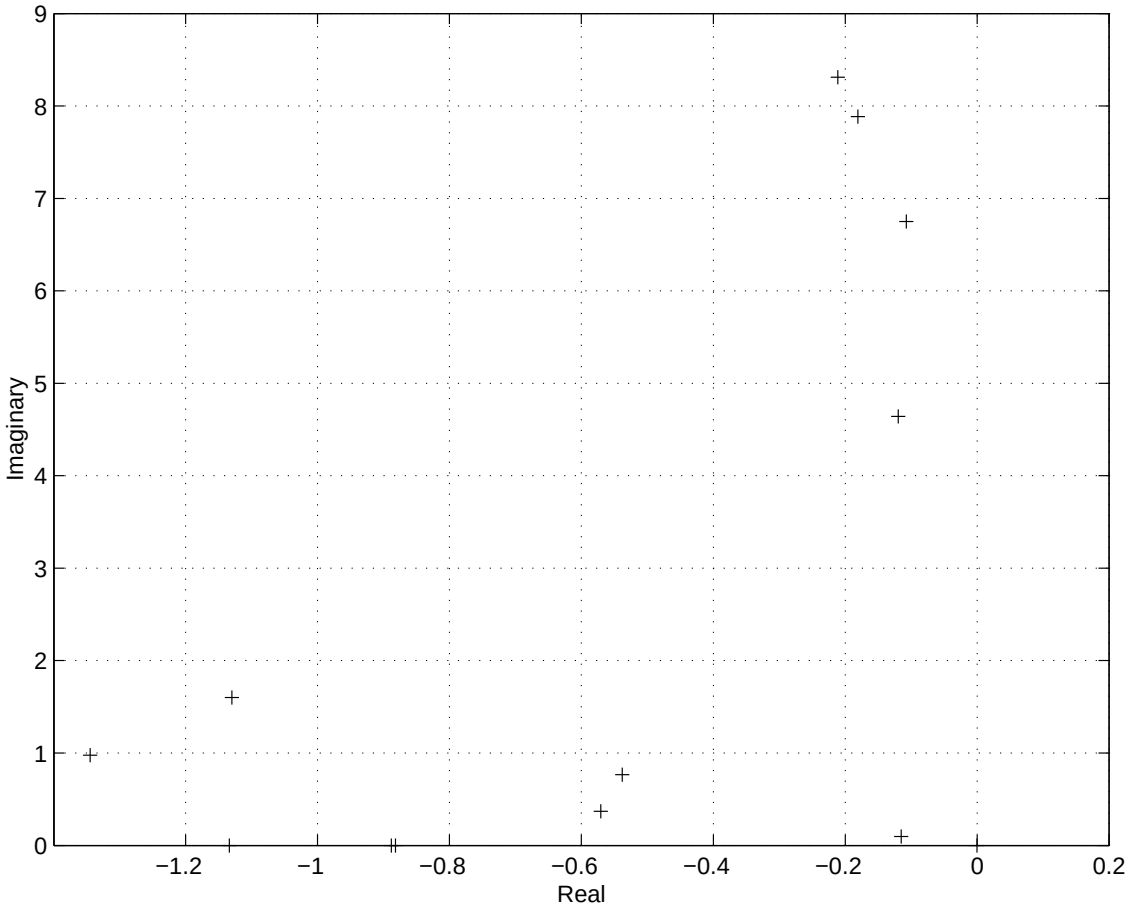

Figure 4.5: Some eigenvalues with PSS at bus 1 for a line 2-4 outage in the IEEE 14-bus test system.

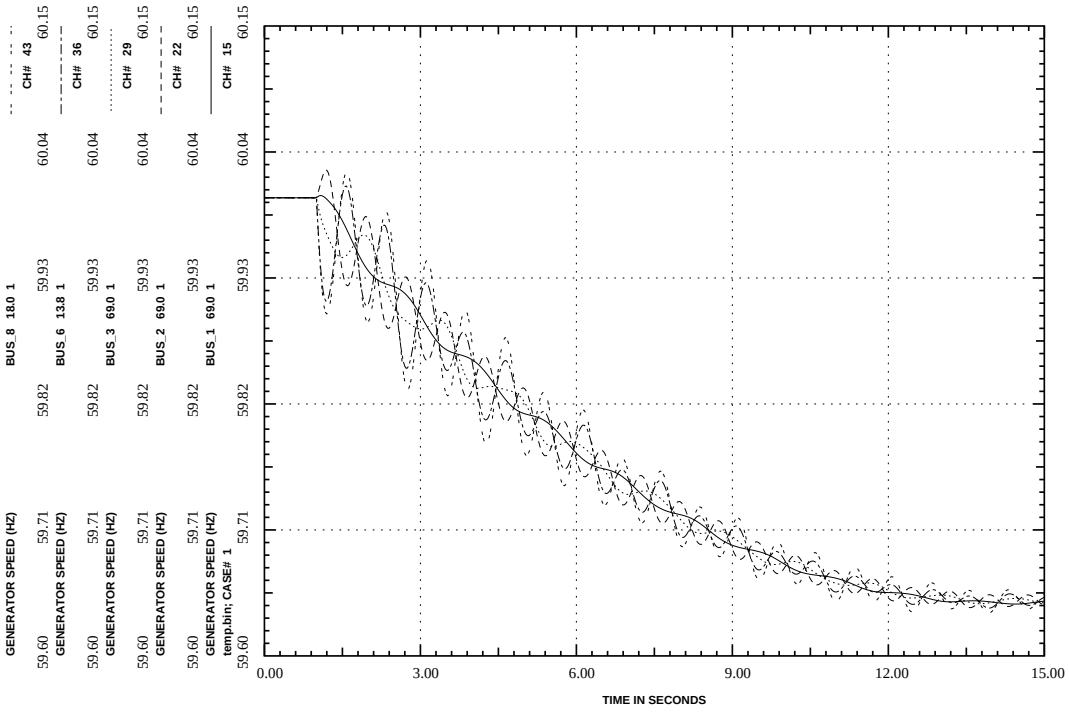

Figure 4.6: Oscillation damping with PSS at bus 1 for a line 2-4 outage in the IEEE 14-bus test system.

Table 4.2: Critical eigenvalue with SVC at various locations for the IEEE 14-bus test system

SVC Location	Critical Eigenvalue	Damping Ratio
Bus 4	$-0.0192 \pm j5.992$	0.0032
Bus 5	$-0.0194 \pm j5.966$	0.0032
Bus 9	$-0.0128 \pm j5.939$	0.0022
Bus 10	$-0.0114 \pm j5.928$	0.0019

best location to improve the loadability margin of the system.

For the best supplementary control input signal, all the possible adjacent line signals (line real power P, line reactive power Q or line current I) were tested. Table 4.3 shows the critical eigenvalue and associated damping for the different signals at the Hopf bifurcation for the base case. Observe that the supplementary control input signal too plays a major role in enhancing the damping of the critical mode. The best control input signal to give maximum damping was the real power flow in line 4-3.

Figure 4.7 shows P-V curves of the system with an SVC at bus 4, notice that there is no Hopf bifurcation. The system maximum loadability margin is also increased in all the cases, along with better steady state voltage at the higher loading levels.

Figure 4.8 shows some eigenvalues plot of the system with an SVC at bus 4 for the line outage; the corresponding time domain simulation is shown in Figure 4.9. The SVC at the appropriate location with the best control input signal removes the oscillation due to the Hopf bifurcation triggered by line 2-4 outage as depicted in Figures 4.8 and 4.9.

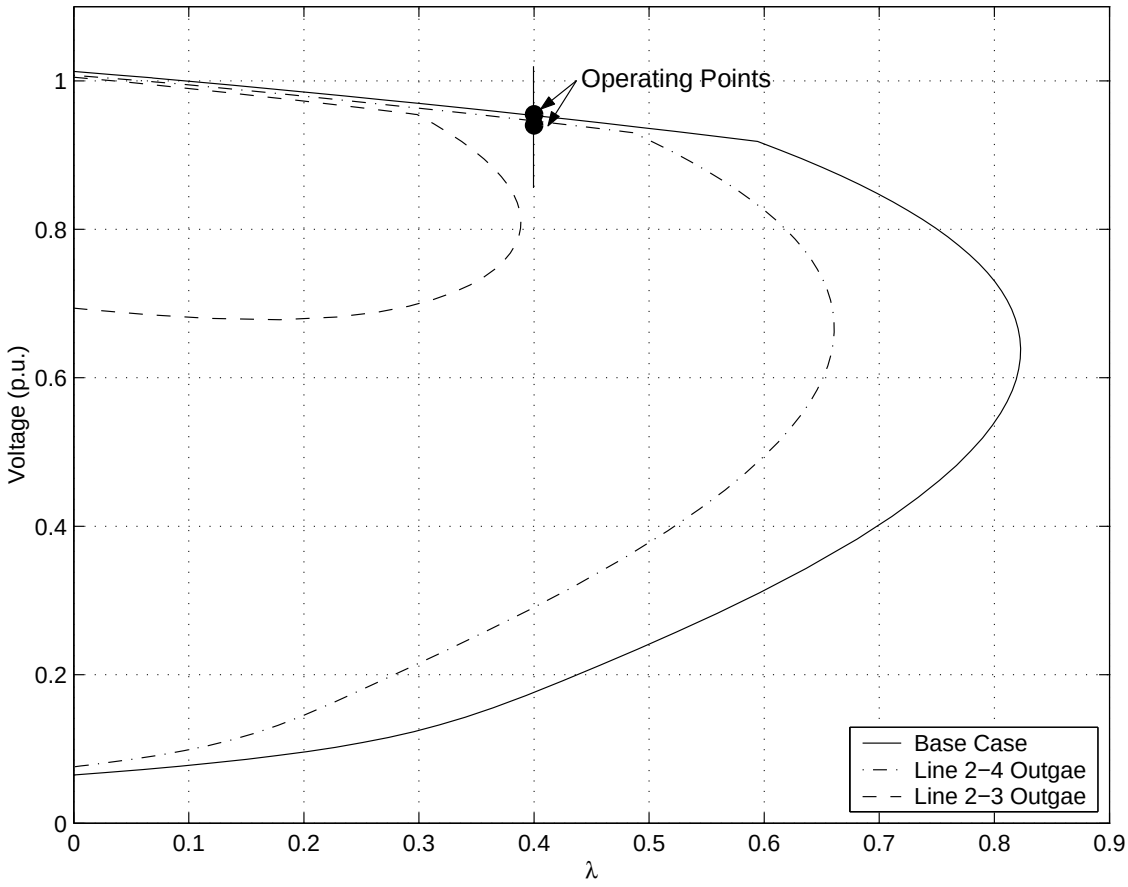

Figure 4.7: P-V curves at bus 14 for different contingencies in the IEEE 14-bus test system with a SVC at bus 4.

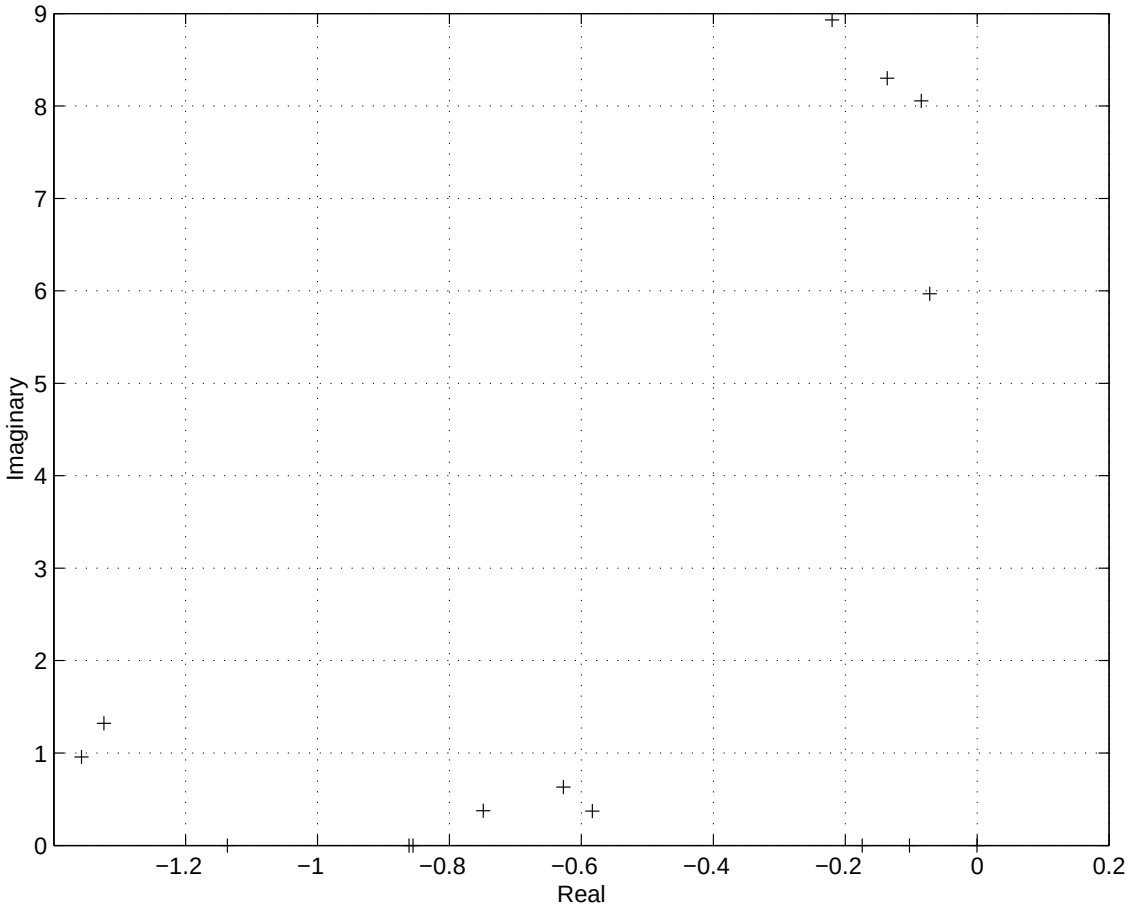

Figure 4.8: Some eigenvalues with a SVC at bus 4 for a line 2-4 outage in the IEEE 14-bus test system.

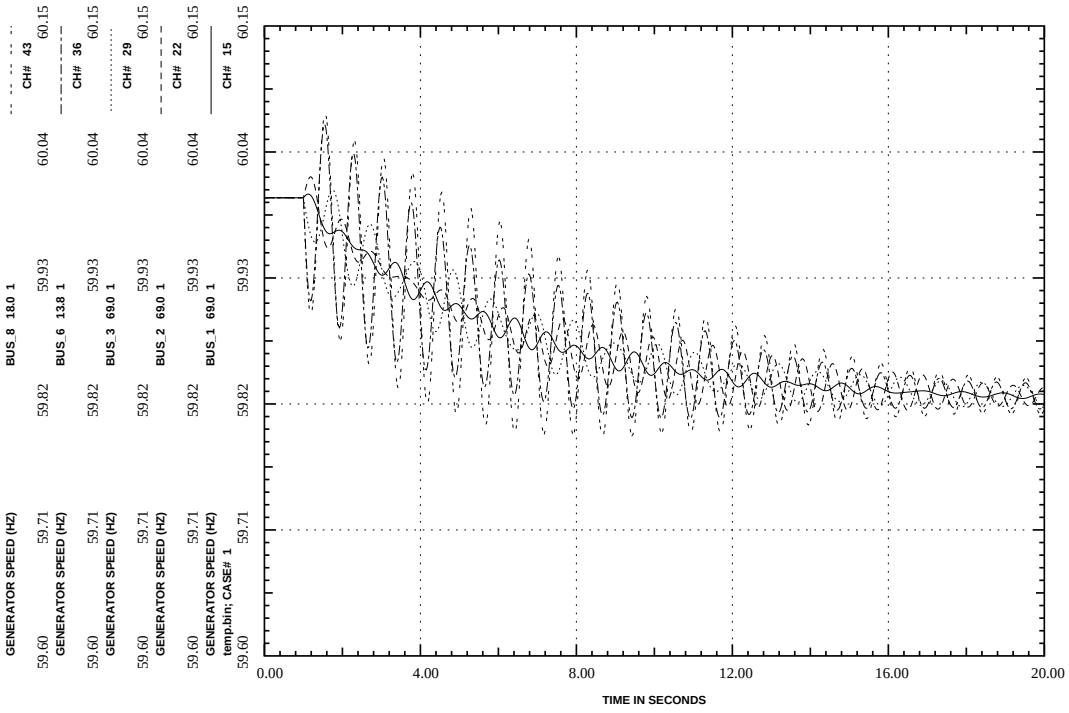

Figure 4.9: Oscillation damping with a SVC at bus 4 and supplementary control loop and signal for a line 2-4 outage in the IEEE 14-bus test system.

Table 4.3: Critical eigenvalue with SVC at bus 4 for various control input signals for the IEEE 14-bus test system

Line	Signal	Critical Eigenvalue	Damping Ratio
4-3	P	-0.0819 ± 5.947	0.0138
	Q	-0.0242 ± 5.995	0.0034
	I	-0.0805 ± 5.960	0.0135
4-5	P	-0.0643 ± 5.964	0.0108
	Q	-0.0112 ± 5.997	0.0019
	I	-0.0734 ± 5.950	0.0123

As a result of these test cases, it seems that an SVC has the potential, in general, to contribute to the alleviation of instability due to Hopf bifurcation.

4.2.3 TCSC Controller

The TCSC controller was considered as another possible alternative to remove the oscillation due to the Hopf bifurcation. Two different user defined controllers, as shown in Figures 2.8 and 2.9, were tried. Both controllers were comparable, as far as the damping introduced by these controllers on the critical mode is concerned. However, the first model was selected because of a better transient performance and its simplicity. The results presented here are based on the the first model (Figure 2.8). Ratings and controller parameters are given in Appendix C (a 40% compensation is considered, in this case).

For the placement of TCSC controller, all heavily loaded lines except lines 2-3 and 2-4 (these are the two lines considered for the outages), were considered as

candidate locations. Line 4-5 was found to be the best TCSC location to remove the oscillation due to the Hopf bifurcation based on the damping introduced by the controllers, as shown in Table 4.4. The line real power was used as the control input signal in all cases.

Table 4.4: Critical eigenvalue with TCSC at various locations for the IEEE 14-bus test system

TCSC Location	Critical Eigenvalue	Damping Ratio
Line 4-5	$-0.0327 \pm j5.9170$	0.0055
Line 3-4	$-0.0185 \pm j5.6960$	0.0033
Line 2-1	$-0.0113 \pm j5.5966$	0.0019
Line 2-5	$-0.0044 \pm j5.8390$	0.0008

Figure 4.10 shows P-V curves for the system with a TCSC in line 4-5 for the base case and the line outages. As indicated in the P-V curves, the TCSC increases the system dynamic loading margins in all cases by diminishing the onset of a Hopf bifurcation.

Figures 4.11 and 4.12 show the beneficial response of the TCSC on the critical eigenvalue and time response of the system, as expected. However, Hopf bifurcations are not completely removed, while the steady state loadability margin is increased.

It is clear from the above example that the placement of FACTS controllers and the input signals are important in achieving best possible damping of the critical oscillation mode. In the Sections 4.3 and 4.4, new methodologies are presented for the selection of best placement for a shunt-FACTS controller and for the selection of the best control input signal for the purpose of oscillation damping.

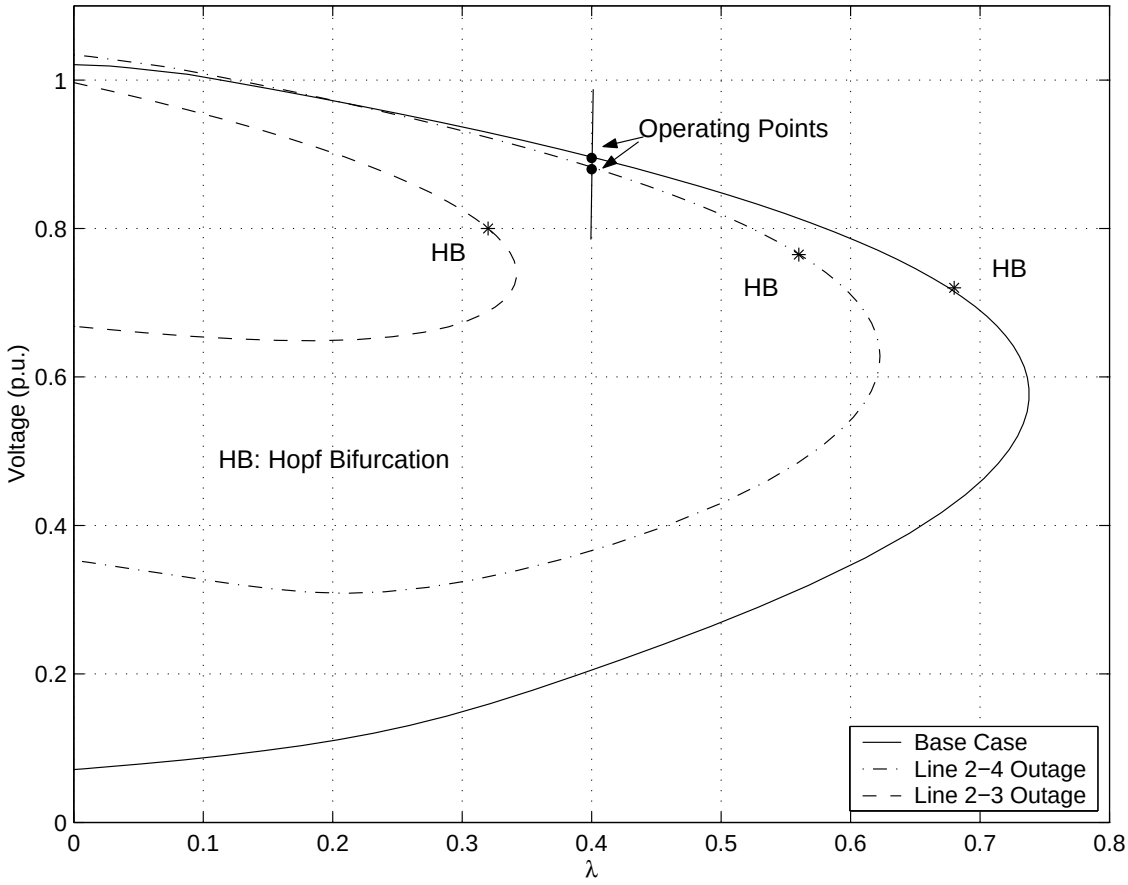

Figure 4.10: P-V curves at bus 14 for different contingencies for IEEE 14-bus test system with a TCSC in line 4-5.

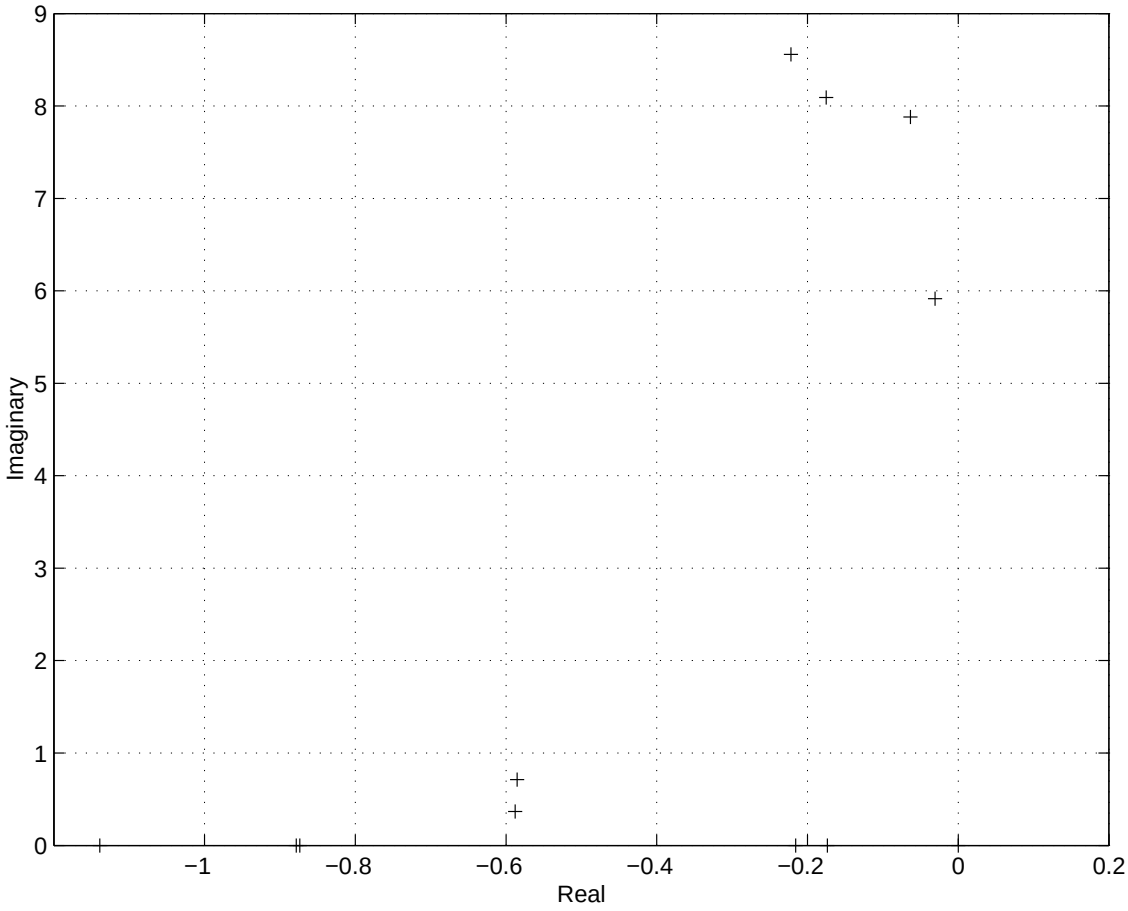

Figure 4.11: Some eigenvalues for the IEEE 14-bus test system with a TCSC in line 4-5 for line 2-4 outage.

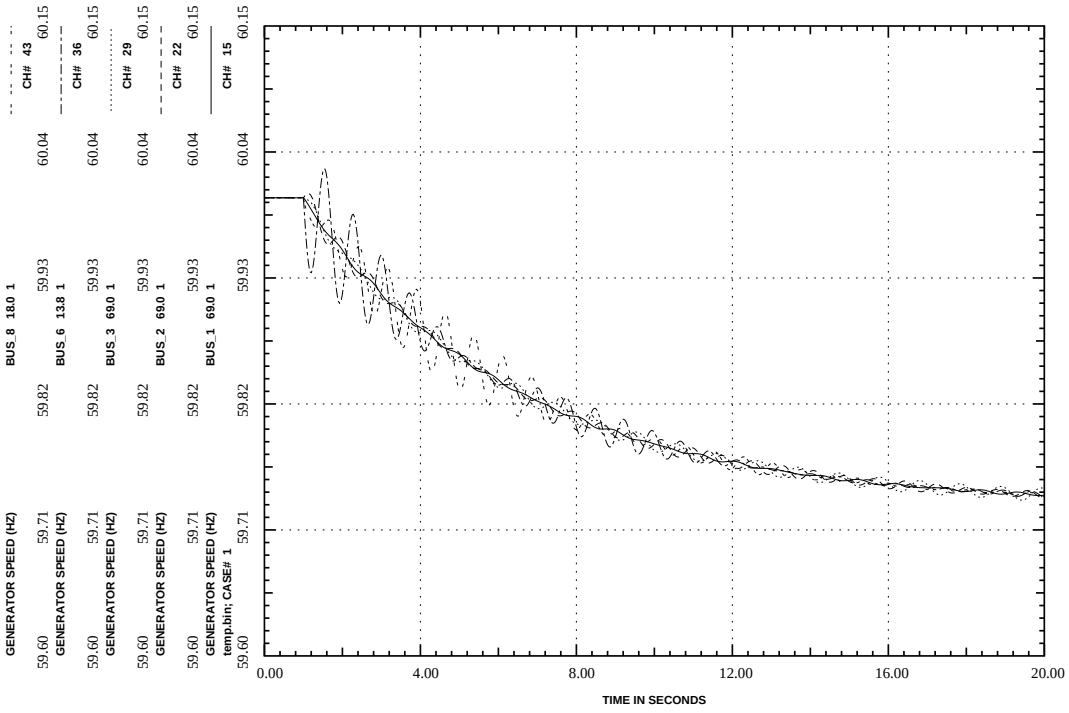

Figure 4.12: Oscillation damping in the IEEE 14-bus test system with a TCSC in line 4-5 for a line 2-4 outage.

4.3 FACTS Controller Placement

The location of a FACTS controller to achieve optimized oscillation damping is one of a number of application strategies. In the event that it is not considered the most vital, it would be useful to know such a location prior to making trade-offs with comparing objectives in the final selection of a FACTS locations. A new placement technique for shunt FACTS controller is proposed below; it is confined to the context of oscillation damping.

4.3.1 Proposed Shunt-FACTS Placement Technique

The linearized DAE system equations can be used instead of the reduced system state matrix for the calculation of eigenvalues, as discussed in Section 2.6.2. The extended eigenvector in this algorithm can be used to identify the dominant algebraic variable associated with the critical mode. Thus, restating the generalized eigenvalue formulation (2.10):

$$\begin{bmatrix} J_1 & J_2 \\ J_3 & J_4 \end{bmatrix} \begin{bmatrix} v_1 \\ v_2 \end{bmatrix} = \mu \begin{bmatrix} v_1 \\ 0 \end{bmatrix} \tag{4.1}$$

where μ is the eigenvalue and $[v_1\ v_2]^T$ is the extended eigenvector of μ, with

$$v_2 = -{J_4}^{-1} J_3 v_1 \tag{4.2}$$

The entries in v_2 correspond to the algebraic variables at each bus (e.g. voltages and angles, or real and imaginary voltages). A shunt FACTS controller, which directly controls voltage magnitudes, can be placed by identifying the maximum entry in v_2 associated with a load bus and the critical mode. Thus, the proposed

methodology can be summarized as follows, in algebraic terms of complex voltages at each bus:

$$v_2 = \begin{bmatrix} v_{2_{V1r}} \\ v_{2_{V1i}} \\ \vdots \\ v_{2_{Vnr}} \\ v_{2_{Vni}} \end{bmatrix} \tag{4.3}$$

$$\Rightarrow \quad Bus \Leftarrow \max_{k=1,..,n} \{ \underbrace{| v_{2_{Vkr}} + j v_{2_{Vki}} |}_{v_{2_{V_k}}} \}$$

where $v_{2_{V_k}}$ corresponds to the complex eigenvector associated with the real (r) and imaginary (i) components of the load bus voltages, i.e. $v_{2_{Vkr}}$ and $v_{2_{Vki}}$, for load bus k. The magnitudes of v_{2_V} are ranked in descending order, the largest entries are then used to identify the candidate load buses for placement of shunt FACTS controllers.

4.3.2 Placement Examples

The placement results obtained for the two-area and IEEE 50-machines test systems are summarized, in this section.

Two-area Test System

According to the Hopf bifurcation analysis presented in Section 3.5.2, for the two-area test system, there is a Hopf bifurcation for the base case when the loading factor is around 0.08 p.u. The participation factor analysis shows that the dominant state variables responsible for the Hopf bifurcations are δ and ω of generator 3 (G3).

Figure 4.13, in showing the proposed placement index $|v_{2_{V_k}}|$ for the two-area test system, identifies bus 11 as the best location; here, generator buses are not considered as voltage control is not an issue at these buses. This was confirmed by modal analysis as summarized in Table 4.5. The PST software tool with SVC and STATCOM models shown in Figures 2.5 and 2.12 are used. The controller parameters for the SVC and STATCOM controllers are given in Tables D.2 and D.4, respectively, in Appendix D. The SVC and STATCOM controllers are arbitrarily rated at ± 100 Mvar without the supplementary control loop for damping oscillations; only load buses were considered as possible candidates. In this case, loadability analysis also fortuitously yields bus 11 as a suitable location for a shunt FACTS controller to increase the loading margin of the system.

Table 4.5: Critical eigenvalues with SVC and STATCOM at different locations for two-area test system

Shunt FACTS Location	$\|v_{2_{V_k}}\|$	Critical eigenvalue	
		SVC	STATCOM
11	0.1461	$-0.0345 \pm j3.5836$	$-0.0471 \pm j3.6637$
10	0.1240	$-0.0163 \pm j3.6517$	$-0.0352 \pm j3.8280$
9	0.1094	$-0.0026 \pm j3.4752$	$-0.0150 \pm j3.8101$
8	0.0432	$0.0366 \pm j3.3674$	$0.1253 \pm j3.8074$

IEEE 50-machine Test System

The proposed placement methodology was also applied to the larger IEEE 50-machines test system (Case I). The results obtained in Section 3.5.4 indicate a Hopf bifurcation for the base case at λ=0.009 p.u. The dominant state variables

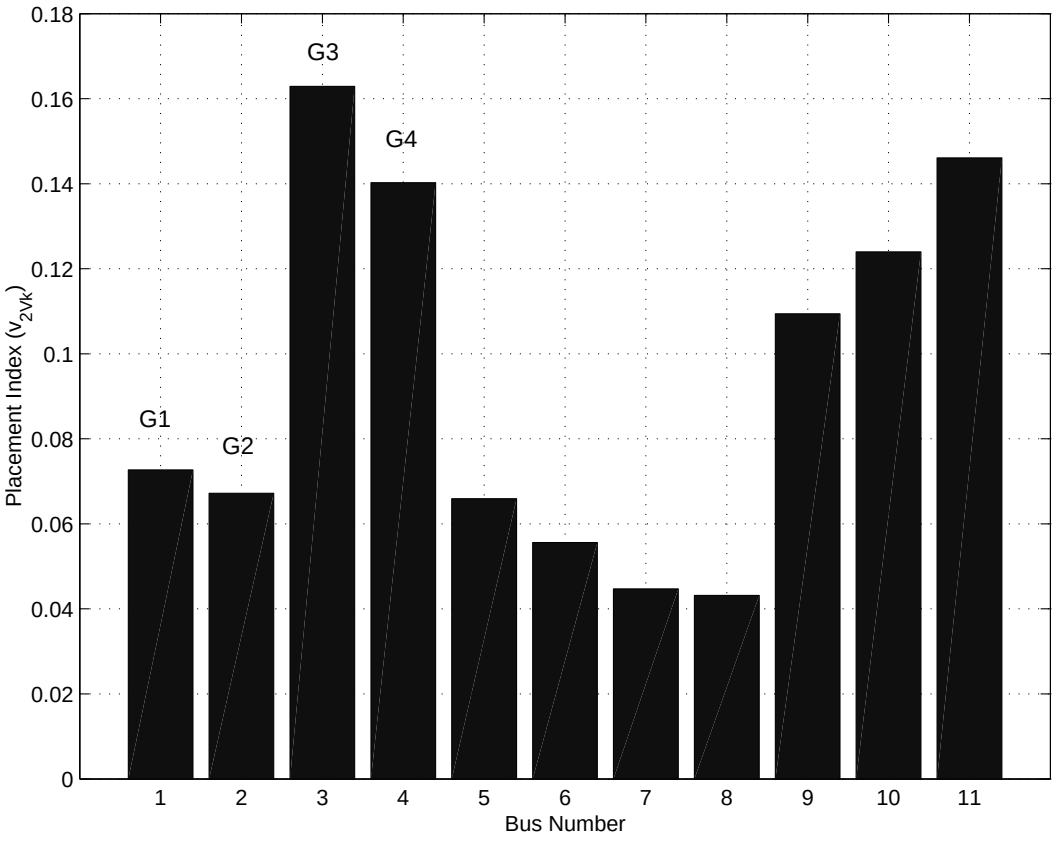

Figure 4.13: Shunt FACTS controller placement index for two-area test system for the base case.

associated with the Hopf bifurcation responsible for the oscillations are δ and ω of the generator at bus 93.

Figure 4.14 shows the placement index results for this test system. According to these results, bus 125 is the best location for a shunt FACTS controller to remove the critical eigenvalues associated with the Hopf bifurcation for the base case. Again the PST software tool is used to obtain these results with a $\pm$ 150 Mvar SVC and STATCOM controllers; the controller data are given in Appendix D.

In order to verify these results, the first seven candidate locations were tested

with SVC and STATCOM controllers; the results are given in Table 4.6, which confirm the placement index. These results were obtained for fixed controller gain and time constant setting in comparing different locations. However, in this case, loadability analysis yields bus 107 as the best location for a shunt FACTS controller to increase the loading margin of the system. Consequently, the best placement for Hopf bifurcation control or oscillation control may not be the same for improving the system loading margin.

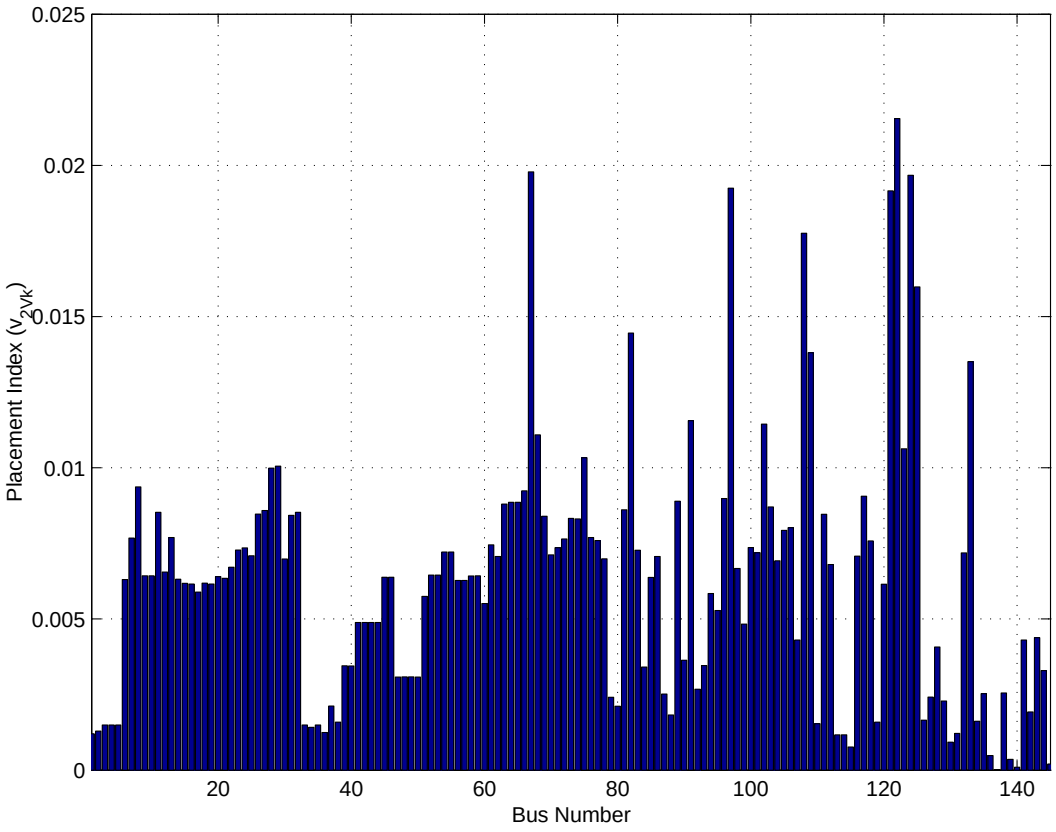

Figure 4.14: Shunt FACTS controller placement index for the IEEE 50-machine test system for the base case.

Table 4.6: Critical eigenvalues with SVC and STATCOM at different locations for IEEE 50-machine test system

Bus	$\lvert v_{2_{V_k}} \rvert$ $\times 10^{-2}$	Critical eigenvalue	
		SVC	STATCOM
125	1.5980	$-0.014 \pm j6.536$	$-0.022 \pm j6.527$
133	1.3450	$-0.006 \pm j6.493$	$-0.018 \pm j6.504$
68	1.0786	$-0.005 \pm j6.480$	$-0.015 \pm j6.501$
123	1.0618	$0.005 \pm j6.481$	$-0.004 \pm j6.491$
75	1.0068	$0.029 \pm j6.433$	$0.020 \pm j6.448$
29	0.9803	$0.016 \pm j6.459$	$0.013 \pm j6.464$
28	0.9736	$0.016 \pm j6.458$	$0.013 \pm j6.464$

4.4 Control Input Signal- General Aspects

For both practical and economical reasons, it is preferable to use locally available control signals. It will be assumed that the combination of remote measurements and communication will be considered only for the most critical circumstances. It is proposed to first considered the most effective control signals without regard to proximity as a useful step before any compromise to minimize the need for communications.

For the PSS controllers, the typical choice of control input signal is the local rotor speed deviation.

The analysis of mode observability can be used to select the effective control signals for the FACTS controller as discussed in [32, 33]. To be able to increase the damping of the critical modes associated with Hopf bifurcation, the selected

signals should have significant observability of the critical modes to be damped. This criterion can be used for selecting the control signals from a range of candidate output signals available at the FACTS controller location.

A similar concept is applied in this thesis to select the best control input signal to damp the oscillatory mode associated with Hopf bifurcation. A line quantities adjacent to the FACTS controller were considered as candidate input signals; typical choices of these signals are real or reactive power flows or line current in each adjacent line. The calculation of the mode observability is follows:

In general, a power system can be approximated by the following linear state equations:

$$\begin{aligned} \dot{X} &= AX + BU \\ Y &= CX \end{aligned} \tag{4.4}$$

where A, B and C are state, input and output matrices, respectively, U is a control vector and Y is the output vector. Assuming $\lambda_i = \pm j\beta$ is the critical mode which is creating an oscillation problem, or the eigenvalue of A of interest,

$$Av_i = \lambda_i v_i$$

$$w_i{}^T A = \lambda_i w_i{}^T$$

If i=j, $w_i{}^T v_j$=1; if $i \neq j$, $w_i{}^T v_j$=0. Also, v_i and $w_i{}^T$ are the left and right eigenvectors of A corresponding to the eigenvalue $\lambda_i = \pm$ jβ, and the mode of observability index OI is defined as:

$$OI = Cv_i = \begin{bmatrix} OI_1 \\ OI_2 \\ \vdots \\ OI_m \end{bmatrix} \tag{4.5}$$

moreover,

$$\Rightarrow \ Best \ \ Signal \Leftarrow \max_{l=1,..,m} \{|OI_l|\}$$

where C is the matrix corresponding to the candidate signals and m is the number of candidate signals. The signal providing the maximum value of OI is considered the most useful.

Similar to the mode observability matrix, a mode controllability matrix can be defined as $v^{-1}B$, which indicates the controllability of the corresponding modes. The mode controllability matrix could be used to select FACTS controller placements, by analyzing the magnitude of the elements in the mode controllability matrix. However, this methodology requires extensive computations as compared to the new methodology proposed in Section 4.3.1.

4.5 Hopf Bifurcation Control for the IEEE 50-machine Test System

For the IEEE 50-machine system (Case I), PSS, SVC, and STATCOM controllers were considered for the control of the oscillations associated with Hopf bifurcations. This system was used to test the proposed placement technique for shunt-FACTS controller augmented by consideration of the effect of various control input signals in the transient response of the system. For the stability studies, PST software was used. A TCSC model was not considered here because it is not supported by the PST software tool.

All the stability results related to the IEEE 14-bus test system were obtained with MASS and ETMSP as explained in Section 4.2. MASS does not produce the outputs needed for the calculation of the proposed placement and control input

signal techniques. Since, the oscillation in the IEEE 14-bus test system could not be reproduced by the PST, due to the modeling differences, the above mentioned techniques were not applied to the IEEE 14-bus test system.

Figure 4.15 shows P-V curves for the base case and two different contingencies (lines 90-79 and 90-92). Hopf bifurcations can be observed in all the cases. These P-V curves were obtained for a specific load and generation pattern. All the loads in the system were increased by a factor of λ according to (2.3) and the required generation was shared among all the generators in proportion to their initial dispatches. The current operating conditions are assumed to correspond to a value of $\lambda = 0.002$ p.u. The operating load line depicted on Figure 4.15 defines the steady state points for the base system topology and two contingencies under consideration, assuming that the load is being modeled as a constant impedance in the transient stability studies.

As can be seen from the P-V curves in Figure 4.15, a Hopf bifurcation is triggered by a line 90-92 outage. In order to study the system effect of this bifurcation, a time domain simulation was performed for the corresponding contingency at the given operating conditions. Thus, Figure 4.16, shows how the Hopf bifurcation leads the system to an oscillatory unstable condition, as expected.

4.5.1 PSS Controller Aspects

The dominant state variables related to the Hopf bifurcation mode, which are responsible for the oscillation, were identified through a participation factor analysis. The state variables of the machines associated with the Hopf bifurcations for the base case and a line 90-92 outage together with the corresponding participation factors are shown in Table 4.7.

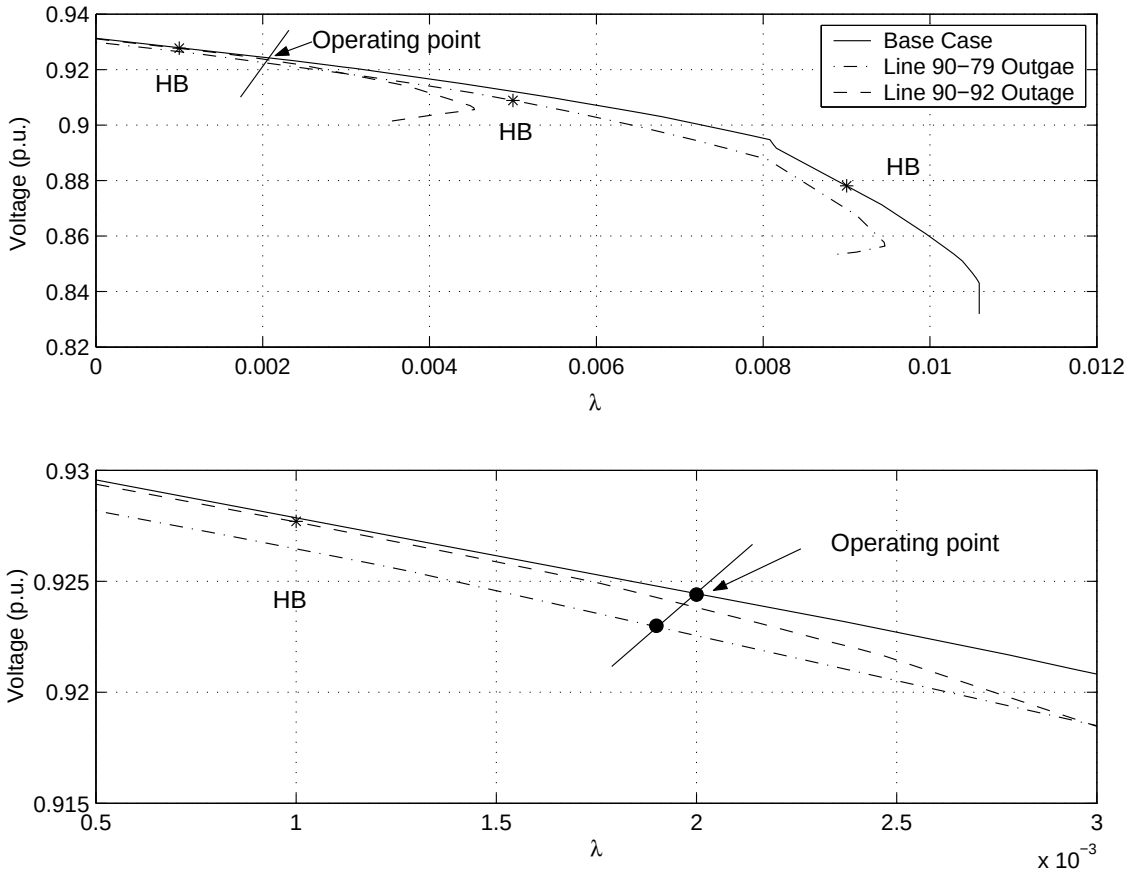

Figure 4.15: (a) P-V curves at bus 92 for different contingencies; in the IEEE 50-machine test system (b) enlarged P-V curves around the operating point.

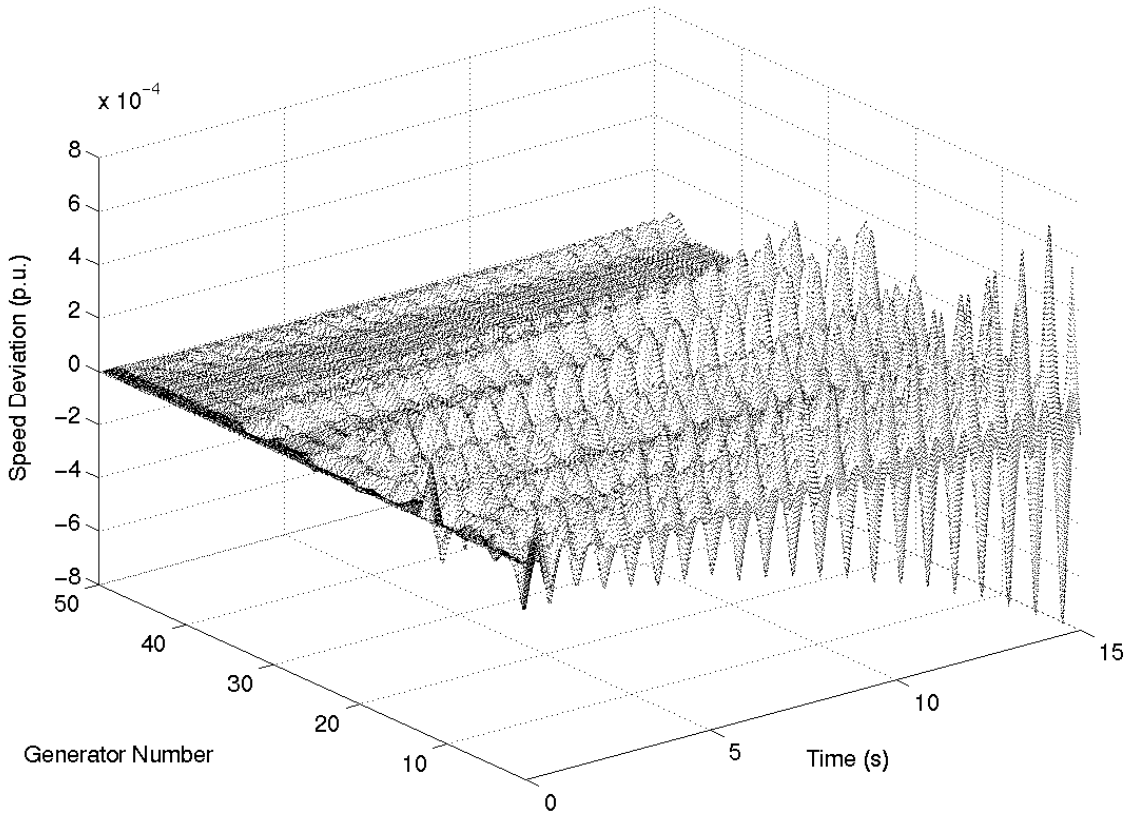

Figure 4.16: Oscillations due to a Hopf bifurcation in IEEE 50-machine test system triggered by line 90-92 outage at λ=0.002 p.u.

Table 4.7: Participation factor analysis for the IEEE 50-machine test system

Base Case			Line 90-92 outage		
State	Bus	P. Factor	State	Bus	P. Factor
ω	93	1.0000	δ	104	1.0000
δ	93	1.0000	ω	104	1.0000
E'_q	93	0.3452	E'_q	104	0.1715
ω	124	0.1734	δ	111	0.2622
δ	124	0.1728	ω	111	0.2622
Ψ''_q	93	0.1720	δ	121	0.1713
ω	121	0.1206	ω	121	0.1709

Observe that the line 90-92 outage yields a different critical mode than for the base case. Thus, in the base case, bus 93 would be chosen as the best candidate for a PSS; however, this will not help in removing the oscillatory problem triggered by the line 90-92 contingency, since for the latter bus 104 would be the best location for a PSS. This is corroborated by time domain analyses where the introduction of a PSS at generator bus 93 removed the Hopf bifurcation in the base case, but it did not remove the Hopf bifurcation problem triggered by a line 90-92 outage, as shown in Figure 4.17. By adding a second PSS at bus 104, the instability generated by the line 90-92 outage was removed; this is clearly demonstrated by the results depicted in Figures 4.17 and 4.18.

It is important to mention that for these tests, only certain oscillation modes and contingencies were considered so that only two of these controllers were introduced. In practice, PSS's would be considered for all generators with fast static exciters; for the given test system it would correspond to 7 generators.

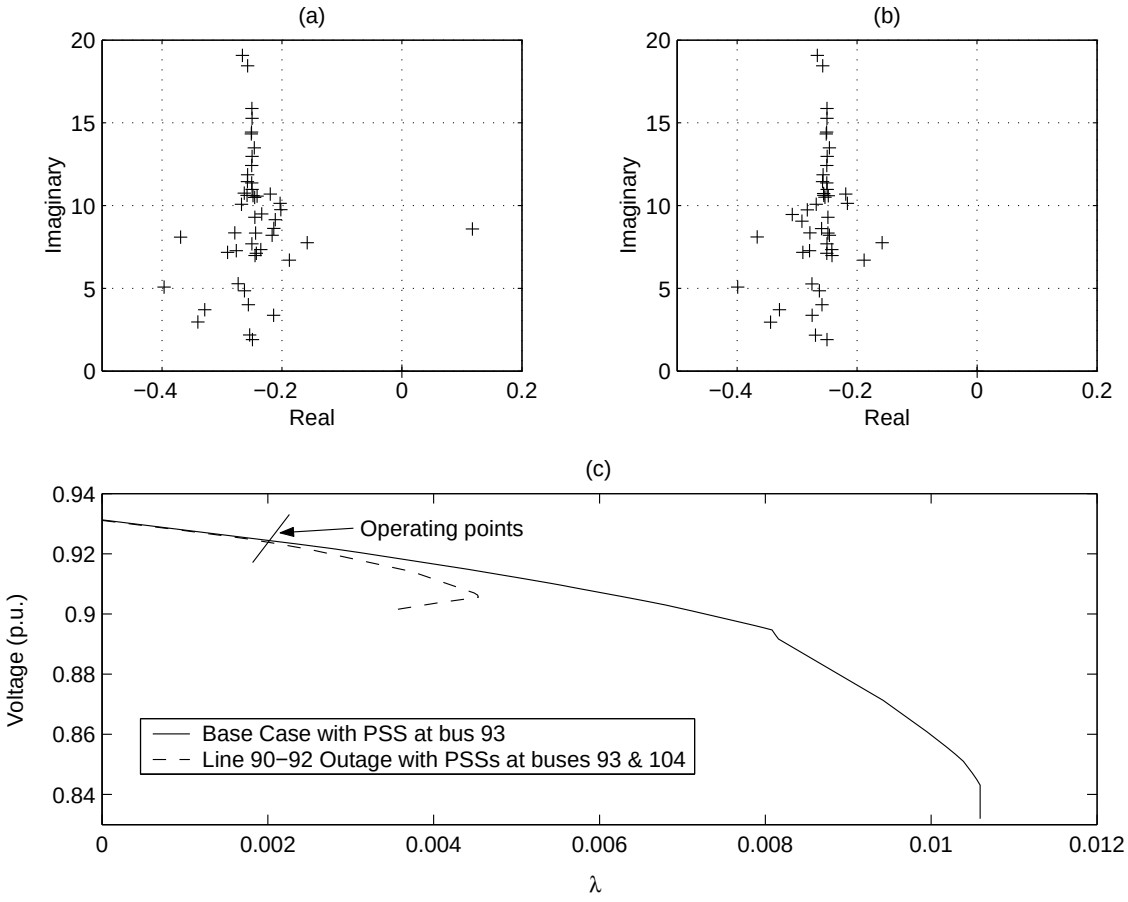

Figure 4.17: Line 90-92 outage for the IEEE 50-machine test system for λ=0.002 p.u. (a) Some eigenvalues with PSS at bus 93; (b) eigenvalues with PSS's at bus 93 and 104; (c) P-V curves at bus 92.

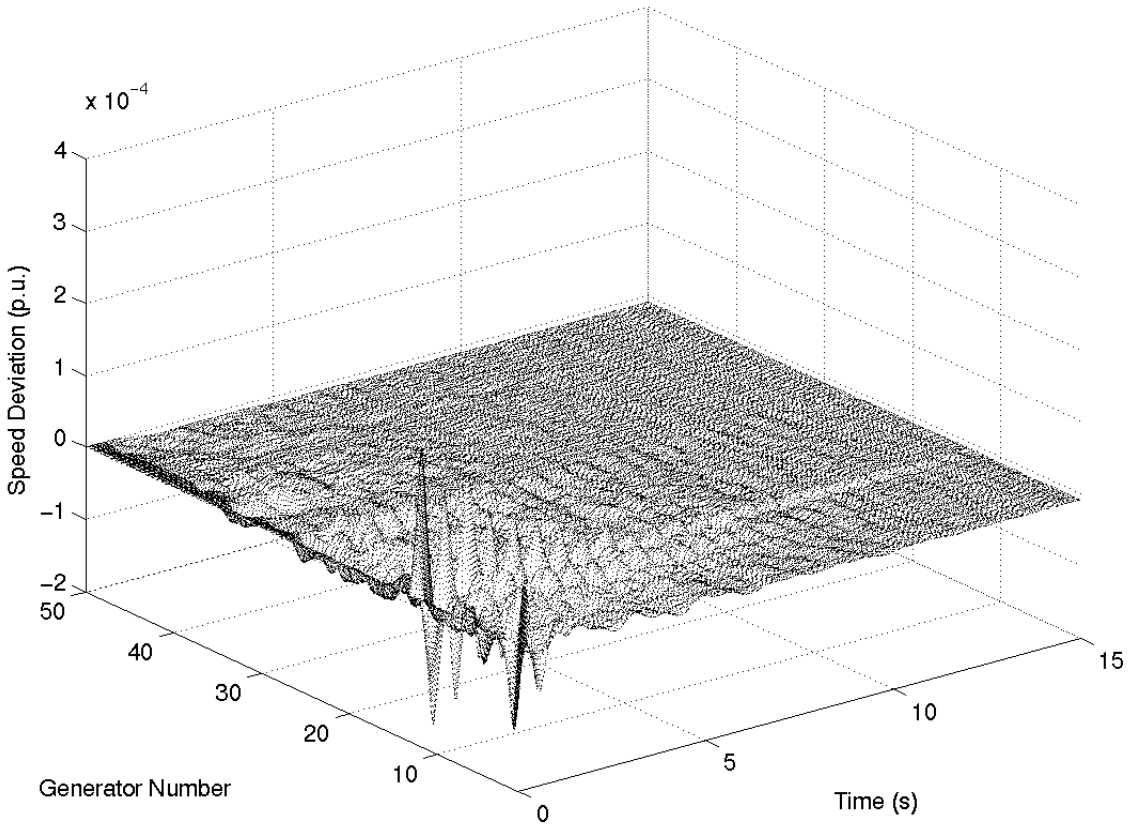

Figure 4.18: Oscillation damping with PSS's at bus 93 and 104 for a line 90-92 outage in IEEE 50-machine test system at λ=0.002 p.u.

4.5.2 Test of SVC and STATCOM Placement and Control

SVC and STATCOM controllers were considered to control system oscillations due to Hopf bifurcations. The control models of SVC and STATCOM with supplementary control input signals for oscillation damping used here are given in Figures 2.5 and 2.12. The rating of the controllers and the parameters used are similar to the ones used in the Section 4.3. The placement technique introduced in section 4.3 was used to determine a suitable location of both shunt FACTS controllers considered in turn. The placement results are listed in Table 4.6; bus 125 emerges as the best location for a shunt-FACTS controller to control the oscillation associated with Hopf bifurcation.

Figure 4.19 shows P-V curves for SVC and STATCOM controllers located at bus 125, showing that the Hopf bifurcation can be removed for the base case. Observe that the loadability margin for the system does not increase significantly because loadability analyses yield bus 107 as the best location to maximize system loadability. Also, a modest var control range is needed. Table 4.8 shows the maximum loadability margins for different system conditions and controllers under study. Notice, the SVC and STATCOM controllers increase system loadability by 136% when the contingency is applied.

Figure 4.20 shows the eigenvalue plot with SVC and STATCOM controllers at bus 125, and the corresponding P-V curves for the line 90-92 outage case.

The SVC and STATCOM perform well for the given contingency, even though the optimal placement in this case should be bus 77 based on the proposed placement technique. The P-V curves show that both the static loading margin and the dynamic stability margin (margin between the current operating point and the Hopf bifurcation point) increase when SVC and STATCOM controllers are introduced.

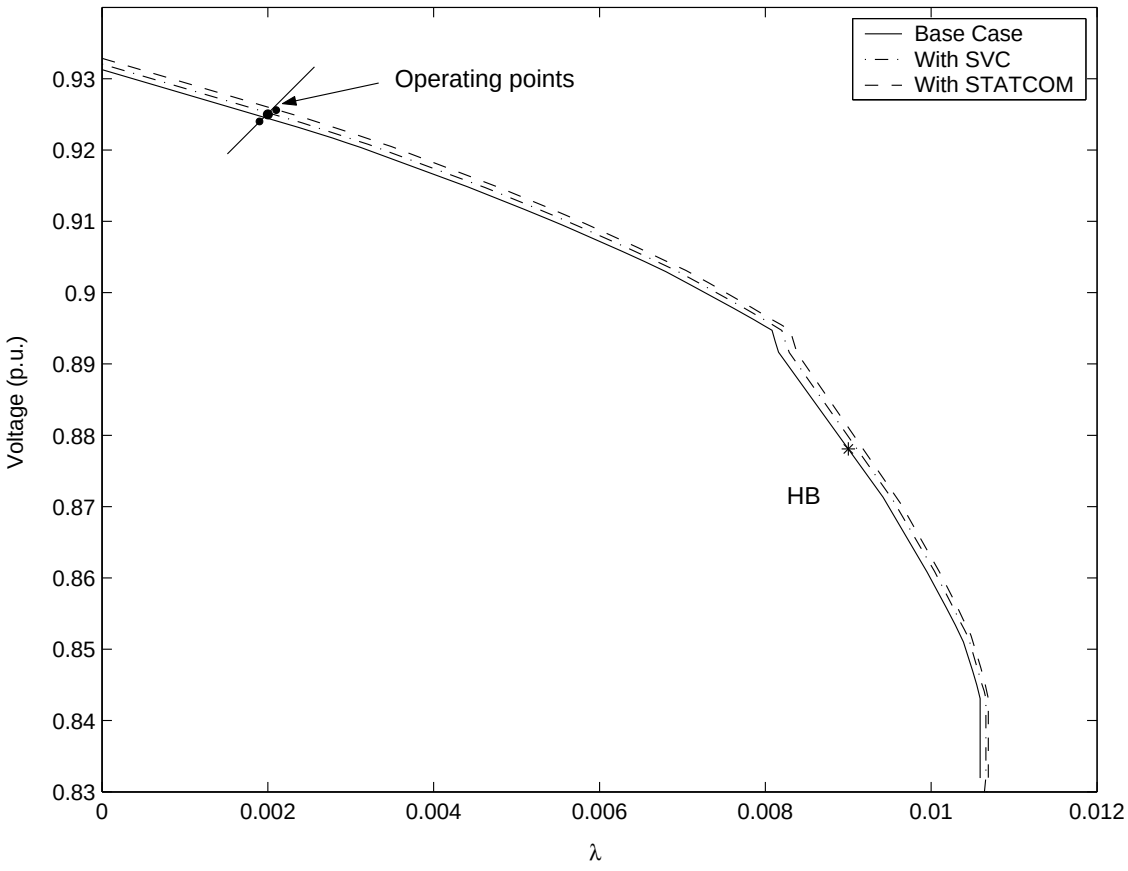

Figure 4.19: P-V curves at bus 92 with SVC and STATCOM controllers at 125 for the IEEE 50-machine test system at the base case.

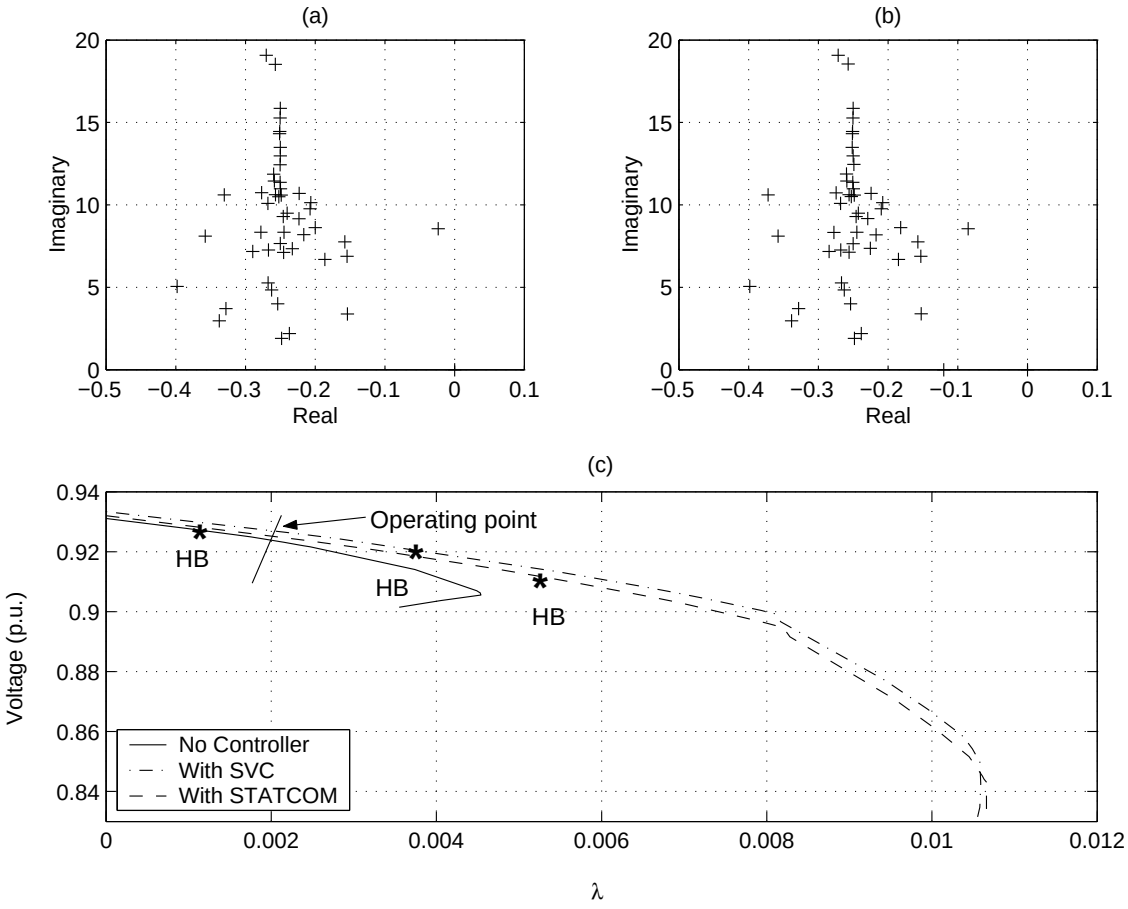

Figure 4.20: Line 90-92 outage in the IEEE 50-machine test system: (a) Some eigenvalues with SVC; (b) eigenvalues with STATCOM; (c) and P-V curves at bus 92 with SVC and STATCOM.

Table 4.8: Static loading margins for different controllers for the IEEE 50-machine test system

Controllers	Maximum Loading Margin (p.u.)	
	Base Case	Line 90-92 outage
no controller	0.01059	0.00454
PSS	0.01059	0.00454
SVC at 125	0.01066	0.01059
STATCOM at 125	0.01069	0.01066
SVC at 107	0.01069	0.01061
STATCOM at 107	0.01078	0.01071

The damping introduced by the SVC and STATCOM controllers with basic control is lower than that provided by the PSS's (see Figures 4.17 and 4.20). Hence, supplementary control signals were introduced to enhance damping, using mode observability indices to identify the best supplementary control signal as explained in Section 4.4. Table 4.9 shows the mode observability indices obtained for different control input signals from the adjacent lines, and that real power (P) flow in line 67-125 is the best choice. This was confirmed by time domain simulation as illustrated in Figures 4.21 and 4.22.

The best oscillation damping is obtained with the PSS controller, as expected, in directly controlling the state variables in the generator, exhibiting the oscillation. SVC and STATCOM controllers also damping the oscillation associated with Hopf bifurcation. They also increase the maximum loading margin of the system, especially in contingency condition. The STATCOM provides better damping than the SVC, which is to be expected, as this controller is able to transiently modulate

Table 4.9: Supplementary control input signals for the SVC and STATCOM controllers for the IEEE 50-machine test system

Line	Signal	OI	Line	Signal	OI
67-125	I	1.0955	121-125	I	0.3269
	P	1.1099		P	0.3319
	Q	0.5473		Q	0.0165
125-132	I	0.6656	122-125	I	0.1090
	P	0.6809		P	0.1123
	Q	0.1075		Q	0.0165

active power.

4.6 Summary

Following the preliminary test example, a new technique for the placement of shunt-FACTS controller is presented together with two examples of application of the proposed technique to damp the oscillation associated with Hopf bifurcations. A methodology to select the best control input signal for the shunt-FACTS controllers is also presented using the Mode Observability Technique. Finally, Hopf bifurcation control is demonstrated in IEEE 50-machine test system using the PSS, SVC and STATCOM controllers, including the application of all the proposed techniques.

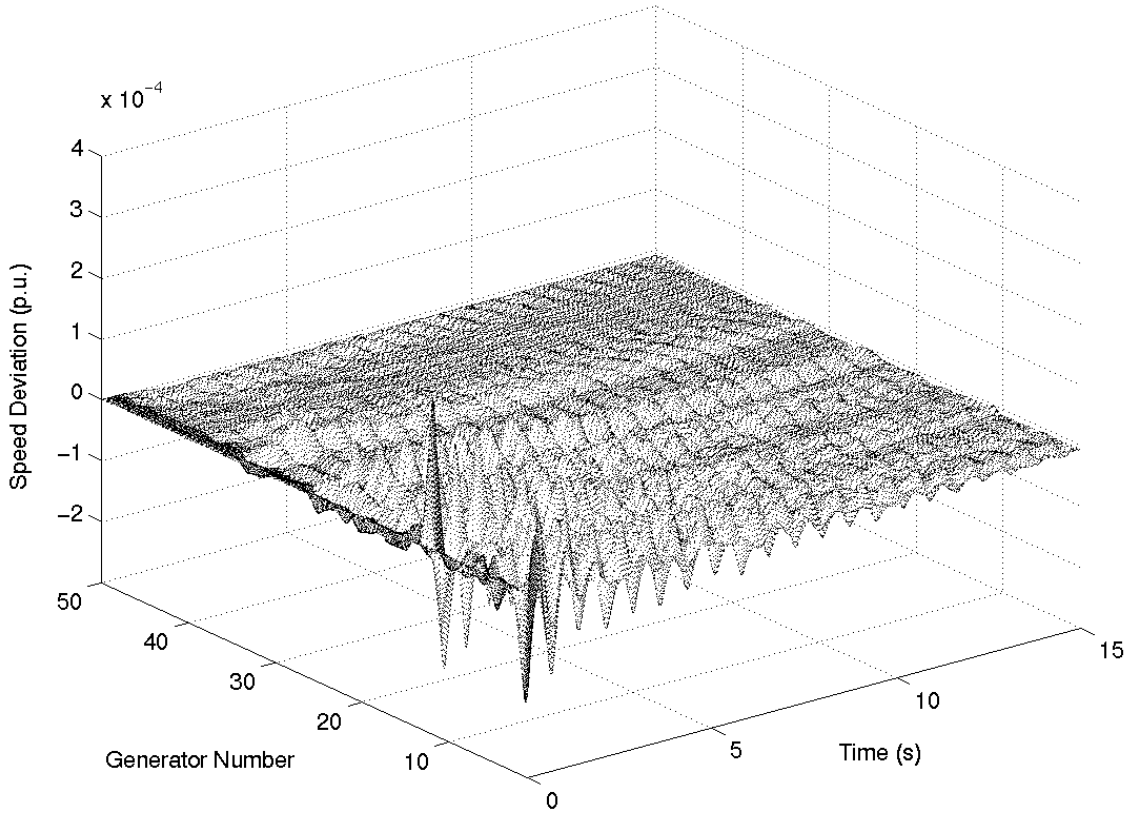

Figure 4.21: Oscillation damping with SVC and supplementary control loop for line a 90-92 outage at $\lambda = 0.002$ p.u. for the IEEE 50-machine test system.

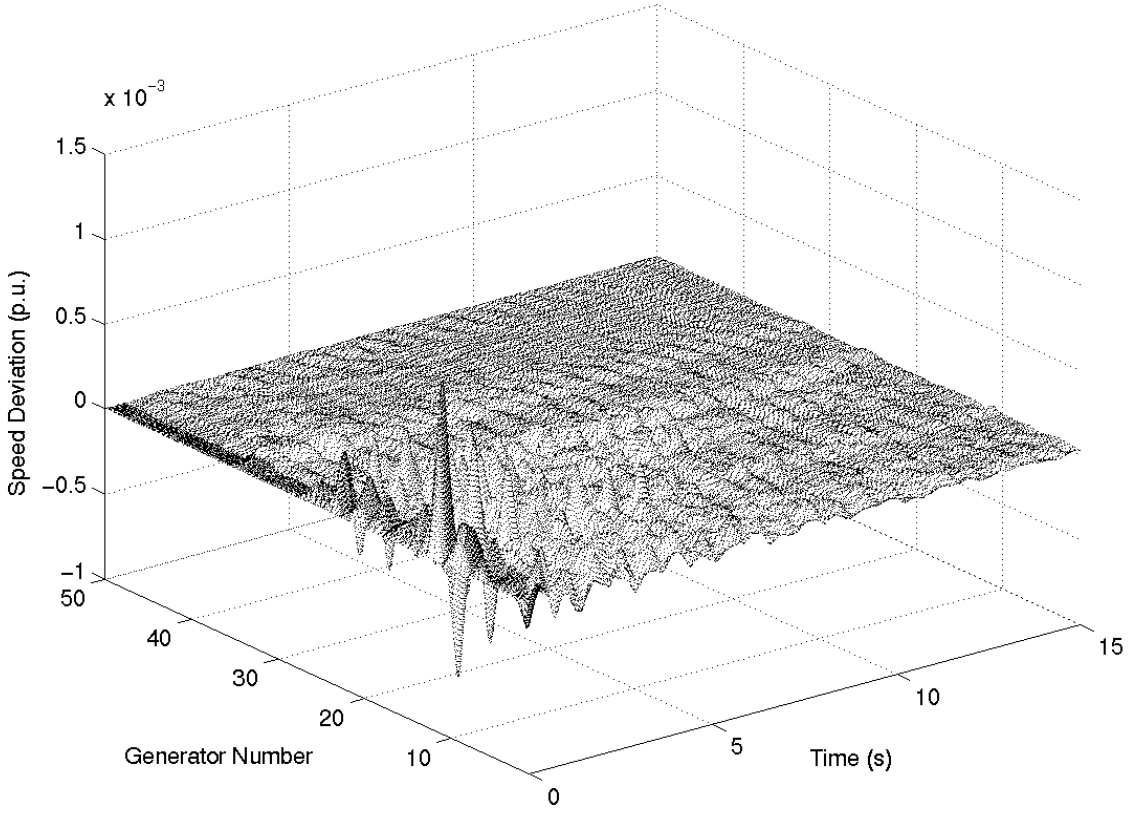

Figure 4.22: Oscillation damping with STATCOM and supplementary control loop for a line 90-92 outage at $\lambda = 0.002$ p.u. for the IEEE 50-machine test system.

Chapter 5

CONTROLLER PERFORMANCE AND INTERACTIONS

5.1 Introduction

Power system controllers play a vital role in improving the dynamic performance of power systems. For a stable and economic operation of a power system, these controllers should perform well at different operating conditions associated with varying load levels, and faults. These controllers are typically introduced and/or tuned to avoid instabilities in the system [16]. For example, in the case of a Hopf bifurcation, controllers may be tuned to bring the complex mode associated with the Hopf bifurcation back to the open left-half plane. However, the tuning process should be carried out with care, as certain gain values could actually worsen the situation. Furthermore, in the case of having multiple controller, tuning of one

controller could lead to problems with other controllers located in the same region; these interactions may enhance or trigger other oscillatory modes in the system [63].

In this chapter, tuning of PSS, SVC and TCSC controllers and their performance, including additional benefits, under a wide range of loading conditions and faults are studied and discussed using the IEEE 14-bus test system. Possible negative impact on the system dynamic performance or undesirable interactions among various types of controllers, as well as the effect that tuning one controller has on another controller in the same area, are studied and discussed.

5.2 Controller Performance

The effects of controller gain tuning on Hopf bifurcations, as well as the system overall performance are studied and discussed in this section. The performance of these controllers under a wide variety of operating conditions that include credible contingencies is also compared. The eigenvalue analysis and the time domain simulation results are obtained using the MASS and ETMSP analytical tools, respectively.

Figure 5.1 depicts the IEEE 14-bus test system with PSS, SVC and TCSC controllers. These controllers are placed at their best locations for controlling Hopf bifurcation in the system; these locations were chosen based on the maximum damping on the critical mode associated with the Hopf bifurcation as described in Chapter 4. In order to compare performance of the controllers in the system, simulations were first carried out with one controller at a time. The results are discussed below.

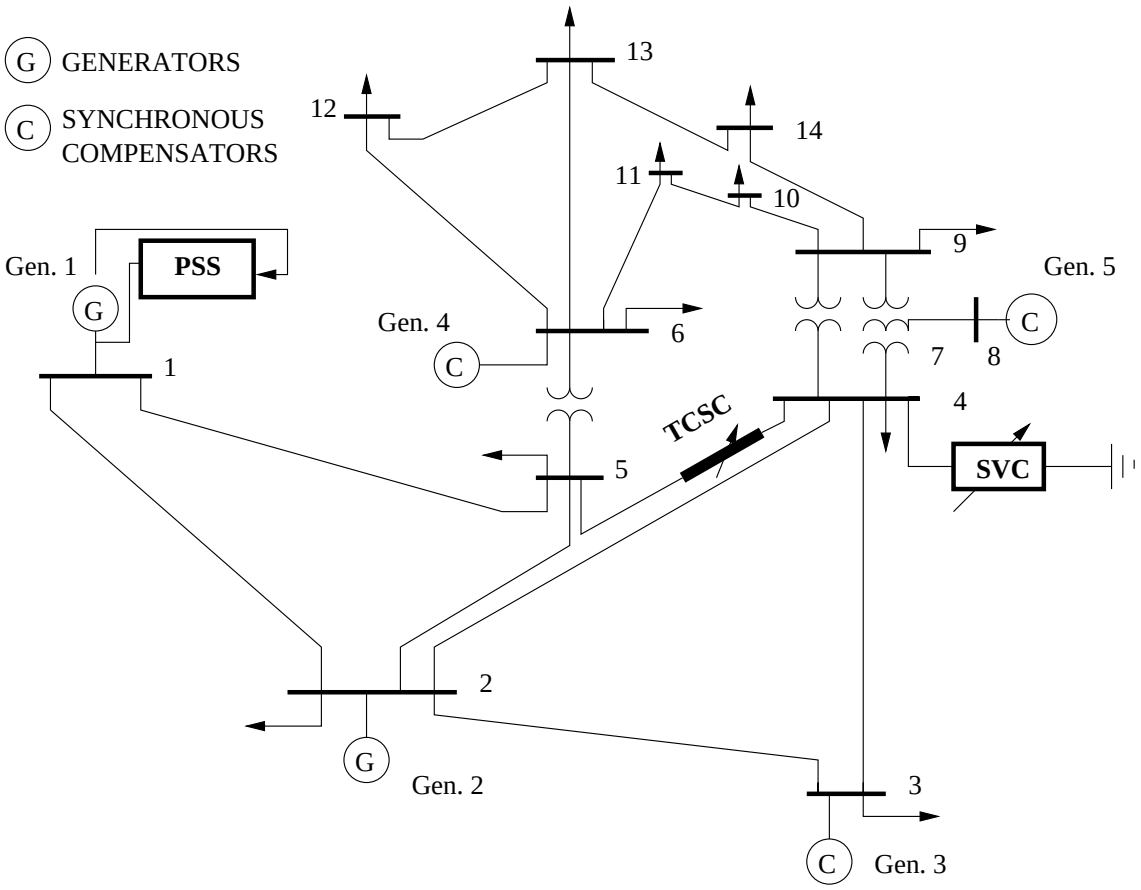

Figure 5.1: IEEE 14-bus test system with different controllers.

5.2.1 PSS

The PSS controller gain was varied and the movement of some eigenvalues was traced at the Hopf bifurcation point for the base case i.e. for load factor λ=0.47. Figure 5.2 shows the locus of these eigenvalues, the electromechanical modes in particular, for variations in the PSS controller gain K_{PSS}. It is seen that as K_{PSS} is increased, the damping of the critical mode associated with the Hopf bifurcation increases; damping of the electromechanical mode associated with generator 2 decreases after reaching a maximum value; and a complex mode with very low frequency has crossed the imaginary axis and moved into the right-half plane.

A time domain simulation was carried out to see the effect of the complex mode on the system dynamic performance for a line 2-4 outage. The system becomes oscillatory unstable, as shown in Figure 5.3; a participation factor analysis reveals that the dominant state variables related to this mode are associated with generator 1.

Table 5.1 shows the static and dynamic loading margins with PSS for different cases. Both margins are the same for all cases i.e. the PSS controller removes the Hopf bifurcation completely. However, there is no improvement in the static loading margin of the system when compared with no PSS controller case (see Figures 4.1 and 4.4).

Voltage profiles of some buses 2, 4, 5, 12 and 14 during the transient without and with the PSS controller for a line 2-4 outage at $\lambda = 0.4$ are shown in Figures 5.4 and 5.5, respectively. These results were obtained for a PSS controller gain setting that gives maximum damping on the critical mode associated with the Hopf bifurcation. Observe that during the transient, the voltages at some buses drop about 11-15%, before they recover to the steady state values after 24 seconds.

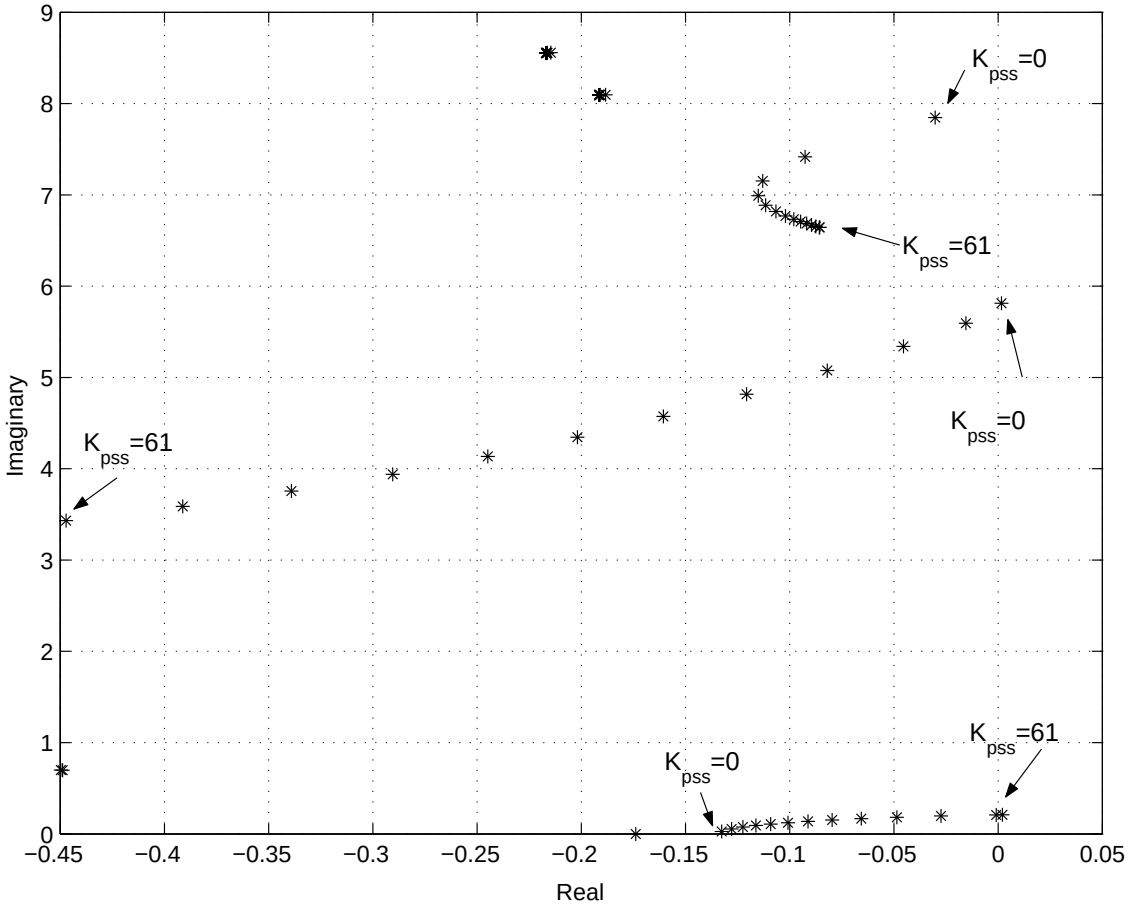

Figure 5.2: Locus of some eigenvalues vs. PSS gain at the base case Hopf bifurcation point (λ=0.47).

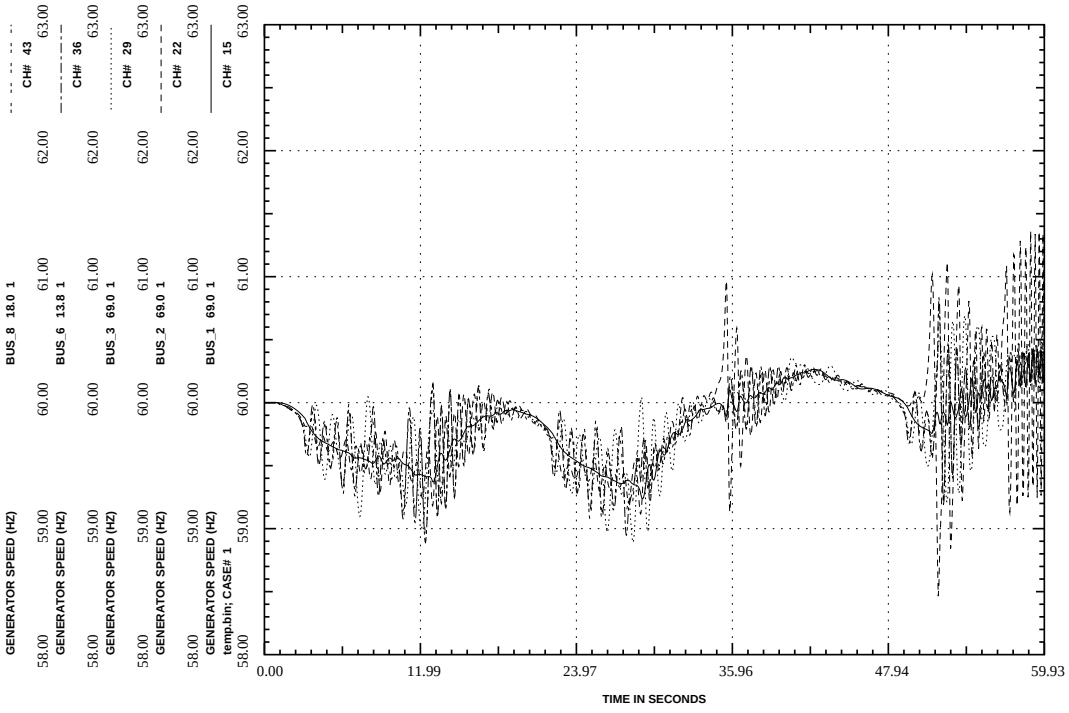

Figure 5.3: Generator frequency plot for a line 2-4 outage with PSS for K_{PSS}=61 (λ=0.47).

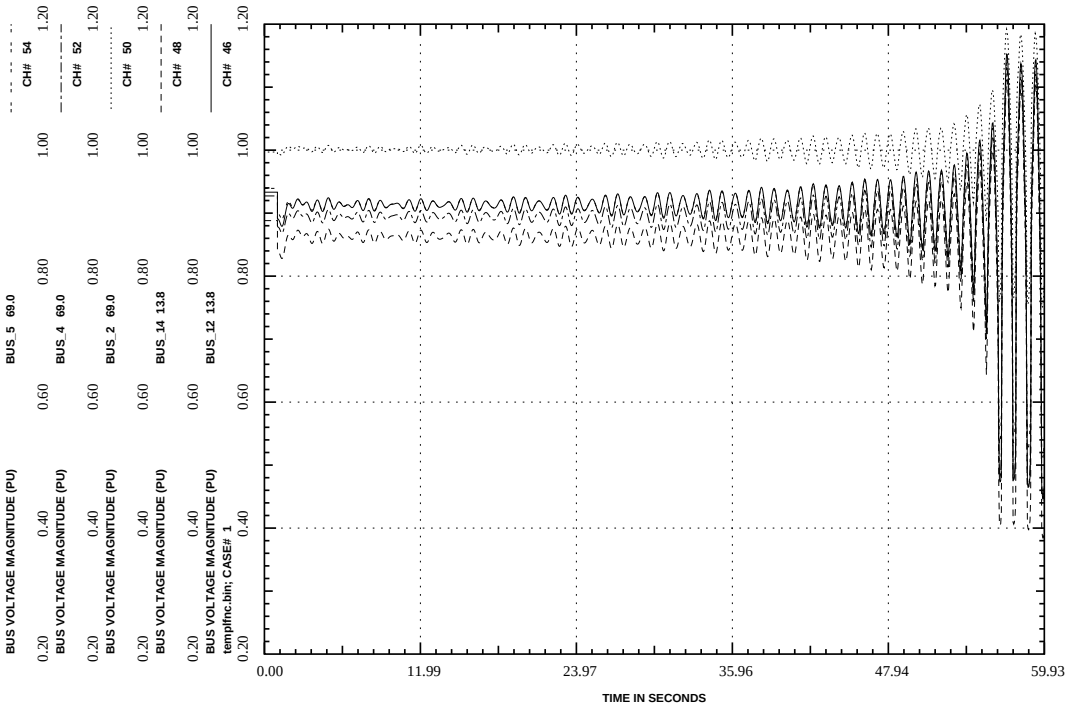

Figure 5.4: Voltage profiles for a line 2-4 outage with no controllers (λ=0.4).

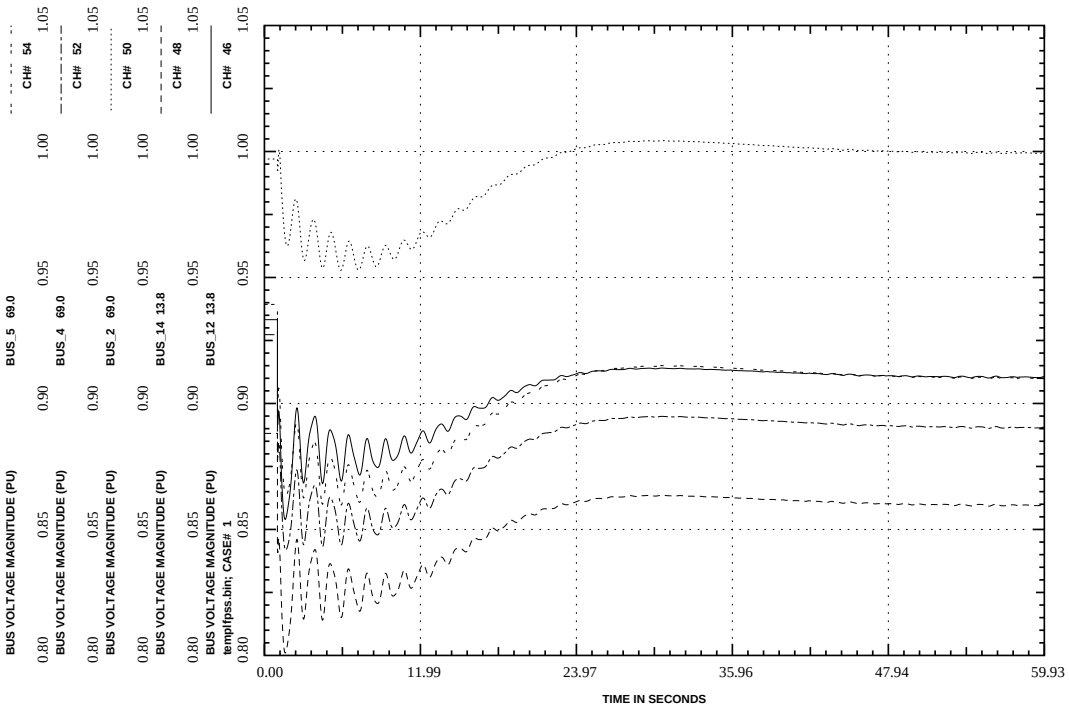

Figure 5.5: Voltage profiles for a line 2-4 outage with PSS for K_{pss}=20 (λ=0.4).

Table 5.1: Static and dynamic loading margins with PSS

Different Cases	Loading Margins (p.u.)	
	Static	Dynamic
Base Case	0.68	0.68
Line 2-4 Outage	0.51	0.51
Line 2-3 Outage	0.25	0.25

5.2.2 SVC

The SVC controller gain was varied to observe the effect on the Hopf bifurcation and the system overall performance. Figure 5.6 shows the locus of some eigenvalues with respect to the SVC main controller gain K_{SVC}. Most of the electromechanical modes move to the left as K_{SVC} increases. However, an increase in the SVC supplementary control gain Ka_{SVC} creates problems as depicted in Figure 5.7, since a complex mode associated with the SVC controller itself crosses the imaginary axis at Ka_{SVC}=0.26 with a frequency approximately 11 Hz. The effect of this complex mode on the system dynamic performance for a line 2-4 outage is shown in Figure 5.8. Tuning the supplementary control gain above 0.26 is problematic as the system goes oscillatory unstable for the line 2-4 outage as shown in the Figure 5.8.

With appropriate gain settings (bellow the problematic gain), the supplementary control in the SVC controller can play a vital role in improving the performance of the SVC. Thus, Table 5.2 shows the dynamic loading margins of the system with the SVC with and without a supplementary control, for the base and line (2-4 and 2-3) outage cases. It is clear that the dynamic loading margins of the system are significantly increased (upto the maximum static loading margins; see Figure 4.8) with the introduction of the supplementary control input signal in the SVC

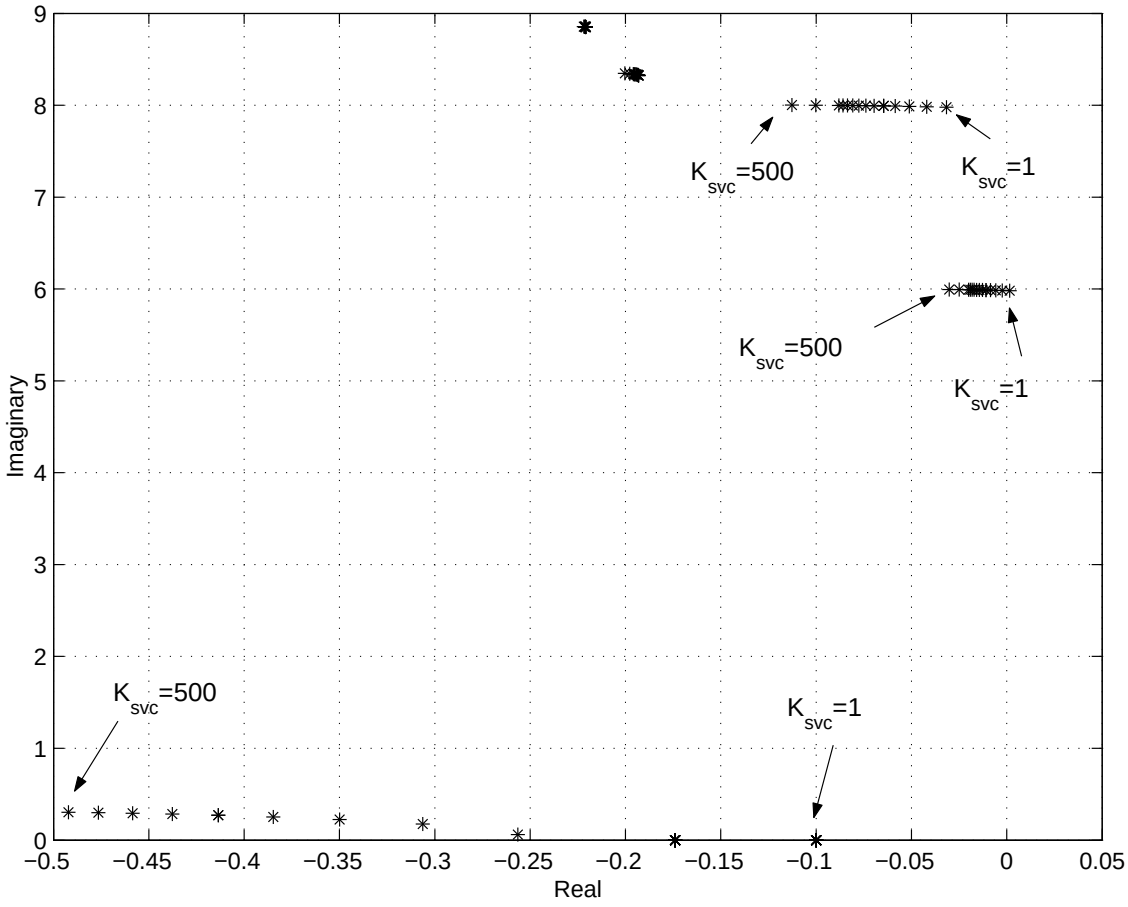

Figure 5.6: Locus of some eigenvalues vs. SVC gain, at the base case Hopf bifurcation point (λ=0.47).

controller.

Voltage profiles of some buses 2, 4, 5, 12 and 14 in the system during the transient generated by a line 2-4 outage are shown in Figure 5.9. Notice that the SVC controller increases the overall system steady state voltages (2-3%) as well as allowing the system voltages to recover much faster than in the case of the PSS controller shown in Figure 5.5. The voltages drop about 5-6 % before they recover after 12 seconds, during the transient.

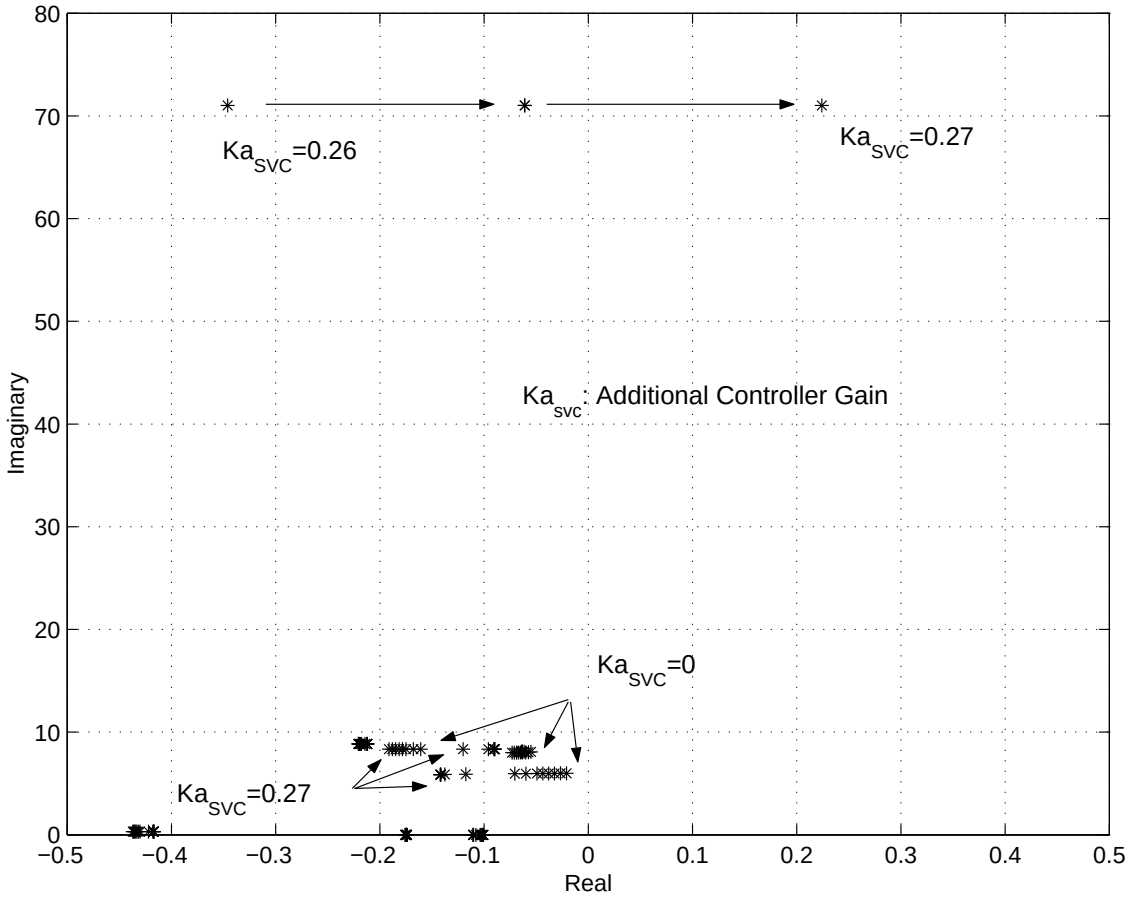

Figure 5.7: Locus of some eigenvalues vs. SVC supplementary control gain, at the base case Hopf bifurcation (λ=0.47).

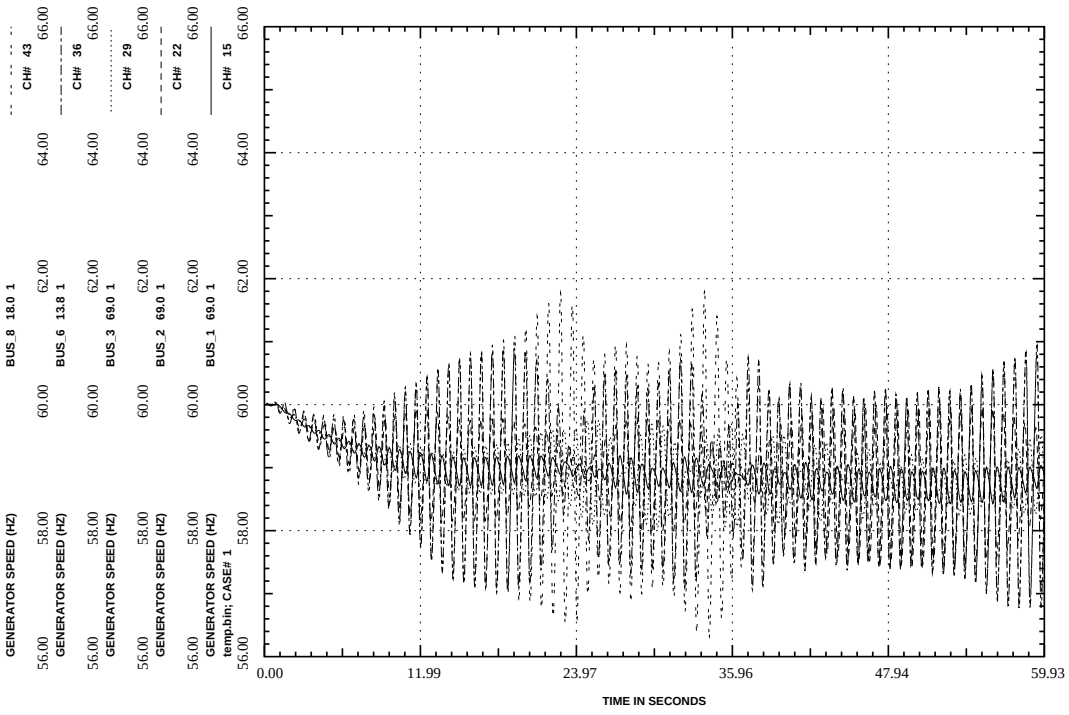

Figure 5.8: Generator frequency plot for a line 2-4 outage with SVC for Ka_{SVC}=0.26 (λ=0.47).

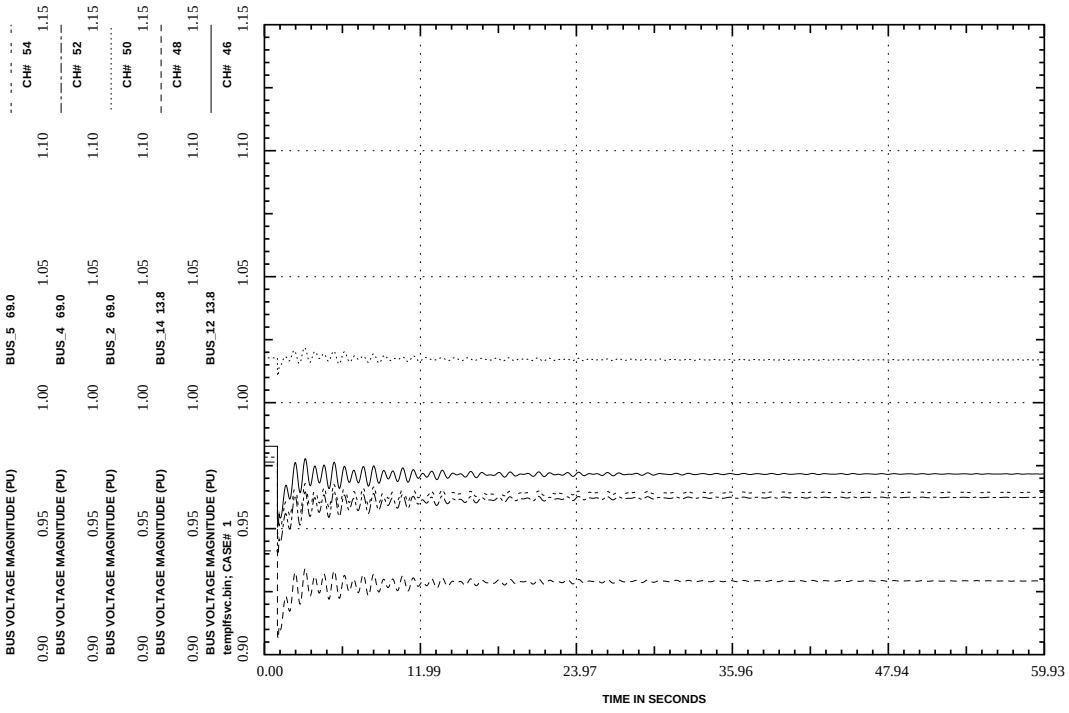

Figure 5.9: Voltage profiles for a line 2-4 outage with SVC for K_{SVC}=400 and Ka_{SVC}=0.06 (λ=0.4).

Table 5.2: Dynamic loading margins with SVC

Different Cases	Dynamic Loading Margins (p.u.)	
	no Supp. Control	with Supp. Control
Base Case	0.72	0.82
Line 2-4 Outage	0.57	0.65
Line 2-3 Outage	0.31	0.38

5.2.3 TCSC

The TCSC controller gain K_{TCSC} was varied to observe its effect on the system critical eigenvalues. Thus, as the gain is increased, the eigenvalue associated with the Hopf bifurcation at the base case loading conditions moves to the left; however, a complex mode associated with the TCSC crosses the imaginary axis as shown in Figure 5.10 for K_{TCSC}=7.8.

Static loading margin and dynamic loading margin of the system with the TCSC controller are given in the Table 5.3. As can be seen from the table the TCSC increases both stability margins of the system. However, the TCSC controller could not remove the Hopf bifurcation completely as in the case of PSS and SVC controllers.

Figure 5.11 shows the voltages profile of some buses 2, 4, 5, 12 and 14 with the TCSC controller for a line 2-4 outage. These results are comparable to the results obtained with the SVC controller (Figure 5.9), i.e. voltages at some buses drop only 5-6% before they recover after 12 seconds. Notice, the overall steady state voltage improves (1-1.5%) to results in an increase in the static loading margin.

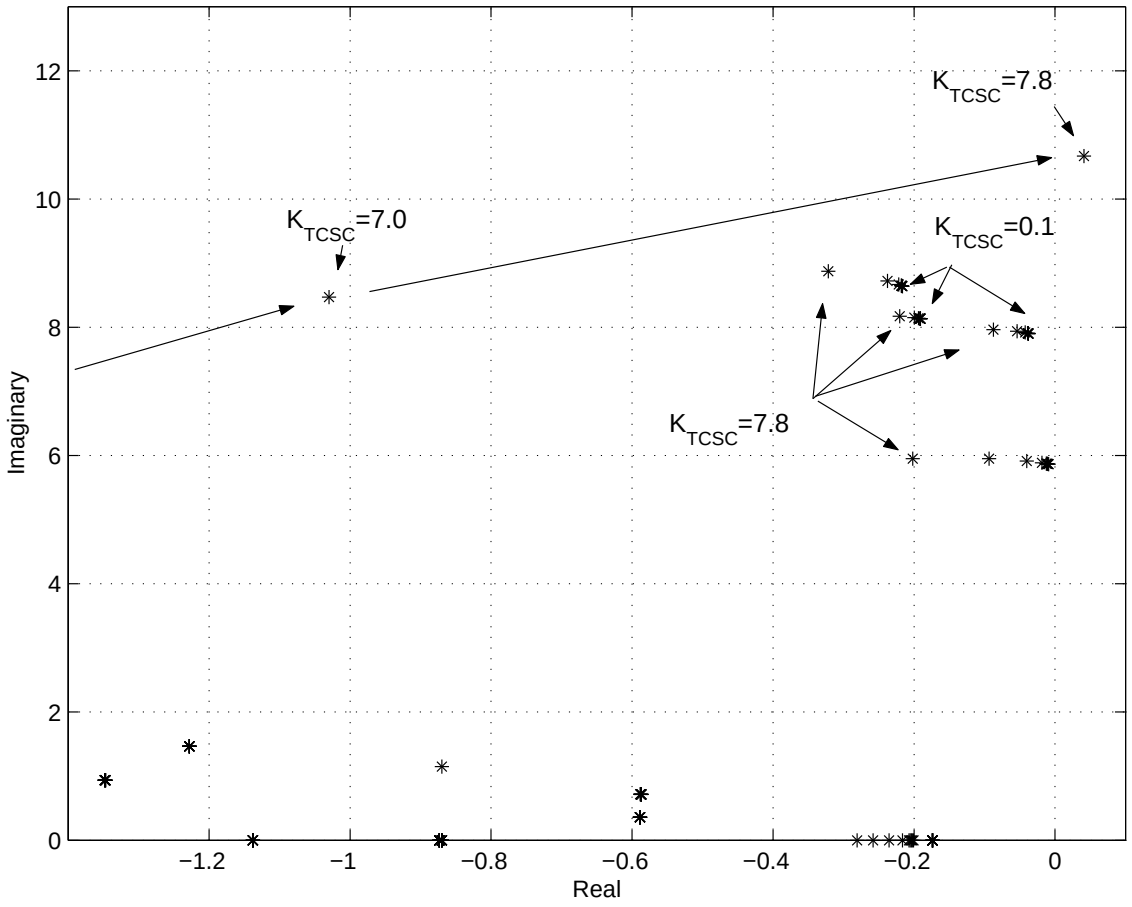

Figure 5.10: Locus of some eigenvalues vs. TCSC gain the base case Hopf bifurcation point (λ=0.47).

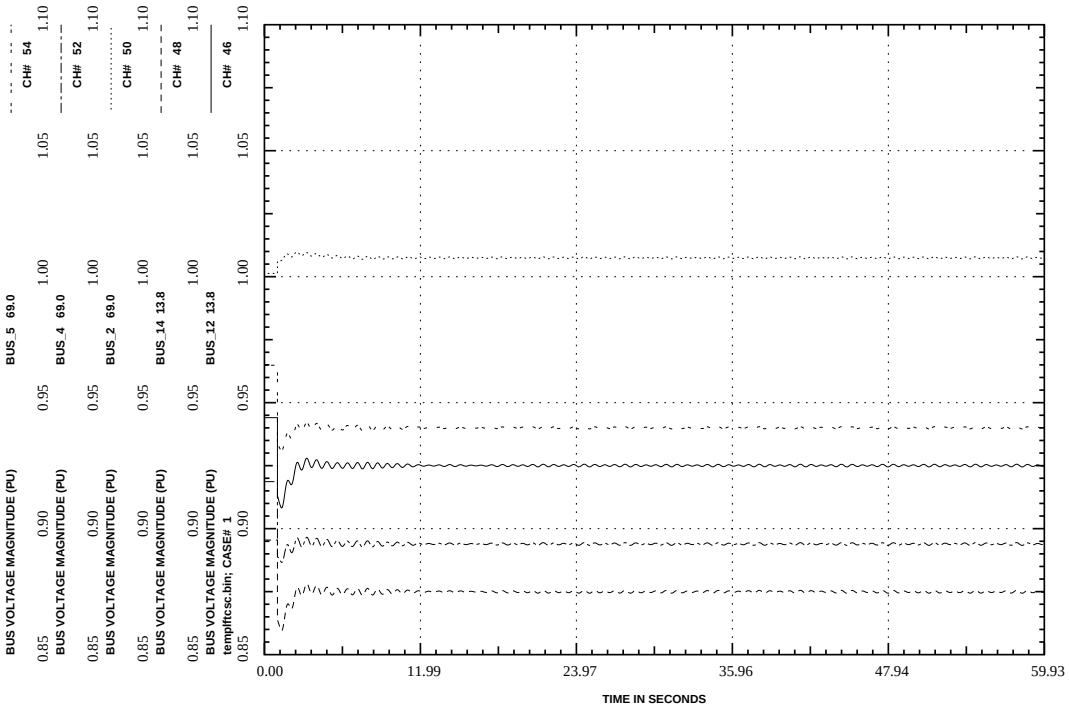

Figure 5.11: Voltage profile for a line 2-4 outage with TCSC for K_{TCSC}=1.0 (λ=0.4).

Table 5.3: Static and dynamic loading margins with TCSC

Different Cases	Loading Margins (p.u.)	
	Static	Dynamic
Base Case	0.74	0.68
Line 2-4 Outage	0.62	0.55
Line 2-3 Outage	0.34	0.32

5.2.4 Comparison of Performance

Performance of these controllers with respect to a three-phase fault on line 2-4 and a sudden load change at bus 9 were also studied at the Hopf bifurcation point associated with the base case loading. Table 5.4 shows the maximum sudden load increase (SLI) as a percentage of the load at that bus that the system can withstand at bus 9, which is the 5th weakest bus in the system, before losing stability. This table also shows the maximum fault clearing time (MFCT) for a three-phase fault at the middle of the line 2-4 for various controllers. The fault was cleared by disconnecting line 2-4. The SLI studies were carried out for different load buses, but only the worst case scenario results are reported here. Table 5.4 indicates that both the PSS and SVC have a markedly superior performance with regard to SLI and MFCT.

Static and the dynamic loading margins with various controllers are compared in Table 5.5 for different outage cases to show that each controller increases the system dynamic loading margin. Also, the PSS and SVC controllers have removed the Hopf bifurcation completely up to the tip of the system nose curve in each case (see Figures 4.4 and 4.7); TCSC controller has increased the dynamic loading margin by delaying the appearance of the Hopf to a higher loading level (Figure

Table 5.4: Susceptibility of different controllers

Controller	SLI (%)	MFCT (cycles)
PSS	110	18
SVC	110	15
TCSC	25	3

4.10). SVC and TCSC controllers have also increased the static loading margin of the system. On the other hand, the PSS controller increases only the dynamic stability margins but has no effect on static loading margins.

Table 5.5: Dynamic and static loading margins with and without controllers

		Base Case	Line 2-4 Outage	Line 2-3 Outage
DLM p.u	No cont.	0.47	0.35	0.14
	PSS	0.68	0.51	0.25
	SVC	0.82	0.65	0.38
	TCSC	0.68	0.55	0.32
SLM p.u.	No cont.	0.68	0.51	0.25
	PSS	0.68	0.51	0.25
	SVC	0.82	0.65	0.38
	TCSC	0.74	0.62	0.34

The most effective damping was observed with a PSS; however, the SVC and TCSC controllers not only increased the dynamic loading margins but also the static loading margins, thus yielding a better voltage profile during post fault tran-

sients and improving overall steady state voltage profiles. Dynamic loading margin greatly improved with a supplementary SVC control loop. The PSS and SVC controllers show less susceptibility to sudden load increase and three phase faults. In evaluating the combined implication of Tables 5.4 and 5.5, SVC controller shows the best overall performance potential for oscillation control. However, a cost benefit analysis for specific application has to be carried out to justify the economical viability, along with the typical need for an SVC, for example, for voltage control, before any firm conclusions can be drawn.

5.3 Controller Interactions

Following the account of the individual controller performance in Section 5.2, this section is concerned with the interactions between the different controllers operating simultaneously. Comparison is made between the amount of damping produced by each controller individually with the case with another controller present. Sensitivity to gains is also explored.

After arriving at gain settings of a PSS controller acting alone using root locus techniques to improve damping of one electromechanical mode an example of adverse interactions would be the degradation the damping of another mode being controlled by a FACTS controller.

It is not feasible by using root locus analysis alone to determine the reason for this interactions, as pointed out in [35]. Some sensitivity based techniques are proposed in [63] to study this problem. It is beyond the scope of this thesis which is confined to revealing potential interactions, including the interaction when controller gains are individually tuned.

5.3.1 PSS with SVC

Figure 5.12 shows some eigenvalues of the system for the PSS alone, SVC alone and both combined. In latter case, damping on some of the modes is reduced, especially on three electromechanical modes.

The effect of tuning the PSS controller gain K_{PSS} on the system was studied using the preferred SVC gain obtained in Section 5.2 for maximum damping on the critical mode. An increase in PSS controller gain above 80 p.u. results in the complex mode associated with generator 1 crossing to the right-half plane, as shown in Figure 5.13.

A time domain simulation for line 2-4 outage for the same critical gain K_{PSS}=80, is shown in Figure 5.14, illustrating how is the system becomes oscillatory unstable. It is noteworthy that the introduction of the SVC in fact has the benefit of increasing the tunable range of the PSS controller which produced a mode crossing at K_{PSS}=61 when operating alone. Consequently, the interaction between the PSS and SVC, appears not to be problematical, in this test scenario.

The next scenario is concerned with tuning with SVC beyond the needs of damping to include the supplementary SVC control loop for mitigation of Hopf bifurcation. Tuning of the main controller gain was free of problems, but tuning the supplementary control gain led to a complex mode cross the imaginary axis. This is comparable to Section 5.2.2 (Figures 5.7 and 5.8), but now the system becomes unstable at Ka_{SVC}=0.20 rather than 0.26. In turn retuning the PSS controller gain redresses the problem by eliminating the Hopf bifurcation as illustrated in Figure 5.15. While iterative tuning between the controller for optimum combined, interactive performance has not been thoroughly studied for this thesis, the described test example indicates the potential for mutually enhancing tuning between multiple

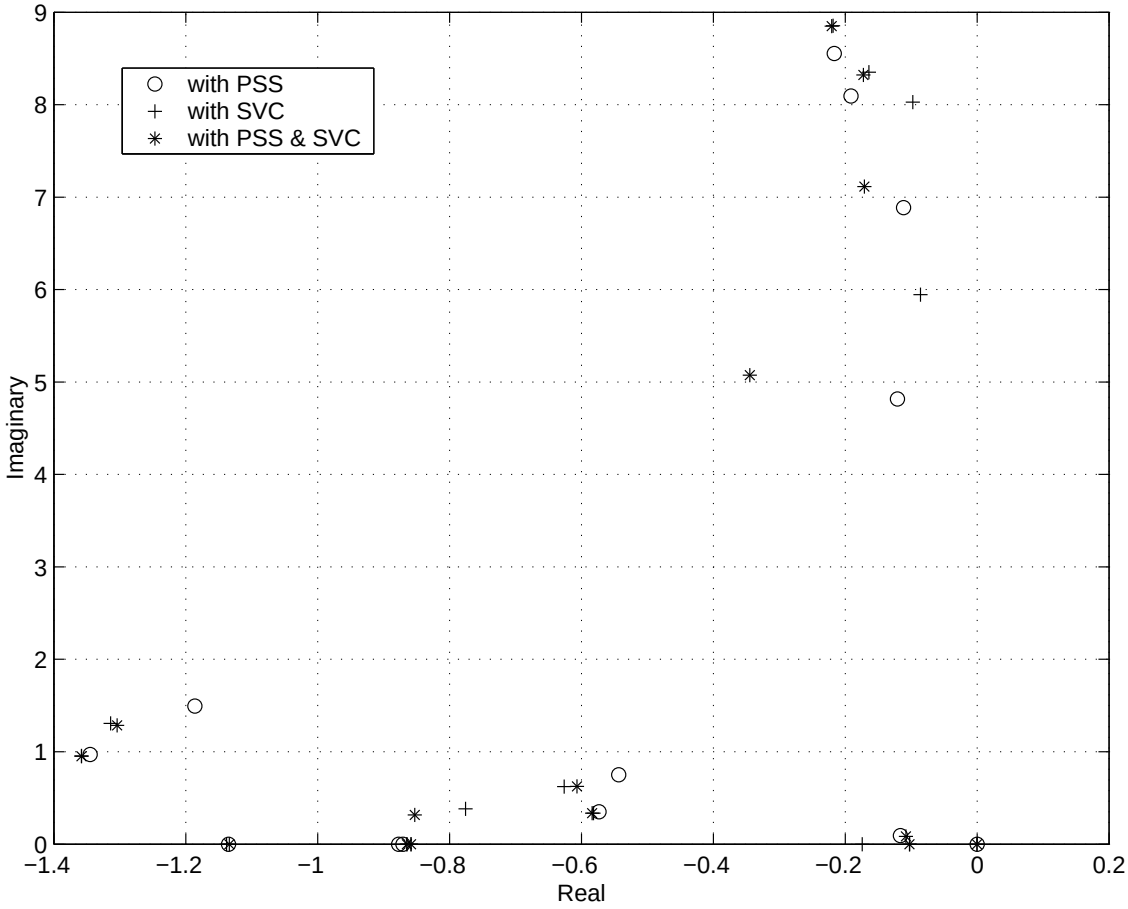

Figure 5.12: Some eigenvalues with PSS, SVC, and PSS and SVC combined at base case Hopf bifurcation (λ=0.47).

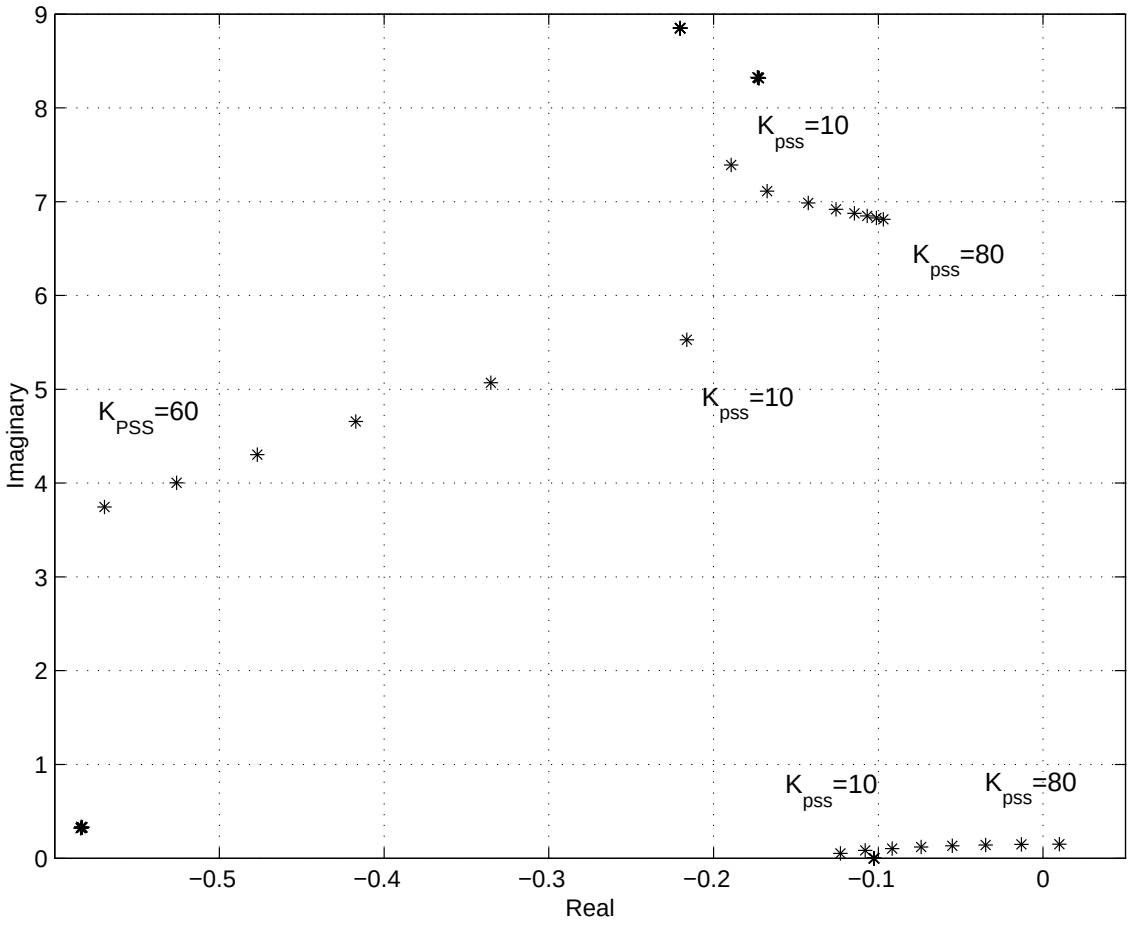

Figure 5.13: Locus of some critical eigenvalues of the system with a tunned SVC vs. PSS controller gain (λ=0.47).

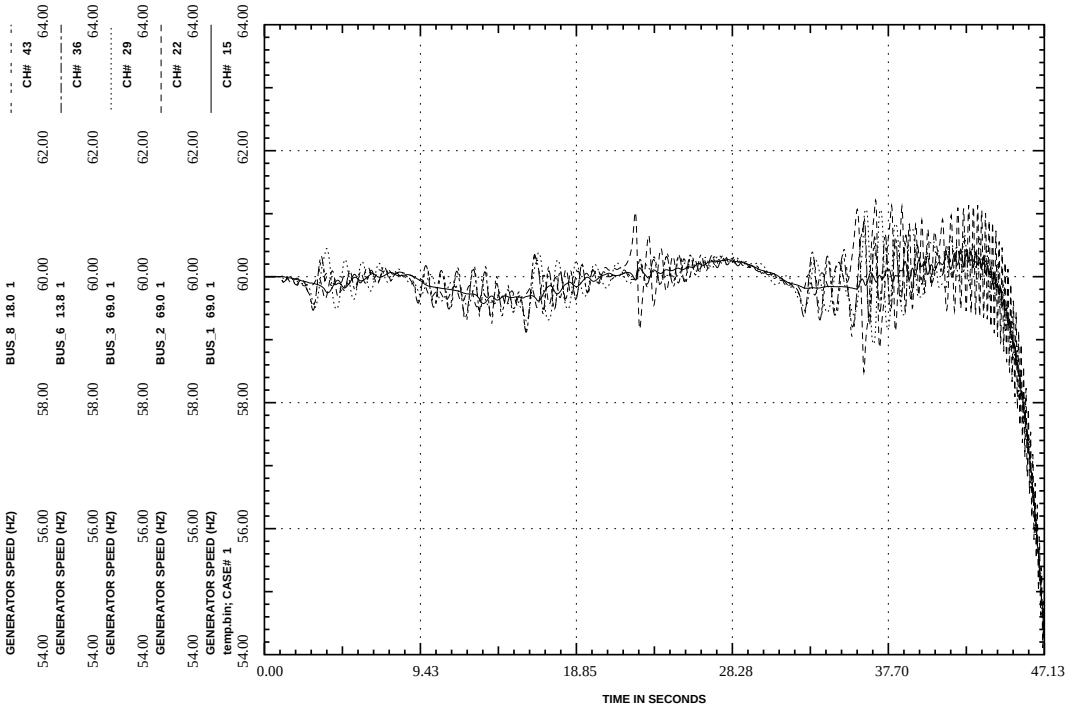

Figure 5.14: Generator frequency plot for a line 2-4 outage with tuned SVC, K_{SVC}=400, Ka_{SVC}=0.06 and PSS, K_{PSS}=80 (λ=0.40).

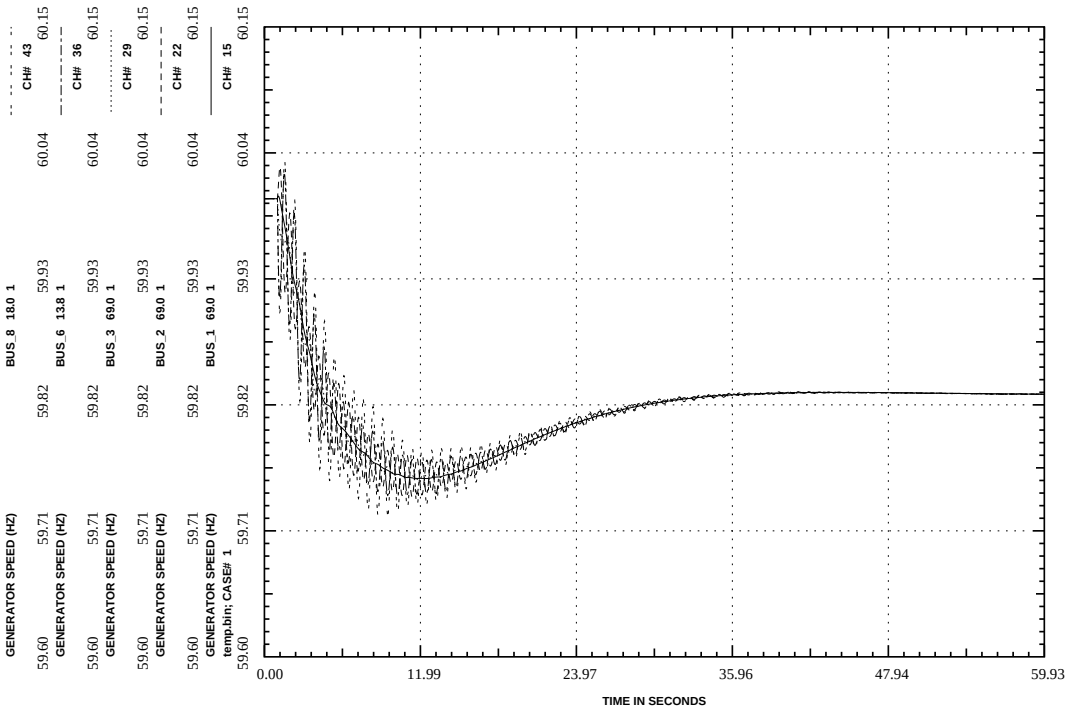

Figure 5.15: Generator frequency plot for a line 2-4 outage with tuned PSS and SVC for K_{PSS}=20, K_{SVC}=400 and Ka_{SVC}=0.06 (λ=0.40).

controllers.

5.3.2 PSS with TCSC

Figure 5.16 shows some eigenvalues of the system with the PSS alone, TCSC alone and both controllers combined at the base case for Hopf bifurcation point. The introduction of the TCSC to supplement the PSS increases damping to the electromechanical modes with the exception of that associated with generator 1 (bottom right-hand corner of Figure 5.16).

In order to observe the movement of some eigenvalues of the system with these

two controllers, the PSS controller gain was first varied. Figure 5.17, in showing the locus of some eigenvalues of the system for variations in K_{PSS} reveals that the complex mode associated to generator 1 crosses the imaginary axis for K_{PSS}=45. Hence, the introduction of the TCSC has reduced the tunable range of the PSS gain, which is clearly an example of a negative interaction among controllers contrary to the comparable case in Section 5.3.1.

Figures 5.18 and 5.19 show the oscillation in frequency for a line 2-4 outage for a PSS gain setting of K_{PSS}=45 with tuned TCSC, and Tuned PSS and TCSC controllers, respectively. Figure 5.18 confirms the mode crossing at K_{pss}=45, whereas Figure 5.19 illustrates that PSS and TCSC controllers can be further tuned to avoid the oscillations due to a Hopf bifurcation.

When TCSC gain was varied independently for a given PSS tuning, non of the electromechanical modes were affected; however, a complex mode associated with the TCSC controller itself crosses the imaginary axis at K_{TCSC}=7.8. The result in this case is similar to the one shown in Figure 5.10. This implies a threshold maximum TCSC gain which may be limiting on other performance objectives of the TCSC.

5.3.3 TCSC with SVC

Interactions studies were also performed with combined SVC and TCSC controllers. When considered independently, both controllers were intended to improve the damping of one particular electromechanical mode associated with generator 3. As depicted in Figure 5.20, the combination action degrades the damping of the electromechanical mode compared to each acting individually.

Figure 5.21 shows the movement of some eigenvalues with respect to the sup-

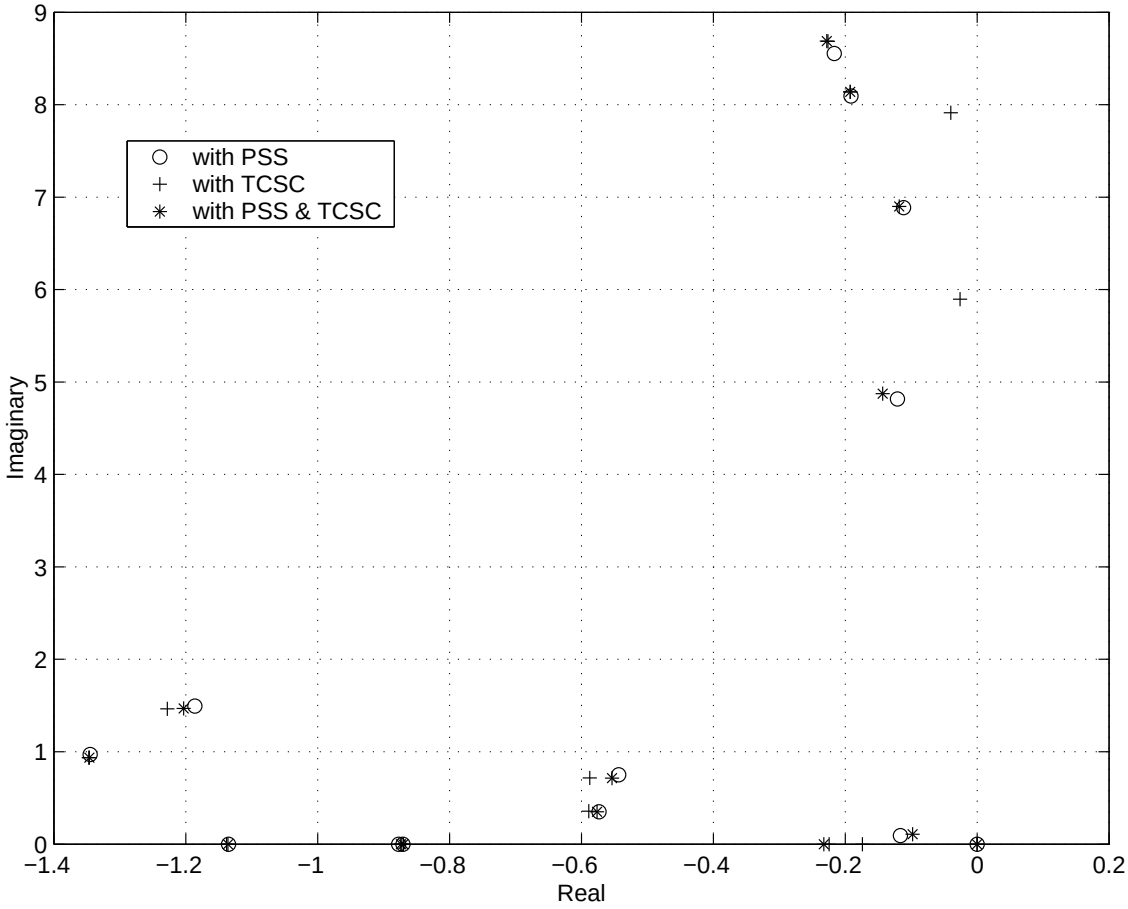

Figure 5.16: Some eigenvalues with PSS, TCSC and PSS and TCSC, at the base case Hopf bifurcation point (λ=0.47).

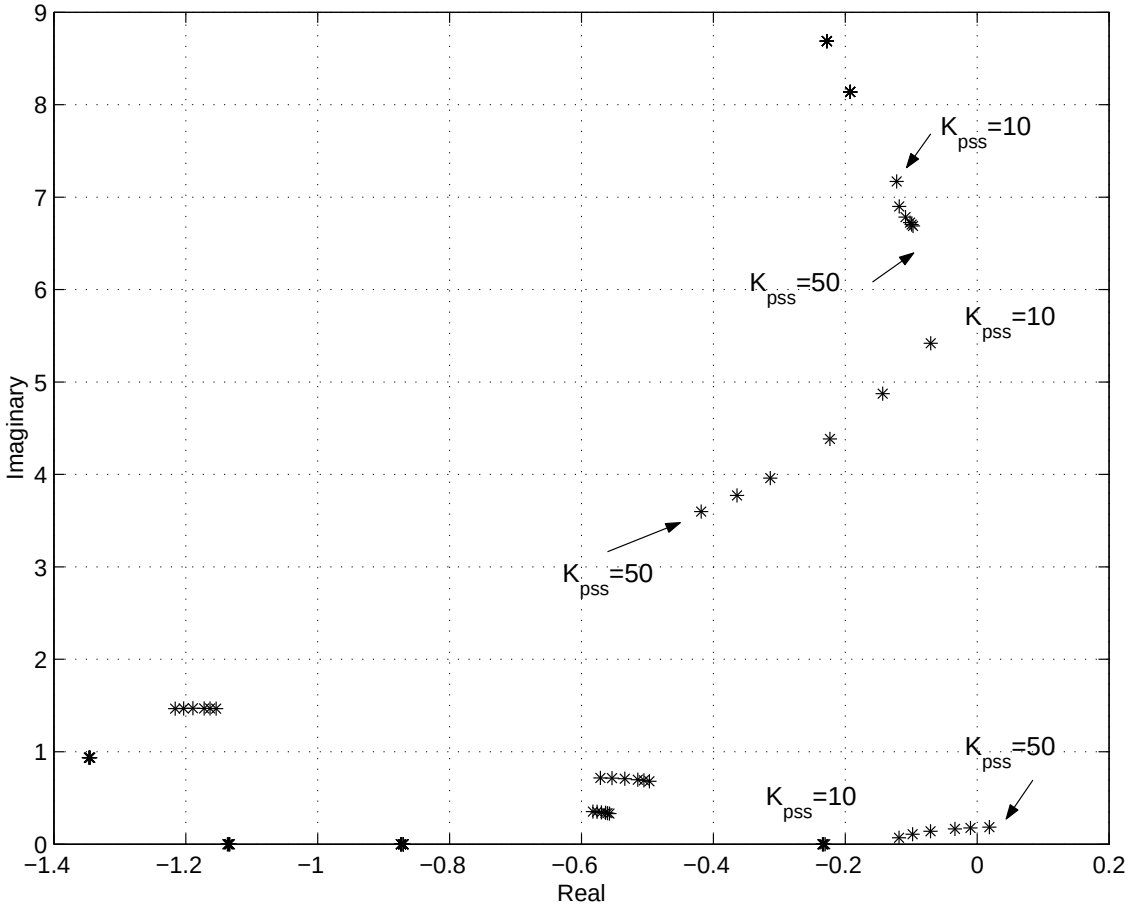

Figure 5.17: Locus of some critical eigenvalues of the system with tuned TCSC vs. PSS controller gain (λ=0.47).

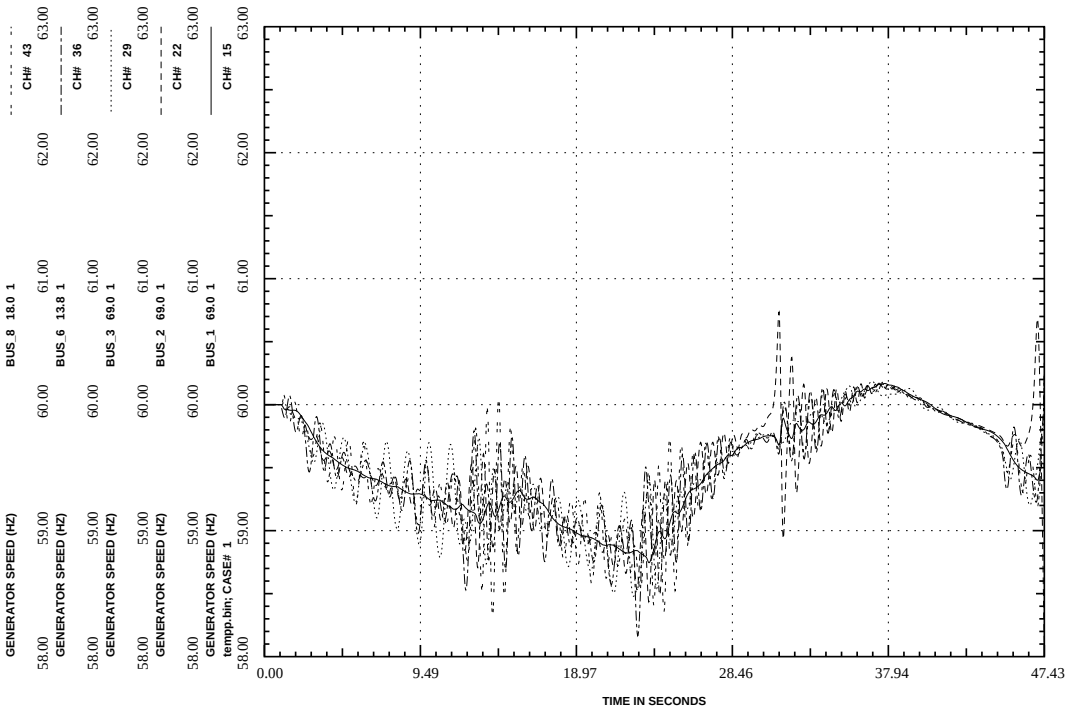

Figure 5.18: Generator frequency plot for a line 2-4 outage with PSS and TCSC for K_{TCSC}=1.0 and K_{PSS}=45 (λ=0.4).

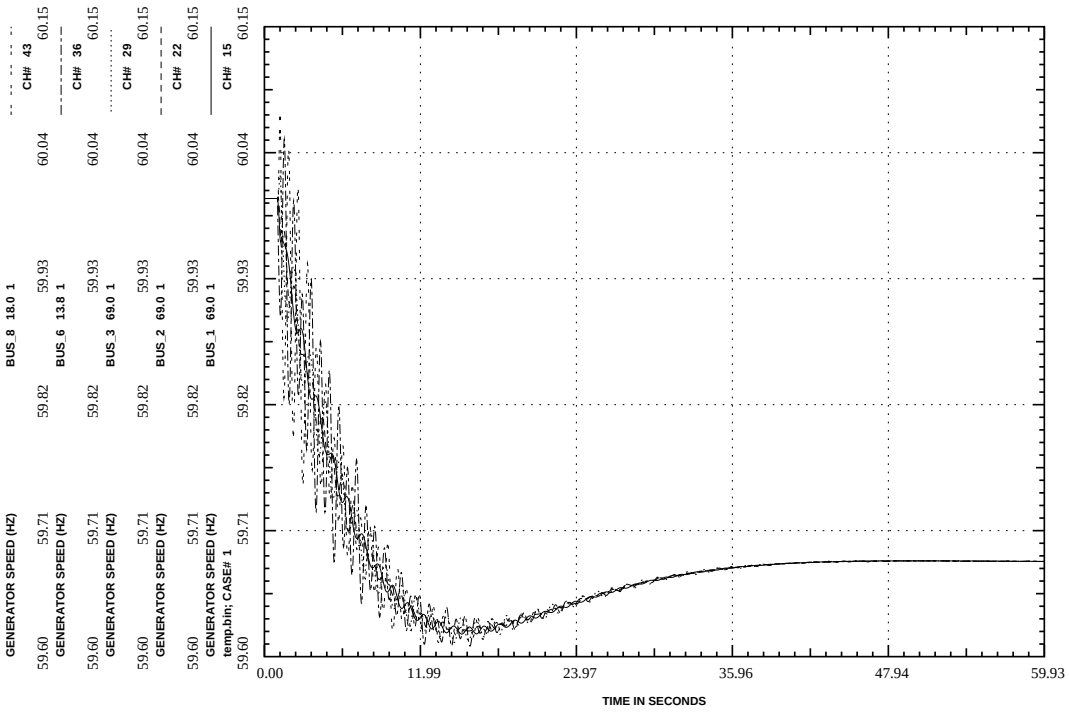

Figure 5.19: Generator frequency plot for a line 2-4 outage with tuned PSS and TCSC for K_{TCSC}=1.0 and K_{PSS}=20 (λ=0.4).

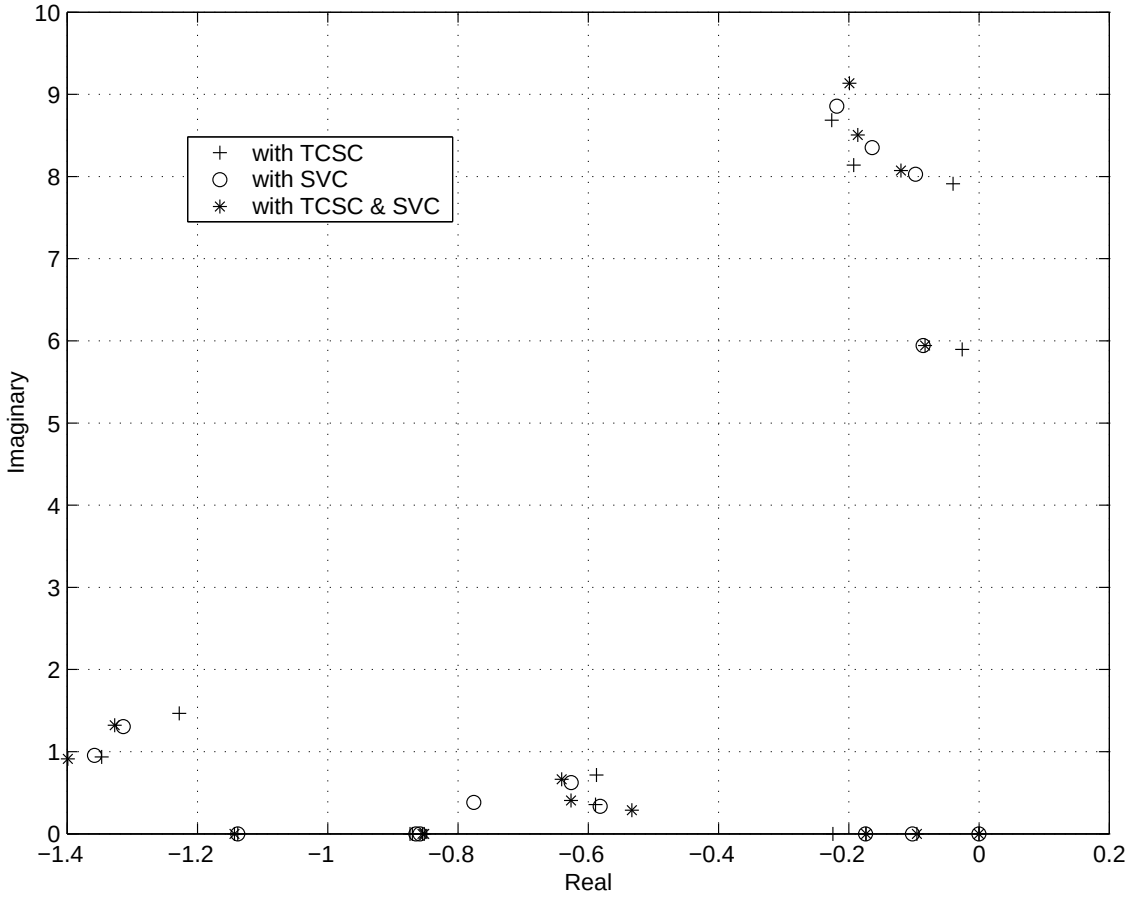

Figure 5.20: Some eigenvalues with SVC, TCSC, and SVC and TCSC, at the base case Hopf bifurcation point (λ=0.47).

plementary control gain Ka_{SVC}. Of concern is that in electromechanical modes associated with the synchronous compensator located at bus 8 crosses the imaginary axis yielding a Hopf bifurcation, while the mode associated with generator 3 moves to the left side. In all other cases, variations in the Ka_{SVC} lead to a complex mode associated with the controller itself crossing the imaginary axis, which can be viewed as a negative interaction between the SVC and TCSC controllers. To further expose the interaction, Figure 5.22 shows the time domain simulation corresponding to the same controller gain settings. It confirms that system becomes oscillatory unstable.

Contrary to the previous performance degradation, test were performed to determine more appropriate gain settings, for combined performance. Of these, using the most effective settings, the frequency plot in Figure 5.23 shows that the oscillations due to Hopf bifurcation have been avoided.

Tuning of the SVC main controller gain K_{SVC} and the TCSC controller gain K_{TCSC} did not produce interactive problems. The electromechanical modes are less sensitive to these gains, TCSC controller gain in particular.

5.3.4 PSS, SVC and TCSC combined

Finally, interaction studies were performed with all the controllers i.e. PSS, SVC and TCSC.

Figure 5.24, shows some eigenvalues of the system with PSS alone, SVC alone, TCSC alone and all combined, at the base case Hopf bifurcation point. Observe that damping on all the electromechanical modes are increased with the exception of that associated with the generator 1, bottom right hand corner of Figure 5.24.

The effect of tuning the PSS controller gain K_{PSS} on the system was studied

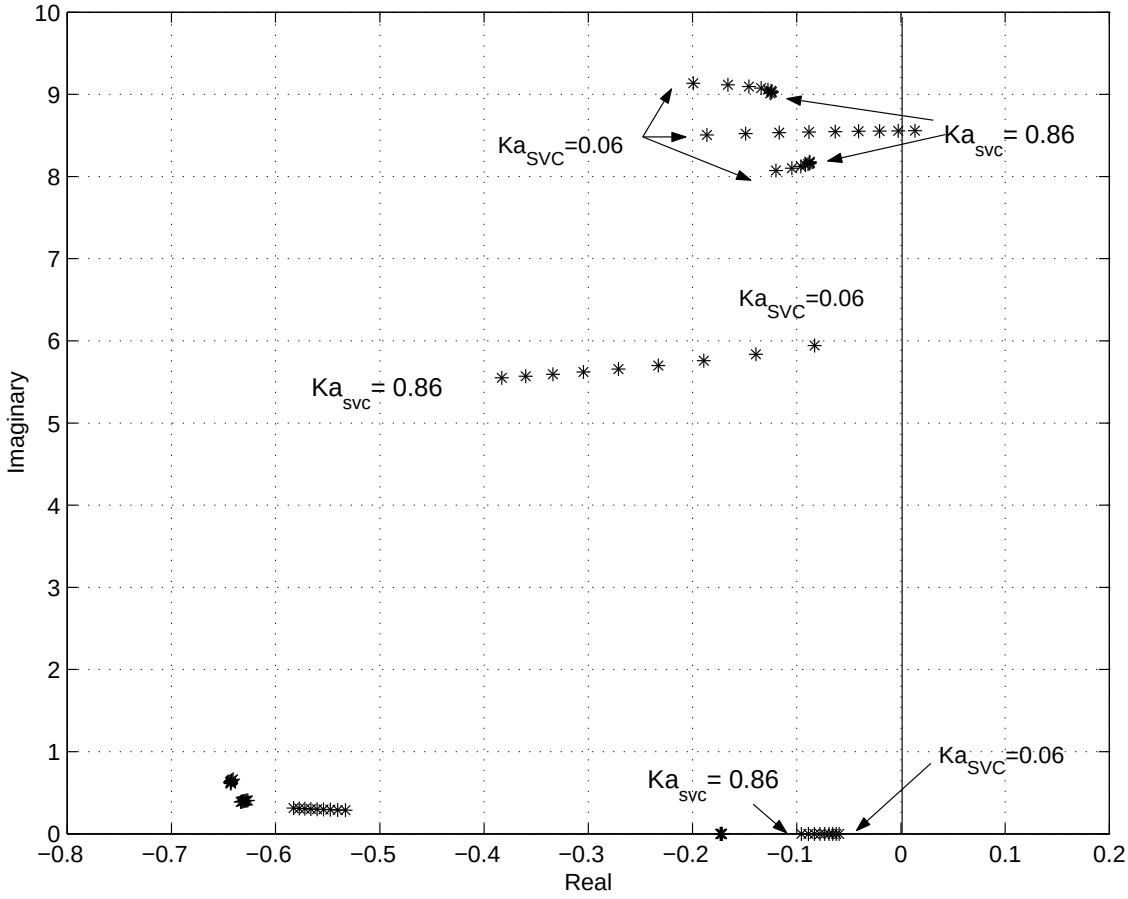

Figure 5.21: Locus of some critical eigenvalues of the system with tuned TCSC vs. SVC supplementary control gain Ka_{SVC} (λ=0.47).

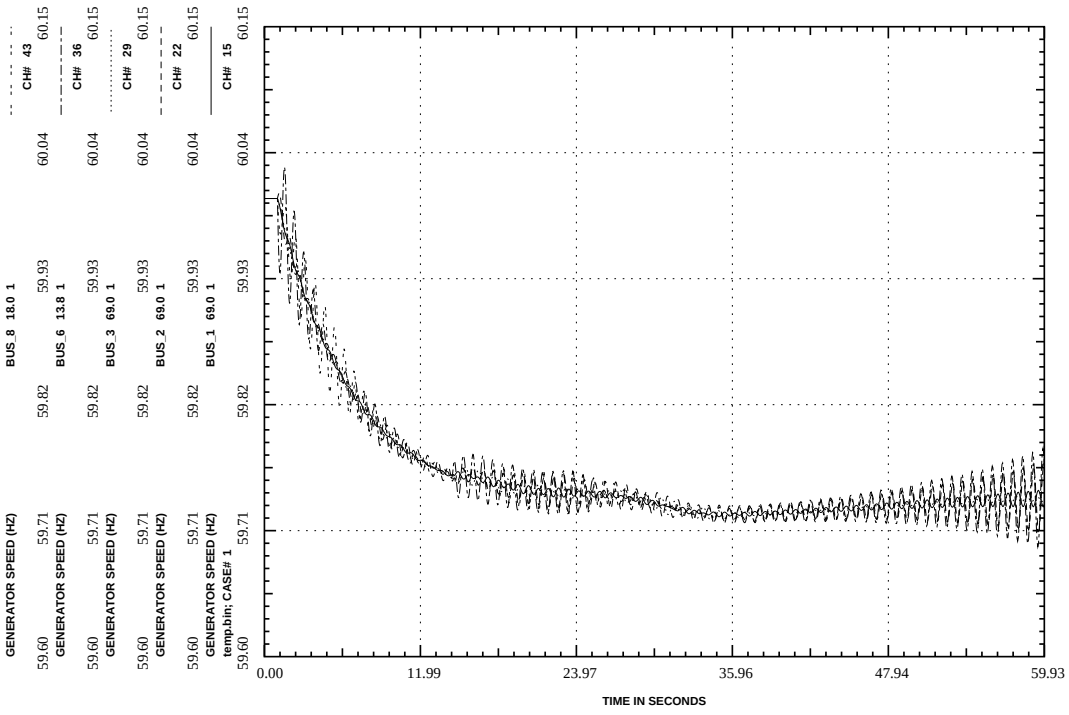

Figure 5.22: Generator frequency plot for a line 2-4 outage with SVC and TCSC for K_{TCSC}=1.0 and K_{SVC}=400, Ka_{SVC}=0.8 (λ=0.4).

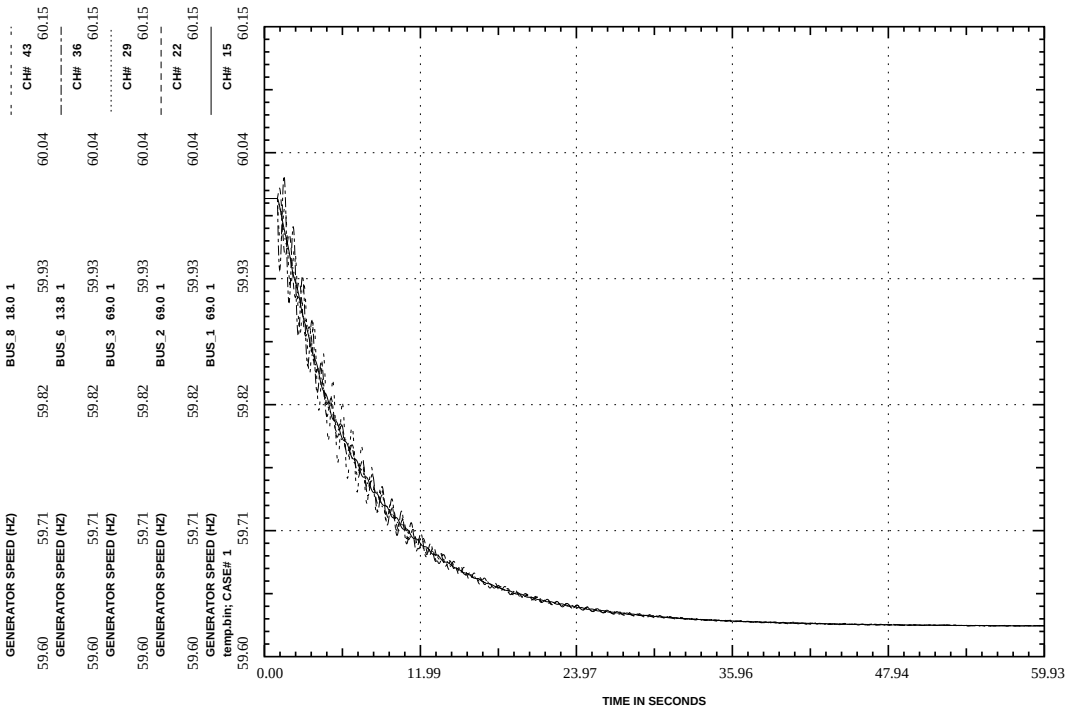

Figure 5.23: Generator frequency plot for a line 2-4 outage with tuned SVC and TCSC for K_{TCSC}=1.0, K_{SVC}=400, and Ka_{SVC}=0.06 (λ=0.4).

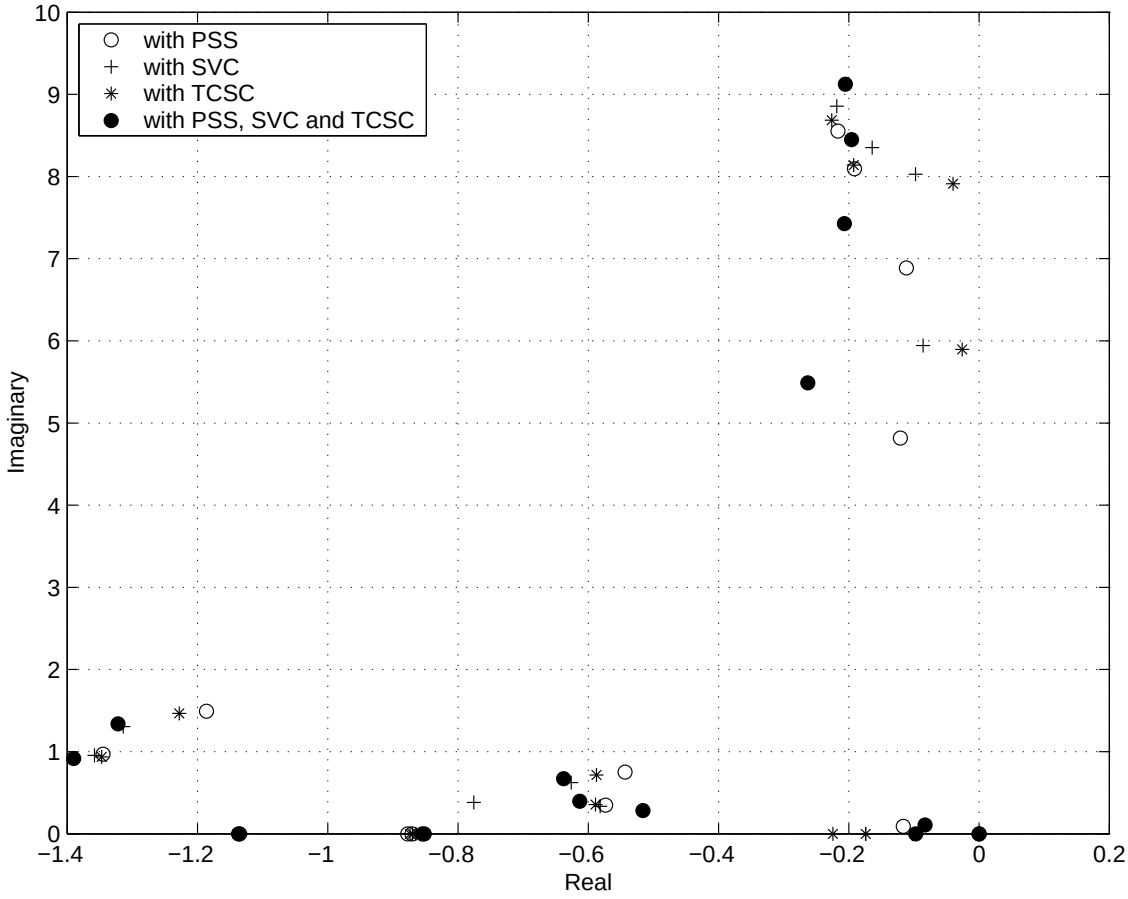

Figure 5.24: Some eigenvalues with PSS, SVC, TCSC and all combined, at the base case Hopf bifurcation point (λ=0.47).

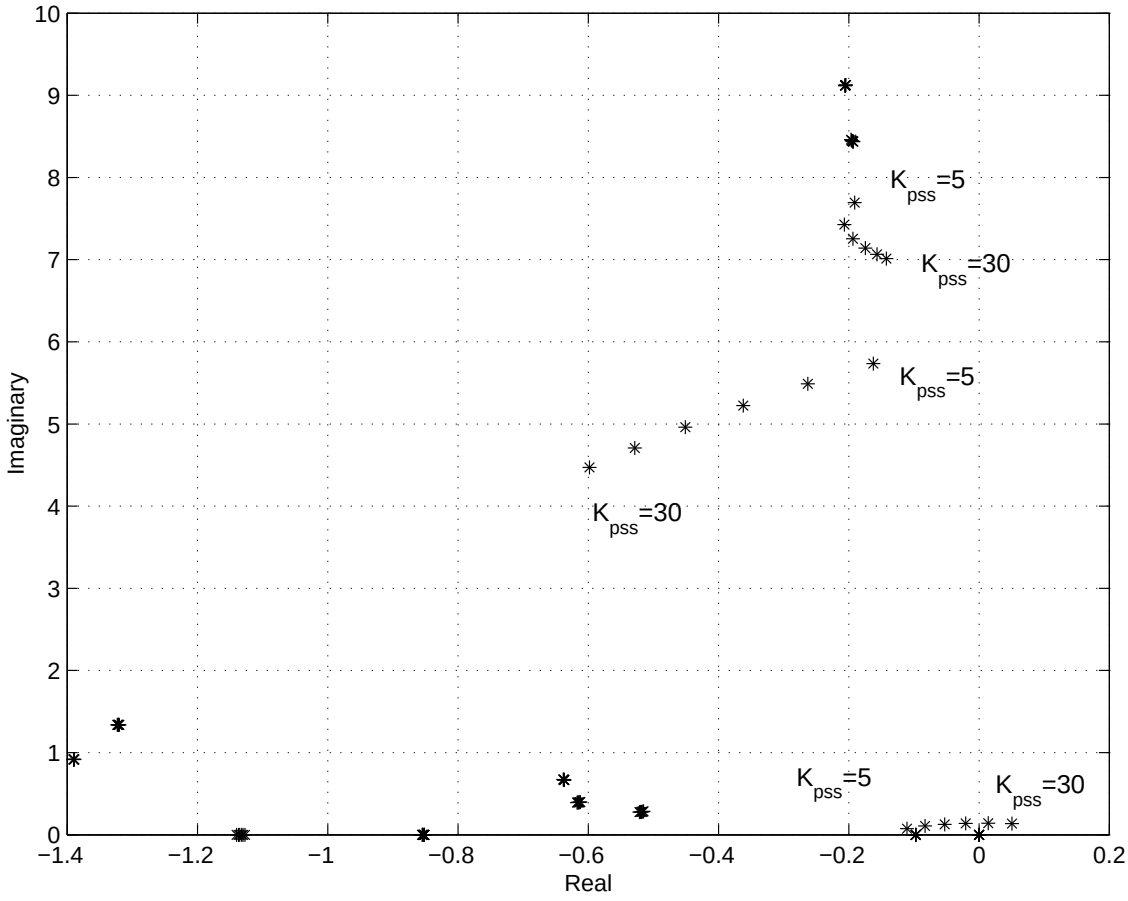

Figure 5.25: Locus of some critical eigenvalues of the system with tuned SVC and TCSC vs. PSS controller gain K_{PSS} (λ=0.47).

using the preferred gain settings of SVC and TCSC obtained in Section 5.2. An increase in the PSS controller gain above 25 p.u. results in the complex mode associated with generator 1 crossing to the right-half plane as shown in Figure 5.25. Recall that the tunable ranges of the PSS controller are 0-80 p.u. with tuned SVC and 0-45 with the tuned TCSC. This means that the tunable range of the PSS controller gain is reduced significantly when SVC and TCSC controllers are present in the system. This is clearly a case of negative interactions.

Tuning of the SVC and TCSC main controller gains was free from problems, but tuning of the supplementary control gain of SVC led a complex mode (electromechanical mode of generator 2) to cross the imaginary axis as shown in Figure 5.26. This is similar to the result given in Section 5.3.3, but here a different mode becomes critical as the gain is varied. Results given in Figures 5.25 and 5.26 were confirmed by time domain simulations. Nevertheless by retuning the PSS and the SVC supplementary control gain oscillation associated with Hopf bifurcation can be removed as shown in Figure 5.27 Observe, the overall best damping and low amplitude oscillation in this case.

5.3.5 Comparison of Controller Combination

For each of the controller combinations presented in Section 5.3 it is evident, as intuitively would be expected, that the most effective settings of each controller to separately control electromechanical modes may be inappropriate for combined operation. When all the controllers operate together, interaction does not produce degradation of stability performance with the exception of some limitation on the gain of the PSS and some additional sensitivity to the SVC supplementary control gain. In comparison, the other test cases in which the controllers operate in pairs, is indicative of the performance with an outage of one controller. For the specific circumstances of the test system in the context of Hopf bifurcations control, the combined controllers appear to be robust to a controller outage.

A number of remedial options can be considered. The most theoretically comprehensive while being the most difficult to implement practically would be an overall centralized control system with communication of control variables between the various PSS and FACTS locations. A simple alternative, as explored in prelim-

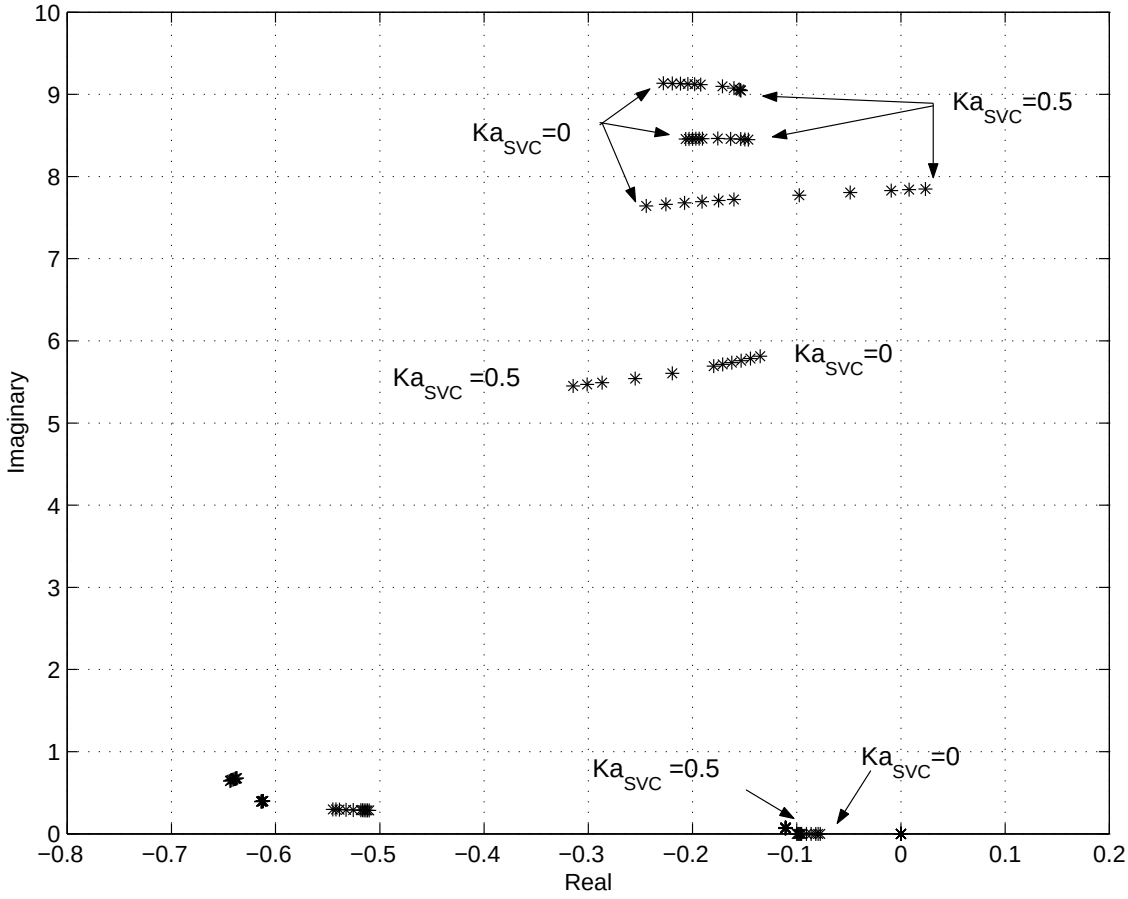

Figure 5.26: Locus of some critical eigenvalues of the system with tuned PSS and TCSC vs. SVC supplementary control gain Ka_{SVC} (λ=0.47).

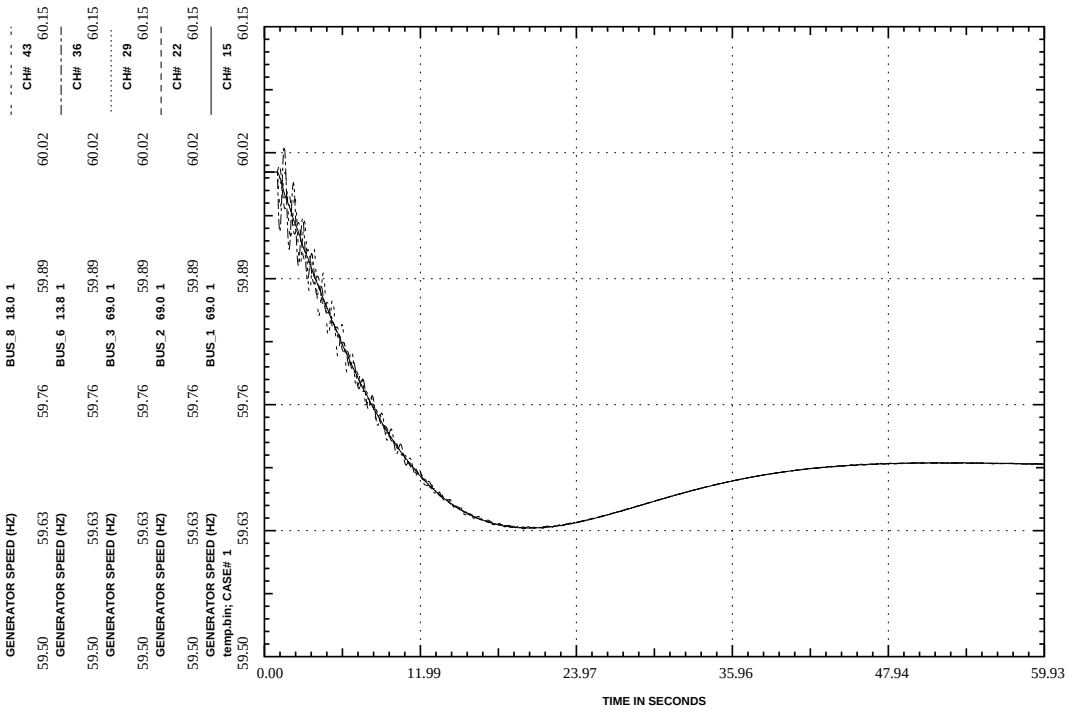

Figure 5.27: Generator frequency plot for a line 2-4 outage with tuned PSS, SVC and TCSC for K_{PSS}=5, K_{TCSC}=1.0, K_{SVC}=400, and Ka_{SVC}=0.06 (λ=0.4).

inary form in Section 5.3 is to reveal problematical mode through system analysis and simulation, as described, and then to select modified control settings to avoid unacceptable (interactive) instability modes. This may well result in some depredation of other control performance objectives. Should no compromise solution be found, it would be indicative of a inadmissible planning case for FACTS location.

A solution to problematical interaction was found, in each of four combinations of controllers in Section 5.3, through re-adjustment of individually optimized control gains. However, since this can not be extrapolated to the performance of other and large systems in general the research presented here is principally confined to the methodology for defining and revealing interactions.

It is also clear from the presented results that the interaction in certain cases can be beneficial. Without the results having generality for all combinations of controllers for any power system, the specific test cases showed that the best performance, in term of the highest damping and lowest amplitude of an oscillation due to Hopf bifurcation was achieved by PSS, SVC and TCSC combined, followed by the SVC and TCSC combination. In considering either SVC or TCSC combined with a commonly applied PSS controllers, the SVC was more effective than the TCSC.

5.4 Summary

Following illustration of performance of various power system controllers to the variation in their respective gains, the interactions of FACTS controller with power system stabilizer and among FACTS controllers are presented in the IEEE 14-bus test system.

Chapter 6

CONCLUSIONS

6.1 Concluding Observations

This thesis has presented the study of oscillatory problems in power systems using Hopf bifurcation theory; indices have been proposed to detect and predict these problems. The use of PSS and FACTS controllers to control them has been described. Further to observations made in individual chapter, the following conclusions are made:

(i) The two proposed indices to detect and predict Hopf bifurcation show a smooth and predictable (linear) behavior with respect to load changes, making them adequate for predicting proximity of the system operation to Hopf bifurcation (oscillation problems). HBI_2 index has a significant computational advantages that makes it suitable for on-line applications. It is also shown that the proposed indices can be readily applied to any nonlinear system for detecting and predicting Hopf and saddle-node bifurcations.

(ii) The effect of system limits on the linearity of indices has been analyzed as well, demonstrating the sensitivity of the indices with respect to the loading factor can be used to offset limit induced nonlinearity. By this means, an alternative pair of linearized indices has been introduced.

(iii) The effect of contingencies and load modeling on Hopf bifurcations through the computation of dynamic stability margins is also discussed in this thesis. It is shown that constant PQ load models yield the lowest dynamic loading margins, followed by constant current and then constant impedance load models, as expected.

(iv) The direct association between electromechanical oscillations and Hopf bifurcation has been demonstrated and Hopf bifurcation theory has used to develop analysis techniques. Valuable information such as critical loading levels at which the system may become vulnerable to an oscillatory problem, as well as the initial frequency of the oscillations, can be obtained by applying this theory.

(v) The oscillation problems associated with Hopf bifurcations, typically triggered in practice by line outages, can be controlled by the use of PSS controllers on generators or FACTS controllers on the transmission system. A new shunt FACTS controller placement technique is proposed, so that users can effectively identify and rank suitable locations for the purpose of controlling oscillations associated with Hopf bifurcations. It is also shown that the best locations to place FACTS controller for oscillation damping is not necessarily the same as the locations obtained through voltage stability analysis.

(vi) While FACTS placement is typically aimed at increasing such primary objectives as voltage control and system power transmission capability, the place-

ment for oscillation control can be considered as a useful part of an overall FACTS planning study.

(vii) This thesis demonstrates that SVC, TCSC and STATCOM controllers, appropriately tuned and located make them a viable alternative to the traditional PSS controller or to enhance PSS controller for oscillation control. The latter is especially true considering the significant improvements to both dynamic and static loading margins, which are reflected in better voltage profiles throughout the system during contingencies, compared to PSS controllers alone. However, an overall cost benefit analysis would be necessary for a specific application for oscillation control combined with other application aspects, given their relatively high costs of FACTS controllers when compared to PSS controllers.

(viii) It has been shown in the test cases that tuning of the various controller gains have to be carried out judiciously. A control gain that may be acceptable for, for example, voltage control at a local bus may have a negative effect on system wide oscillations. It can be further concluded that it may well be relevant to explore such dynamic interaction using the proposed indices and methodology, even if a FACTS controller is located to meet other planning objectives. In this case, the concern would not be primarily to enhance the system dynamic but to ensure, at least, that the FACTS controller would not introduce dynamic problems.

(ix) Chapter 5 explored the interaction of FACTS controllers in the context of oscillation induced by Hopf bifurcations, system loading and oscillation damping. Without re-iterating the observations made in section 5.4, it has been shown that the methodology presented in the previous chapter is applicable

to investigating FACTS interactions.

The test cases, by definition can not be considered to provide results general to all power systems. They do indicate that interaction may be both beneficial and unacceptable based on individual control settings established in isolation. Interaction may be sufficient to produce Hopf bifurcation and consequential instability where a controller used alone and tuned accordingly would be stable.

6.2 Main Contributions

The major contributions of this thesis can be summarized as follows:

- **Hopf bifurcation prediction**:

  1. Development of two indices to predict and detect Hopf bifurcations in power systems, including a methodology to linearize these indices. One of these indices may be used as an on-line index.
  2. Influence of the non-linear static load models on Hopf bifurcation points and associated oscillations in a power system.

- **Hopf bifurcation control**:

  1. Development of a methodology for the placement of shunt-connected FACTS controllers to control Hopf bifurcations in power systems.
  2. Hopf bifurcation control using PSS, SVC, TCSC and STATCOM controllers in power systems, including the implementation of a detailed STATCOM model in a commercial software package (PST).

- **Controllers performance and interactions**:

    1. Exploration of additional benefits of these controllers under wide variety of operating conditions.
    2. Exploration of undesirable controller interactions on power system performance.

This thesis has resulted in a number of papers published and under review [31, 48, 58, 64, 65, 66].

6.3 Future Directions

There are a number of issues that are still to be addressed in the area of Hopf bifurcation prediction, control and controller interactions:

1. Thus, the effect of dynamic and other nonlinear static load models (other than the "standard" ones) on Hopf bifurcation points of a power system can be studies by using the proposed indices.
2. The methodology for Hopf bifurcation control can be extended to other types of FACTS controllers, such as SSSC and UPFC, including placement techniques for series and other FACTS controllers, by extending the placement technique proposed in this thesis for shunt-FACTS controllers.
3. Another area of study is the coordination of FACTS planning studies for both power/voltage control and for dynamic control. In this case, various control objectives of these controllers can be combined for the best location and performance, not only for oscillation control, but also to increase the overall system loadability.

4. Due to the expensive nature of FACTS controllers, a thorough cost-benefit analysis has to be carried out to justify the economic viability of these controllers by translating various benefits of the use of the controllers on system performance (e.g. static and dynamic loading margins increase, improved voltage profiles) in financial terms. This would be a very useful contribution, especially in the framework of open electricity markets.

5. There is a need for more research in coordinating the controls of multiple FACTS devices, not only to avoid undesirable interactions, but also to provide composite enhanced performance. Studies should be carried out to understand the reasons for different types of interactions. Furthermore, sensitivity analysis of eigenvalues with respect to controller's gain should be carried out to identify the range of the controller gains in which the gains become problematic.

Appendix A

THREE-BUS TEST SYSTEM

A.1 Static and Dynamic Data

```
% Three-bus test  system
% detailed generator,exciter and governor
% bus data format
% bus:
% col1 number
% col2 voltage magnitude(pu)
% col3 voltage angle(degree)
% col4 p_gen(pu)
% col5 q_gen(pu)
% col6 p_load(pu)
% col7 q_load(pu)
% col8 G shunt(pu)
% col9 B shunt(pu)
% col10 bus_type
%       bus_type - 1, swing bus
%                - 2, generator bus (PV bus)
%                - 3, load bus (PQ bus)
% col11 q_gen_max(pu)
% col12 q_gen_min(pu)
%  the voltage on bus 2 is adjusted for zero Q at machine 1
```

```
bus = [ 1 1.05   0.0   4   1.5  0.0  0.0  0.0  0.0  2     10  -2;
        2 1      0.0   5   1.5  0.0  0.0  0.0  0.0  1  999  -999;
        3 1.0    0     0     0  9    3    0.0  0.0  3    0     0];

% line data format
% line: from bus, to bus, resistance(pu), reactance(pu),
%       line charging(pu), tap ratio, phase shifter angle

line = [1  3  0.0  0.05    0.  1.0 0.0;
        2  3  0.0  0.03999 0.  1.0 0.0;
        2  3  0.0  0.03999 0.  1.0 0.0];

% Machine data format
% machine:  1. machine number
%           2. bus number
%           3. base mva
%           4. leakage reactance x_l(pu)
%           5. resistance r_a(pu)
%           6. d-axis sychronous reactance x_d(pu)
%           7. d-axis transient reactance x'_d(pu)
%           8. d-axis subtransient reactance x"_d(pu)
%           9. d-axis open-circuit time constant T'_do(sec)
%          10. d-axis open-circuit subtransient time
%                constant T"_do(sec)
%          11. q-axis sychronous reactance x_q(pu)
%          12. q-axis transient reactance x'_q(pu)
%          13. q-axis subtransient reactance x"_q(pu)
%          14. q-axis open-circuit time constant T'_qo(sec)
%          15. q-axis open circuit subtransient time
%                constant T"_qo(sec)
%          16. inertia constant H(sec)
%          17. damping coefficient d_o(pu)
%          18. damping coefficient d_1(pu)
%          19. bus number
%          20. S(1.0) - saturation factor
%          21. S(1.2) - saturation factor

mac_con = [...
1 1 555.5   0.16 0 1.81   0.300 0.217 7.8  0.022 ...
```

```
                  1.76   0.610 0.217 0.9  0.074 ...
                  3.53   1.0   0     1    0.0959    0.3477;
2 2 700.0   0.16 0 1.81   0.300 0.217 7.8  0.022 ...
                  1.76   0.610 0.217 0.9  0.074 ...
                  3.53   1.0   0     2    0.0959    0.3477];

%Exciter data format
%Exciter:  1. Exciter type 7 for AC4a
%          2. Machine number
%          3. Rc compensation resistance
%          4. Xc compensation reactance
%          5. Transuducer time constant
%          6. Voltage regulator gain Kg
%          7. Voltage regulator time constant Ta
%          8. Tb
%          9. Tc
%         10. Maximum voltage regulator output Vmax
%         11. Minimum voltage regulator output Vmin

exc_con = [...
7  1   0.0  0.0  0.0  100  0.01   0.0    0.0   6.43  -6.0   0.0  999    -999 ...
0  0   0    0    0    0    0      0       0     0     0      0    0      0 ;
7  2   0.0  0.0  0.0  100  0.01   0.0    0.0   6.43  -6.0   0.0  999    -999 ...
0  0   0    0    0    0    0      0       0     0     0      0    0      0 ;
];

% Hydraulic turbine governor data format

hgt_con = [
   1 .04 0.4 5.0 0.05 5.0 0.2 .16 -.16 0  500 1.41 0.16 0.94 1;
   2 .04 0.4 5.0 0.05 5.0 0.2 .16 -.16 0 1000 1.41 0.16 0.94 1;
];

pss_con = []; gsib_idx = [1]; geib_idx = []; load_con = [];
svc_con = []; tcsc_con = []; lmod_con= []; rlmod_con = []; tgt_con = [];
```

Appendix B

TWO-AREA TEST SYSTEM

B.1 Static and Dynamic Data

```
% Two-area system [1]
% 100 MVA base
% Reference P. Kundur 'Power System Stability and Control',
% McGraw-Hill Inc.,New York, 1993


% The following bus solution is within one iteration of the actual
%    1   2     3       4      5      6      7       8
%   bus volt angle   p_gen  q_gen  p_load q_load  G_shunt
%     9       10   11    12    13     14    15
% B_shunt type q_max q_min v_rate v_max v_min

bus = [
    1  1.0300  26.8490 7.0000 1.7919 0    0    0.00 0.00 2 5.0 -5.0  20.0 1.1  .9;
    2  1.0100  17.0998 7.0000 2.2026 0.00 0.00 0.00 0.00 2 5.0 -2.0  20.0 1.1  .9;
    3  1.0300   0.0    7.1850 1.6898 0.00 0.00 0.00 0.00 1 9.0 -9.0  20.0 1.1  .9;
    4  1.0100 -10.1588 7.0000 1.8521 0.00 0.00 0.00 0.00 2 5.0 -2.0  20.0 1.1  .9;
    5  1.0074  20.3799 0.00   0.00   0.00 0.00 0.00 0.00 3 0.00 0.0  230  1.5  .5;
    6  0.9804  10.3201 0.00   0.00   0.00 0.00 0.00 0.00 3 0.00 0.0  230  1.5  .5;
    7  0.9652   1.9560 0.00   2.00   9.67 1.00 0.00 0.00 3 0.00 0.0  230  1.5  .5;
    8  0.9536 -11.7915 0.00   0.00   0.00 0.00 0.00 0.00 3 0.00 0.0  230  1.5  .5;
```

```
    9  0.9763 -25.2580 0.00   3.50  17.67 1.00 0.00 0.00 3 0.00 0.0  230  1.5  .5;
   10  0.9862 -16.8988 0.00   0.00   0.00 0.00 0.00 0.00 3 0.00 0.0  230  1.5  .5;
   11  1.0093  -6.6276 0.00   0.00   0.00 0.00 0.00 0.00 3 0.00 0.0  230  1.5  .5];

% line data format
% line: from bus, to bus, resistance(pu), reactance(pu),
%       line charging(pu), tap ratio, tap phase, tapmax, tapmin, tapsize

line = [...
1   5   0.0     0.0167   0.00    0 0 0 0 0;
5   6   0.0025  0.025    0.04375 0 0 0 0 0;
2   6   0.0     0.0167   0.00    0 0 0 0 0;
6   7   0.001   0.01     0.0175  0 0 0 0 0;
7   8   0.011   0.110    0.1925  0 0 0 0 0;
7   8   0.011   0.110    0.1925  0 0 0 0 0;
8   9   0.011   0.110    0.1925  0 0 0 0 0;
8   9   0.011   0.110    0.1925  0 0 0 0 0;
9  10   0.001   0.01     0.0175  0 0 0 0 0;
4  10   0.0     0.0167   0.00    0 0 0 0 0;
10 11   0.0025  0.025    0.04375 0 0 0 0 0;
3  11   0.0     0.0167   0.00    0 0 0 0 0];


statcom_data=[9 12 0 0.145 0 1.0 0 0.0017 2.0 100 1.0 1.0 1.10 1.0 0.9];%

%Initial Values for STATCOM variables
  %col 1 Vsat   Volatge at the statcom terminal
  %col 2 Delta  Angle at the statcom terminal (rad)
  %col 3 Vdc    Voltage at the dc bus
  %col 4 Alpha  Angle at the inverter terminal (rad)
  %col 5 I      Statcom current (should not be zero)
  %col 6 Theta  Statcom current phase Angle (rad)
  %col 7 Psat   Statcom Real Power (pu)
  %col 8 Qsat   Statcom Reactive power (pu)

  Xsat=[1.000 -0.369 1.3400 -0.370 1.500 1.199 0.003 -1.607];

%Machine data
mac_con = [ ...
```

```
1 1 900 0.200  0.0025  1.8  0.30  0.25 8.00  0.03...
                       1.7  0.55  0.25 0.4   0.05...
                       6.5  2   0  3 0.0377 0.1821;
2 2 900 0.200  0.0025  1.8  0.30  0.25 8.00  0.03...
                       1.7  0.55  0.25 0.4   0.05...
                       6.5  2   0  3 0.0377 0.1821;
3 3 900 0.200  0.0025  1.8  0.30  0.25 8.00  0.03...
                       1.7  0.55  0.25 0.4   0.05...
                       6.175 2 0  3 0.0377 0.1821;
4 4 900 0.200  0.0025  1.8  0.30  0.25 8.00  0.03...
                       1.7  0.55  0.25 0.4   0.05...
                       6.175  2  0 3 0.0377 0.1821];

exc_con = [
7     1     0.0   0.0   0.0  100   0.01   0.0    0.0   6.43  -6.0   0.0  999    -999 ...
0     0     0     0   0     0     0      0       0     0     0      0     0      0 ;
%7     2     0.0   0.0   0.0  100   0.01   0.0    0.0   6.43  -6.0   0.0  999    -999 ...
%0     0     0     0   0     0     0      0       0     0     0      0     0      0 ;
7     3     0.0   0.0   0.0  100   0.01   0.0    0.0   6.43  -6.0   0.0  999    -999 ...
0     0     0     0   0     0     0      0       0     0     0      0     0      0 ;
7     4     0.0   0.0   0.0  100   0.01   0.0    0.0   6.43  -6.0   0.0  999    -999 ...
0     0     0     0   0     0     0      0       0     0     0      0     0      0 ;
];

tg_con = [...
 1  1  1  25.0  1.0  0.1  0.5 0.0 1.25 5.0;
 1  2  1  25.0  1.0  0.1  0.5 0.0 1.25 5.0;
 %1  3  1  25.0  1.0  0.1  0.5 0.0 1.25 5.0;
 1  4  1  25.0  1.0  0.1  0.5 0.0 1.25 5.0
];

lmon_con = [2 3 4 5]';

% STATCOM data
%       col1  statcom number
%       col2  Bus number
%       col3  Mmax
%       col4  Mmin
%       col5  Mo
%       col6  k(first loop)
```

```
%       col7  kD (first loop)
%       col8  T1
%       col9  T2
%       col10 Kmac
%       col11 Tmac
%       col12 vref
%       col13 Almax
%       col14 Almin
%       col15 Alo
%       col16 kI
%       col17 kP
%       col18 kmdc
%       col19 Tmdc
%       col20 vdcref

statcom_con = [ 1   9   1.69   1.56   1.63    100  10  0.05  0.01  20 0.02...
                1.0   pi    -pi  -0.32    10  100  10.0  0.01  1.0; ];

load_con = [11 0 0 0 0];

svc_con = [
    11 100  2  -2  100  0.02  0.05 0.01 0.2;
];

pss_con = [];
hgt_con = [];
tgt_con = [];
lmod_con = [];
rlmod_con  = [];
uel_con=[];
gsib_idx = [];
geib_idx = [];
```

Appendix C

IEEE 14-BUS TEST SYSTEM

C.1 Static and Dynamic Data

```
HDG
   IEEE 14 BUS SYSTEM
   EPRI DATA FORMAT
   NOVEMBER 2001
BAS
C
C  AC Buses
C
C        1         2         3         4         5         6         7         8
C 345678901234567890123456789012345678901234567890123456789012345678901234567890
C                              | SHUNT |
C  |Ow|Name   |KV |Z|PL  |QL  |MW |MVA|PM |P   |QM  |Qm  |Vpu|Vm |Name   |KV |Q
BQ    BUS_1   69.0IE.0000.0000.000.0009999232.6990.0 -9891060   0            0.0
BQ    BUS_2   69.0IE21.7012.70.000.000999940.0050.00-40.01045   0            0.0
BQ    BUS_3   69.0IE94.2019.00.000.0009999.000040.00.00001010   0            0.0
B     BUS_4   69.0IE47.804.000.000.000.000.0000.0000.0000   0   0            0.0
B     BUS_5   69.0IE7.6001.600.000.000.000.0000.0000.0000   0   0            0.0
BQ    BUS_6   13.8IE11.207.500.000.0009999.000024.00-6.001070   0            0.0
B     BUS_7   13.8IE.0000.0000.000.000.000.0000.0000.0000   0   0            0.0
BQ    BUS_8   18.0IE.0000.0000.000.0009999.000024.00-6.001090   0            0.0
B     BUS_9   13.8IE29.5016.60.000.000.000.0000.0000.0000   0   0            0.0
```

```
B     BUS_10  13.8IE9.0005.800.000.000.000.0000.0000.0000   0   0           0.0
B     BUS_11  13.8IE3.5001.800.000.000.000.0000.0000.0000   0   0           0.0
B     BUS_12  13.8IE6.1001.600.000.000.000.0000.0000.0000   0   0           0.0
B     BUS_13  13.8IE13.505.800.000.000.000.0000.0000.0000   0   0           0.0
B     BUS_14  13.8IE14.905.000.000.000.000.0000.0000.0000   0   0           0.0
C
C AC Lines
C
C        1         2         3         4         5         6         7         8
C 345678901234567890123456789012345678901234567890123456789012345678901234567890
C                 M            CS
C |Own|Name_1 |KV1||Name_2 |KV2|||In || R   | X   | G/2 | B/2 |Mil|
L     BUS_1   69.01BUS_2   69.011.0001.01938.05917.00000.02640
L     BUS_1   69.01BUS_5   69.011.0001.05403.22304.00000.02460
L     BUS_2   69.01BUS_3   69.011.0001.04699.19797.00000.02190
L     BUS_2   69.01BUS_4   69.011.0001.05811.17632.00000.01870
L     BUS_2   69.01BUS_5   69.011.0001.05695.17388.00000.01700
L     BUS_3   69.01BUS_4   69.011.0001.06701.17103.00000.01730
L     BUS_4   69.01BUS_5   69.011.0001.01335.04211.00000.00640
L     BUS_6   13.81BUS_11  13.811.0001.09498.19890.00000.00000
L     BUS_6   13.81BUS_12  13.811.0001.12291.25581.00000.00000
L     BUS_6   13.81BUS_13  13.811.0001.06615.13027.00000.00000
L     BUS_7   13.81BUS_8   18.011.0001.00000.17615.00000.00000
L     BUS_7   13.81BUS_9   13.811.0001.00000.11001.00000.00000
L     BUS_9   13.81BUS_10  13.811.0001.03181.08450.00000.00000
L     BUS_9   13.81BUS_14  13.811.0001.12711.27038.00000.00000
L     BUS_10  13.81BUS_11  13.811.0001.08205.19207.00000.00000
L     BUS_12  13.81BUS_13  13.811.0001.22092.19988.00000.00000
L     BUS_13  13.81BUS_14  13.811.0001.17093.34802.00000.00000
C Transformers
C
C        1         2         3         4         5         6         7         8
C 345678901234567890123456789012345678901234567890123456789012345678901234567890
C                 M            CS
C  |Ow|Name_1 |KV1||Name_2 |KV2|||Sn  | R   | X   | G   | B   |Tap1|Tap2|
T     BUS_4   69.01BUS_7   13.811.0001.00000.20912.00000.0000067.4813.80
T     BUS_4   69.01BUS_9   13.811.0001.00000.55618.00000.0000066.8613.80
T     BUS_5   69.01BUS_6   13.811.0001.00000.25202.00000.0000064.3113.80
ZZ
C        1         2         3         4         5         6         7         8
```

```
C 345678901234567890123456789012345678901234567890123456789012345678901234567890
C                     |Iter| |Slack  |KV |  |Ang      |           |#
A  IEEE14    BUS_2   69.0     0.00 IE
ZZ
SOL1                      20  BUS_1   69.0       0.0000    1.1000    1    1.00
END

% DYNAMIC DATA IN PSAPAC FORMAT
 DESC
CASE ID
EDATA
 DGEN
BUS_1   69.0    1 100. 100.
    0    0    1    1    0    0    0    0    0    0    0    0
   0.00000   0.89800   0.64600   0.23900   0.29950   0.64600   0.00000   0.00000
   7.40000   0.00000   0.00000   0.00000
   5.14797   2.00000   0.00000   615.000   1.00000  60.00000
BUS_1   69.0    1    1    1
 200.00000   0.02000   1.00000   0.00010   0.00000   0.00000   0.00000   0.00000
   0.01000   1.00000   0.00000   0.00000   7.32000   0.00000   0.00000   0.00000
   0.00000   0.00000   0.00000   0.00000  20.00000   0.05000   1.00000   1.98000
BUS_1   69.0    0
 20.00000  10.00000   0.30000   0.01000   0.40000   0.02000   0.00000   0.00000
   0.00000   0.00000   0.00000    0.0000
BUS_2   69.0    1 100. 100.
    0    0    1    0    0    0    0    0    0    0    0    0
   0.00310   1.05000   0.98000   0.00000   0.18500   0.36000   0.00000   0.00000
   6.60000   0.00000   0.00000   0.00000
   6.54167   2.00000   0.00000    60.000   1.00000  60.00000
BUS_2   69.0    1    1    1
  20.00000   0.05000   1.00000   1.98000   0.00160   1.71280   0.00000   0.00000
   0.00000   0.00000   0.00000   0.00000   0.00000   0.00000   0.00000   0.00000
   0.00000   0.00000   0.00000   0.00000  20.00000   0.05000   1.00000   1.98000
BUS_3   69.0    1 0.00 100.
    0    0    1    0    0    0    0    0    0    0    0    0
   0.00310   1.05000   0.98000   0.00000   0.18500   0.36000   0.00000   0.00000
   6.60000   0.00000   0.00000   0.00000
   7.73333   1.00000   0.00000    60.000   1.00000  60.00000
BUS_3   69.0    1    1    1
  20.00000   0.05000   1.00000   1.98000   0.00160   1.71280   0.00000   0.00000
```

```
   0.00000   0.00000   0.00000   0.00000   4.38000   0.00000   0.00000   0.00000
   0.00000   0.00000   0.00000   0.00000  20.00000   0.05000   1.00000   0.70000
BUS_6   13.8    1 0.00 100.
    0    0    1    0    0    0    0    0    0    0    0    0
   0.00140   1.25000   1.22000   0.13000   0.23200   0.71500   0.00000   0.00000
   4.75000   1.50000   0.00000   0.00000
   5.02000   2.00000   0.00000    25.000   1.00000  60.00000
BUS_6   13.8    1    1    1
  20.00000   0.05000   1.00000   0.70000   0.03920   0.88070   0.00000   0.00000
   0.00000   0.00000   0.00000   0.00000   6.81200   1.39500   0.00000   0.00000
   0.00000   0.00000   0.00000   0.00000  20.00000   0.05000   1.00000   0.70000
BUS_8   18.0    1 0.00 100.
    0    0    1    0    0    0    0    0    0    0    0    0
   0.00140   1.25000   1.22000   0.13000   0.23200   0.71500   0.00000   0.00000
   4.75000   1.50000   0.00000   0.00000
   5.01600   2.00000   0.00000    25.000   1.00000  60.00000
BUS_8   18.0    1    1    1
  20.00000   0.05000   1.00000   0.70000   0.03920   0.88070   0.00000   0.00000
   0.00000   0.00000   0.00000   0.00000   6.81200   1.39500   0.00000   0.00000
   0.00000   0.00000   0.00000   0.00000   0.00000   0.00000   0.00000   0.00000
EDATA
 NLBS
BUS_10  13.8    0    0  100  100    0    0    0    0    0    0    0    0    0
BUS_11  13.8    0    0  100  100    0    0    0    0    0    0    0    0    0
BUS_12  13.8    0    0  100  100    0    0    0    0    0    0    0    0    0
BUS_13  13.8    0    0  100  100    0    0    0    0    0    0    0    0    0
BUS_14  13.8    0    0  100  100    0    0    0    0    0    0    0    0    0
BUS_2   69.0    0    0  100  100    0    0    0    0    0    0    0    0    0
BUS_3   69.0    0    0  100  100    0    0    0    0    0    0    0    0    0
BUS_4   69.0    0    0  100  100    0    0    0    0    0    0    0    0    0
BUS_5   69.0    0    0  100  100    0    0    0    0    0    0    0    0    0
BUS_6   13.8    0    0  100  100    0    0    0    0    0    0    0    0    0
BUS_9   13.8    0    0  100  100    0    0    0    0    0    0    0    0    0
EDATA
 NSVC
BUS_4   69.0 SH1    50 0.00    1
? USER DEFINED SVC STARTS

BUS_4   69.0BUS_3   69.01
                LL 100.00000   1.00000   5.00000   0.00000   0.00000   0.00000
```

```
                LL   1.00000   1.00000   5.00000   0.00000   0.00000   0.00000
                GN   1.00000   1.00000   0.00000   0.00000   0.00000   0.00000
                LL   1.00000   0.00000   0.02000   0.00000   0.00000   0.00000
               SD2 100.00000 100.00000   0.00000   0.00000   0.00000   0.00000
                LL   1.00000   0.77000   0.02000   0.00000   0.00000   0.00000
                WO   1.00000  10.00000   0.00000   0.00000   0.00000   0.00000

    1    2    2    3    3    4    4    5    6    1    7    6
    1 VREF  -1.00000    1 VSVC   1.00000    7 PRO1   -4.0600
?
? USER DEFINED SVC ENDS
?
EDATA
BUS_15  69.0BUS_5   69.0    1    50  50.    4
? USER DEFINED TCSC STARTS

BUS_4   69.0BUS_15  69.01
        B1          WO   1.00000   5.00000   0.00000   0.00000   0.00000   0.00000
        B2          LL   1.00000   0.00000   0.01000   0.00000   0.00000   0.00000
        B3          LL   1.00000   0.60000   0.20000   0.00000   0.00000   0.00000
        B4          GN   0.02000   1.00000   0.20000   0.00000   0.00000   0.00000
        B5         SD24000.00000 800.00000   0.02000   0.00000   0.00000   0.00000

    1    2    2    3    3    4    4    5
    1 PRO1  -0.60000    4 VREF   0.01000
?
? USER DEFINED TCSC ENDS
?
EDATA
  END
```

Appendix D

SVC AND STATCOM DATA

D.1 SVC Data

Table D.1: SVC static data

X_c (p.u.)	X_l (p.u.)	α_{min} (deg.)	α_{max} (deg.)	Slope (%)	MVA	kV
2.1708	0.1925	90	175	2	150	100

Table D.2: SVC controller parameters used in the PST software

K	T (s)	T_1 (s)	T_2 (s)	T_w (s)	B_{max} (p.u.)	B_{min} (p.u.)
100	0.02	0.01	0.05	10	2	-2

D.2 STATCOM Data

Table D.3: STATCOM static data

R_c (p.u.)	R (p.u.)	X (p.u.)	C (p.u.)	k	X_{SL} (%)
0.0017	0	0.145	0.1	0.9	2

Table D.4: STATCOM controller parameters used in the PST software

V_{ref}	K_p	K_I	K_M	T_M (s)	T_w (s)	α_{max} (rad)	α_{min} (rad)
1	10	100	1	0.02	10	—	—

Bibliography

[1] H. G. Kwatny, A. K. Pasrija, and L. Y. Bahar, "Static bifurcation in electric power networks: Loss of steady-state stability and voltage collapse," *IEEE Trans. Circuits Systems*, vol. 33, 1986, pp. 981–991.

[2] I. Dobson and H-D. Chiang, "Towards a theory of voltage collapse in electric power systems," *Systems and Control Letters*, vol. 13, 1989, pp. 253–262.

[3] H-D. Chiang, I. Dobson, R. J. Thomas, J. S. Thorp, and L. Fekih-Ahmed, "On voltage collapse in electric power system," *IEEE Trans. on Power Systems*, vol. 5, 1990, pp. 601–611.

[4] E. H. Abed, J. C. Alexander, H. Wang, A. M. A. Hamdan, and H-C. Lee, "Dynamic Bifurcation in a Power System Model Exhibiting Voltage Collapse," technical report, Department of Mathematics, University of Maryland, College Park, MD 20742 USA, February 1992.

[5] W. Zhu, R. R. Mohler, R. Spee, W. A. Mittelstadt, and D. Maratukulam, "Hopf bifurcations in a SMIB Power System with SSR," *IEEE Trans. on Power Systems*, vol. 11, no. 3, 1996, pp. 1579–1584.

[6] A. S. Gugushvilli, G. N. Dalakishvili, N. M. Gomareli, and V. M. Kekenadze.

"Bifurcation and Chaos in Power Systems". In *Proc. of Inter. conference on Control of Oscillation and Chaos*, pp. 349–353, Russia, 1997.

[7] Y. Mitani and K. Tsuji, "Bifurcations Associated with Sub-Synchronous Resonance," *IEEE Trans. on Power Systems*, vol. 13, no. 1, 1998, pp. 139–144.

[8] J. Li and V. Venkatasubramanian. "Study of Hopf bifurcation in a Simple Power System Model". In *Proc. of the 39th Conference on Decision and Control*, pp. 3075–3079, Sydney, December 2000.

[9] C. A. Cañizares, F .L. Alvarado, C. L. DeMarco, I. Dobson, and W. F. Long, "Point of Collapse Method Applied to AC/DC Power Systems," *IEEE Trans. on Power System*, vol. 7, no. 2, May 1992, pp. 673–683.

[10] Editor C. A. Cañizares, "Voltage Stability Assessment, Procedure and Guides," technical report, IEEE/PES Power System Stability Subcommittee, draft, Available at http://www.power.uwaterloo.ca, January 2001.

[11] V. Ajjarapu and B. Lee, "Bifurcation Theory and its Application to Nonlinear Dynamical Phenomena in an Electrical Power System," *IEEE Trans. on Power System*, vol. 7, no. 1, February 1992, pp. 424–431.

[12] C. A. Cañizares and S. Hranilovic. "Transcritical and Hopf Bifurcation in AC/DC Systems". In *Proc. Bulk Power System Voltage Phenomena-III Seminar*, pp. 105–114, Davos, Switzerland, August 1994.

[13] E. H. Abed and P. P. Varaiya, "Nonlinear Oscillations in Power Systems," *International Journal of Electric Power and Energy Systems*, vol. 6, 1984, pp. 37–43.

[14] W. D. Rosehart and C. A. Cañizares, "Bifurcation analysis of various power system models," *International Journal of Electrical Power and Energy Systems*, vol. 12, 1999, pp. 171–182.

[15] N. Mithulananthan and S. C. Srivastava. "Investigation of a Voltage Collapse Incident in Sri Lankan Power System Network". In *Proc. of EMPD'98*, pp. 47–52, Singapore, March 1998.

[16] C. Alsberg, "WSCC issues Preliminary Report on August Power Outage: PRESS RELEASE," technical report, WSCC, Available at http://www.wscc.com/augdist.htm, September 1996.

[17] K. Kim, H. Schattler, V. Venkatasubramanin, J. Zaborszky, and P. Hirsch, "Methods for calculating oscillations in large power systems," *IEEE Trans. on Power System*, vol. 12, November 1997, pp. 1639–1648.

[18] P. Kundur, *Power System Stability and Control*. McGraw Hill, New York, 1994.

[19] C. D. Vournas, M. A. Pai, and P. W. Saure, "The Effect of Automatic Voltage Regulation on the Bifurcation Evolution in Power Systems," *IEEE Trans. on Power System*, vol. 11, no. 4, 1996, pp. 37–43.

[20] J. C. Alexander, "Oscillatory Solution of a Model System of Nonlinear Swing Equation," *International Journal of Electric Power and Energy Systems*, vol. 8, 1986, pp. 130–136.

[21] C. Rajagopalan, P. W. Sauer, and M. A. Pai. "Analysis of Voltage Control System Exhibiting Hopf Bifurcation". In *Proc. of the 28th Conference on Decision and Control*, Tampa, FL, December 1989.

[22] V. Ajjarapu and B. Lee. "Nonlinear Oscillations and Voltage Collapse Phenomena in an Electrical Power System". In *Proc. of the 22nd North America Power Symposium*, Auburn, Alabama, October 1990.

[23] H. O. Wang, E. H. Abed, R. A. Adomaitis, and A. M. A. Hamdan, "Control of Nonlinear Phenomena at the Inception of Voltage Collapse," technical report, Institute for System Research, University of Maryland, College Park, MD 20742, USA, March 1993.

[24] S. K. Joshi and S. C. Srivastava. "Estimation of Closest Hopf Bifurcation in Electric Power System". In *12th Power System Computational Conference*, August 1996.

[25] R. Seydel, *Practical Bifurcation and Stability Analysis: From Equilibrium to Chaos*. Second Edition, Springer-Verlag, New York, 1994.

[26] T. Kim and E. H. Abed, "Closed-Loop Monitoring Systems for Detecting Impending Instability," *IEEE Trans. on Circuits and Systems*, vol. 47, no. 10, October 2000, pp. 1479–1493.

[27] E. H. Abed and J. H. Fu, "Local Feedback Stabilization and Bifurcation Control I. Hopf bifurcations," *System and Control Letters*, vol. 7, 1986, pp. 11–17.

[28] E. H. Abed and J. H. Fu, "Local Feedback Stabilization and Bifurcation Control, II. Stationary Bifurcations," *Systems and Control Letters*, vol. 8, 1987, pp. 467–473.

[29] I. Dobson, F. Alvarado, and C. L.DeMarco, "Sensitivity of Hopf Bifurcation to Power System Parameters," *IEEE Decision and Control*, vol. 3, 1992, pp. 2928–2933.

[30] F. P. DeMello and C. Concordia, "Concept of Synchronous Machine Stability as affected by Excitation Control," *IEEE Trans. Power Apparatus and Systems*, vol. 88, 1969, pp. 189–202.

[31] N. Mithulananthan, C. A. Cañizares, and J. Reeve. "Hopf Bifurcation Control in Power System Using Power System Stabilizers and Static Var Compensators". In *Proc. of NAPS'99*, pp. 155–163, San Luis Obispo, California, October 1999.

[32] N. Yang, Q. Liu, and J. D. McCalley, "TCSC Controller Design for Damping Interarea Oscillations," *IEEE Transactions on Power Systems*, vol. 13, no. 4, November 1998, pp. 1304–1309.

[33] H. F. Wang, "Selection of Robust Installing Locations and Feedback Signals of FACTS-based Stabilizers in Multi-machine Power Systems," *IEEE Transactions on Power Systems*, vol. 14, no. 2, May 1999, pp. 569–574.

[34] M. J. Lautenberg, M. A. Pai, and K. R. Padiyar, "Hopf Bifurcation Control in Power System with Static Var Compensators," *Int. J. Electric Power and Energy Systems*, vol. 19, no. 5, 1997, pp. 339–347.

[35] Task Force 16 of Advisory Group 02 of Study Committee 38, "Impact of Interactions Among Power System Controls," technical report, CIGRE, November 1999.

[36] J. Arrillaga and C. P. Arnold, *Computer Analysis of Power Systems*. John Wiley & Sons, England, 1990.

[37] N. Mithulananthan, M. M. A. Salama, C. A. Cañizares, and J. Reeve, "Distribution System Voltage Regulation and Var Compensation for Different Static Load Models," *IJEEE*, vol. 37, no. 4, October 2000, pp. 384–395.

[38] P. Kundur, M. Klein, G. J. Rogers, and M. S. Zywno, "Application of Power System Stabilizers for Enhancement of Overall Systsem Stability," *IEEE Trans. on Power System*, vol. 4, no. 2, 1989, pp. 614–626.

[39] IEEE FACTS working group 15.05.15, *"FACTS Applications"*. IEEE Power Engineering Society, December 1995.

[40] C. A. Cañizares and Z. T. Faur, "Analysis of SVC and TCSC Controllers in Voltage Collapse," *IEEE Transaction on Power Systems*, vol. 14, no. 1, February 1999, pp. 158–165.

[41] N. G. Hingorani, "Flexible AC Transmission Systems," *IEEE Spectrum*, April 1993, pp. 40–45.

[42] L. Gyugyi, "Dynamic Compensation of AC Transmission Lines by Solid State Synchronous Voltage Sources," *IEEE Transaction on Power Systems*, vol. 9, no. 2, April 1994, pp. 904–911.

[43] L. Gyugyi, N. G. Hingorani, P. R. Nannery, and N. Tai, *" Advanced Static Var Compensators using Gate Turn-off Thyristors for Utility Application"*. CIGRE 23-203, August 1990.

[44] E. Uzunovic, C. A. Cañizares, and J. Reeve. "Fundamental Frequency Model of Static Synchronous Compensator". In *Proc. North American Power Symposium*, pp. 49–54, Laramie, Wyoming, October 1997.

[45] "Guid for Economic Evaluation of Flexible AC Transmission Systems (FACTS) in open Access Environments," technical report, EPRI TR 108500, Final Report Prepared by GE, New York, August 1997.

[46] J. V. Coevering, J. P. Stovall, R. L. Hauth, P. J. Tatto, B. D. Railing, and B. K. Johnson. "The Next Generation of HVDC - needed R&D, Equipment Costs, and Cost Comparisons". *Proc. of EPRI Conference of Future of Power Delivery*, Washington DC, April 1996.

[47] C. A. Cañizares. "Power Flow and Transient Stability Models of FACTS Controllers for Voltage and Angle Stability Studies". In *Proc. of IEEE/PES Winter Meeting*, Singapore, January 2000.

[48] N. Mithulananthan, C. A. Cañizares, J. Reeve, and Graham J. Rogers, "Comparison of PSS, SVC and STATCOM Controllers for Damping Power System Oscillations," *Accepted subjected to changes in IEEE Trans. on Power Systems*, October 2001.

[49] *Small Signal Stability Analysis Program Ver. 3.1: User's Manual.* EPRI, TR-101850-V2R1, May 1994.

[50] *Extended Transient-Midterm Stability Program (ETMSP) Ver. 3.1: User's Manual.* EPRI, TR-102004-V2R1, May 1994.

[51] D. J. Hill and I. M. Y. Mareels, "Stability Theory for Differential/Algebraic System with Application to Power Systems," *IEEE Trans. Circuits and Systems*, vol. 37, no. 11, November 1990, pp. 1416–1423.

[52] C. A. Cañizares and F .L. Alvarado, "Point of Collapse and Continuation Methods for Large AC/DC Systems," *IEEE Trans. on Power System*, vol. 8, no. 1, February 1993, pp. 1–8.

[53] V. Ajjarapu and C. Christy, "The continuation power flow: a tool for steady state voltage stability analysis," *IEEE Trans. on Power System*, vol. 7, 1992, pp. 416–423.

[54] C. A. Cañizares, *"UWPFLOW: Continuation and Direct Methods to Locate Fold Bifurcation in AC/DC/FACTS Power Systems"*. University of Waterloo, Available at http://www.power.uwaterloo.ca, November 1999.

[55] N. Martins, "Efficient Eigenvalue and Frequency Response Methods Applied to Power System Small-Signal Stability Studies," *IEEE Trans. on Power System*, vol. 3, May 1988, pp. 472–480.

[56] *Power System Toolbox Version 2.0: Load Flow Tutorial and Functions.* Cherry Tree Scientific Software, RR-5 Colborne, Ontario K0K 1S0, 1991-1999.

[57] *Power System Toolbox Version 2.0: Dynamic Tutorial and Functions.* Cherry Tree Scientific Software, RR-5 Colborne, Ontario K0K 1S0, 1991-1997.

[58] N. Mithulananthan, C. A. Cañizares, and J. Reeve. "Indices to Detect Hopf Bifurcation in Power Systems". In *Proc. of NAPS-2000*, pp. 15–18–15–23, University of Waterloo, Waterloo, Canada, October 2000.

[59] P. M. Anderson and A. A. Fouad, *Power System Control and Stability.* IEEE Press, 1994.

[60] Chairman V. Vittal, "Transient Stability Test System for Direct Stability Methods," *IEEE Transaction on Power Systems*, vol. 7, no. 1, February 1992, pp. 37–42.

[61] A. Berizzi, P. Finazzi, D. Dosi, P. Marannino, and S. Cors. "First and Second order Methods for Voltage Collapse Assessment and Security Enhancement". In *Proc. of IEEE/PES Winter Meeting*, New York, February 1997.

[62] I. Dobson. "Strong Resonance Effects in Normal Form Analysis and Subsyn-

chronous Resesonance". pp. 470–481, *Proc. of Bulk Power System Dynamics and Control V*, Japan, August 2001.

[63] M. J. Gibbard, D. J. Vowles, and P. Pourbeik, "Interactions Between, and Effectiveness of, Power System Stabilizers and FACTS Device Stabilizers in Multimachine Systems," *IEEE Trans. on Power System*, vol. 15, no. 2, May 2000, pp. 748–755.

[64] C. A. Cañizares, N. Mithulananthan, A. Berizzi, and J. Reeve, "On the linear Profile of Indices for Prediction of Saddle-node and Limit-induced Bifurcation Points in Power Systems," *Submitted for publication in IEEE Trans. on Circuit and Systems*, October 2001, no of pages 8.

[65] C. A. Cañizares, N. Mithulananthan, and J. Reeve, "Linear Profile Indices to Predict Oscillatory Problems in Power Systems," *to be Submitted for publication in IEEE Trans. on Power Systems*, manuscript, no. of pages 8.

[66] N. Mithulananthan, C. A. Cañizares, and John Reeve. "Tuning, Performance and Interactions of PSS and FACTS Controllers". *Accepted for the IEEE/PES Summer Meeting*,Chicago, July 2002.